Dissertation

submitted to the

Combined Faculties for the Natural Sciences and for Mathematics

of the Ruperto-Carola University of Heidelberg, Germany

for the degree of

Doctor of Natural Sciences

presented by

Piotr Fabrowski, M.Sc.

Born in Łask, Poland

Oral examination:……

The endocytic mechanisms underlying apical surface morphogenesis during epithelial development in *Drosophila*.

Referees:

Dr. Anne Ephrussi

Prof. Dr. Walter Nickel

Acknowledgements

My foremost gratitude belongs to Stefano De Renzis, my supervisor, who guided my professional scientific development over the last four years. He is an exceptional scientist, patient and supporting mentor who deeply inspired me throughout my PhD studies. Thank you for your advices, patience and understanding, especially in the most challenging periods where I needed your support the most.

I am also thankful to my scientific advisors Anne Ephrussi, Walter Nickel and Marko Kaksonen for their invaluable scientific inputs that contributed to the development and successful finalizing of my PhD project. I am also grateful to Jan Lohmann for joining my examination committee.

A special thanks goes to all my lab mates, and in particular to Eva, Ale, Tina and Simone for the coffee breaks, rowing classes, BBQs, Korean soap operas and many, many unrelated topics during fly flipping. My most sincere gratitude to Eva for her expertise and help with the experiments and to Ale and Sasha for all great scientific discussions we had.

I would like to thank my friends and my loved one for always being beside me and for keeping my spirits up in this challenging and rewarding period of my life.

Last, but not least, I would like to thank my parents for encouraging me to follow my dreams and for always believing in me,

Dziękuję Wam.

SUMMARY

Cell shape changes are of fundamental importance during morphogenesis. These changes are often initiated by the contraction or expansion of plasma membrane domains. During differentiation the plasma membrane also undergoes more complex functional re-organization that brings about specialized function such as absorption, secretion and photo-transduction. While the role of cytoskeleton elements in controlling the structure and dynamics of the plasma membrane is well-established, little is known about the contribution of membrane trafficking in this process.

The aim of this thesis was to address the contribution of membrane trafficking in controlling cell shape changes during tissue morphogenesis. More specifically I have investigated the role of endocytosis in controlling the remodeling of the plasma membrane during cellularization, the transformation of the syncytial Drosophila embryo is 6000 mononucleated cells. By following the early endocytic regulator Rab5, I identified two pools of endosomes. Early during cellularization endosomes accumulate at the invaginating furrows. Towards the end of cellularization a second pool of endosomes appeared at the apical surface. This increase in apical endosomes coincides with changes in apical morphology. Blocking endocytosis by inhibiting dynamin function prevented the re-absorption of apical protrusions and subsequent membrane flattening. Using a novel genetically-encoded cargo uptake assay I discovered that during apical surface flattening endocytosis is up-regulated of approximately five-fold. Strikingly this assay also revealed that the primary entry route for soluble extracellular cargo is through long tubular intermediates that serve as platform for the generation of Rab5 vacuolar endosomes. Blocking dynamin activity resulted in the complete inhibition of both tubular endocytosis as well as in the disappearance of Rab5 endosomes. These data collectively support a role for membrane trafficking in morphological remodeling. Surface flattening is thus an endocytosis-dependent morphogenetic process driven by the rapid internalization of large quantities of plasma membrane through tubular invagination and up-regulation of Rab5 endosome production. To further characterize the molecular machinery controlling apical endocytosis during cellularization a biochemical approach was undertaken. I performed large-scale affinity purification from 0-4 h embryos in order to identify Rab5 effectors operating during these early stages of embryonic development. This experiment led to the identification of

Rabankyrin-5. Using a combination of live imaging and correlative light-electron microscopy I could show that Rabankyrin-5 controls the budding and processing of apical vacuoles from tubular plasma membrane invagination.

In conclusion, in this thesis I have identified a novel endocytic pathway and linked its function to the remodeling of the apical surface during epithelial morphogenesis.

ZUSAMMENFASSUNG

Während der Morphogenese spielen Veränderung von Form und Größe der Zelle eine enorme Bedeutung und werden zumeist durch Kontraktion oder Expansion bestimmter Bereiche der Plasmamembran eingeleitet. Bei der Differenzierung muss die Plasmamembran eine Reihe von Umstrukturierungen durchlaufen, die zu Spezialisierungen, wie Absorption, Sekretion und Phototransduktion führen können. Eine wichtige und bereits gut erforschte Rolle hat hierbei das Cytoskelett, das die Form und Strukturgebung der Plasmamembran beeinflusst. Im Gegensatz dazu ist nur sehr wenig über die Rolle des Membrantransports auf diesen morphogenetischen Prozess bekannt.

Ziel dieser Arbeit war es, den Einfluss des vesikulären Membrantransports auf die Formgebung der Plasmamembran während der Morphogenese zu untersuchen. Im Speziellen ist hiermit die Rolle der Endozytose auf die Umgestaltung der Plasmamembran während der Zellularisierung des *Drosophila* Embryos gemeint. Während diesem Entwicklungsstadium wird aus einem 6000-zellkernigen Synzytium die erste Zellschicht mit individuellen Zellen gebildet. Hauptaugenmerk lag bei dieser Arbeit auf Rab5, einer GTPase welche in einem frühen Stadium der Endozytose involviert ist. Mit Hilfe von Live Imaging wurde endozytisches Rab 5 verfolgt. Hierbei konnte ich feststellen, dass zwei unterschiedliche Gruppen endosomaler Strukturen vorliegen. Zu Beginn der Zellularisierung akkumulieren Endosomen an den Einstülpungen der Plasmamembran. Gegen Ende dieser Entwicklungsphase tauchte eine zweite Gruppe von Endosomen an der apikalen Oberfläche auf. Dieser Anstieg von Endosomen an der apikalen Oberfläche geht mit einer Veränderung in der Morphologie der apikalen Seite einher. Blockieren der Endozytose durch Inhibierung von Dynamin führte zur Ausbildung von apikalen Ausstülpungen und verhinderte das Abflachen der Plasmamembran. Desweiteren konnte ich durch die Benutzung eines neuen ‚genetisch-codierten' Endozytose Assay zeigen, dass die Endozytoserate während des Abflachens der Plasmamembran um das Fünffache erhöht ist. Dieser Assay brachte auch zum Vorschein, dass der primäre Aufnahmeweg von flüssigen extrazellulären Transportstoffen durch lange tubuläre Intermediate erfolgt. Diese Intermediate dienen als Grundlage für die Herstellung von Rab5-Endosomen. Durch blockieren der Aktivität von Dynamin wurde sowohl die tubuläre Endozytose als auch das Auftreten von Rab5-Endosomen gestoppt.

Diese Daten zeigen den Einfluss von Membrantransport auf die Formgebung während der Morphogenese. Ich konnte zeigen, dass das Abflachen der Membran ein Entwicklungsprozess darstellt, der Endozytose-abhängig ist und durch eine schnelle Aufnahme der Plasmamembran und vermehrte Produktion von Rab5-Endosomen bewerkstelligt wird. Desweiteren wurden biochemische Untersuchungen vorgenommen um die exakten molekularen Mechanismen, die diesem Prozess unterliegen, zu charakterisieren. Hierfür führte ich eine Proteinaufreinigung von 0-4 Stunden alten Embryos durch, um Interaktionspartner von Rab5 zu identifizieren, die während diesem Embryonalstadium aktiv sind. Hierbei wurde Rabankyrin-5 als Interaktionspartner von Rab5 identifiziert. Durch Kombination von Live-Imaging und korrelativer Licht/Elektronen Mikroskopie konnte ich zeigen, dass Rabankyrin-5 das Abknospen und Weiterverarbeiten von apikalen Vakuolen, die aus tubulären Plasmamembran-Einstülpungen resultieren, kontrolliert.

Zusammenfassend, konnte ich mit der vorliegenden Arbeit einen neuen endozytischen Signalweg identifizieren und seine Funktion in Zusammenhang mit der Umgestaltung der apikalen Oberfläche während der embryonalen Morphogenes aufweisen.

Table of Contents

LIST OF FIGURES

Abbreviations

°C	degrees Celsius
AAJ	apical adherens junction
AEE	apical early endosome
ATP	adenosine triphosphate
BAJ	basal adherens junction
BAR	bin–Amphiphysin–Rvs
BEE	basal early endosome
bp	base pairs
BTB	BR-C, ttk and bab
CCV	clathrin-coated vesicle
cDNA	complementary DNA
CLIC	clathrin-independent carriers
CME	clathrin-mediated endocytosis
EE	early endosome
ECM	extracellular matrix
ESCRT	endosomal sorting complex required for transport
F-actin	filamentous actin
Fc	fragment crystallizable region
FYVE	Fab 1, YOTB, Vac 1
GAP	GTPase activating protein
GDI	guanosine nucleotide dissociation inhibitors
GDP	guanosine diphosphate
GEEC	GPI-enriched endosomal compartments
GEF	guanine nucleotide exchange factor
GGT	geranylgeranyltransferase
GPI-AP	glycosyl-phosphatidylinositol-anchored proteins
GTP	guanosine triphosphate
HRP	horseradish peroxidase
HSPGs	heparan sulfate proteoglycans
IgG	immunoglobulin G
IPTG	isopropyl β-D-1-thiogalactopyranoside
kb	kilobase
kDa	kilodalton
LE	late endosome
LYS	lysosome
MDCK	Madin-Darby canine kidney epithelial cells
mRNA	messenger ribonucleic acid
MTC	multi-subunit tethering complexes
NECD	Notch extracellular domain
NICD	Notch intracellular domain
PCR	polymerase chain reaction
PH	pleckstrin homology
PM	plasma membrane
PtdIns	phosphatidylinositol
qPCR	quantitative PCR
RE	recycling endosome
REP	Rab escort protein
RNA	ribonucleic acid
RNAi	RNA interference
RT-PCR	real-time PCR
S2	Schneider 2
secGFP	secreted green fluorescent protein
SH3	Src homology 3
shRNA	short hairpin RNA
SM	Sec1/Munc18
SNARE	SNAP receptor
SV40	Simian virus 40
TGN	trans-Golgi network
TIRFM	total internal reflection fluorescence microscopy
UV	ultraviolet
WGA	wheat germ agglutinin

Gene symbols

AAK1	AP2-associated protein kinase 1
Abl	abelson tyrosine kinase
Amph	amphiphysin
AP2	Adaptor protein 2
Arf6	ADP-ribosylation factor 6
arm	armadillo
aux	auxillin
Bap	Beta Adaptin
bcd	bicoid
bnk	bottleneck
Cav	Caveolin
Cdc14	Cell division cycle 14
Cdk1	Cyclin-dependent kinase 1
Chc	Clathrin heavy chain
Clc	Clathrin light chain
Dap160	Dynamin associated protein 160
dia	diaphanous
dpp	decapentaplegic
EEA1	early endosome antigen 1
EGF	epidermal growth factor
EPS15	epidermal growth factor receptor pathway substrate 15
fog	folded gastrulation
Gap43	growth associated protein 43
gish	gilgamesh
GRAF1	GTPase regulator associated with focal adhesion kinase 1
hh	hedgehog
hsc70	heat shock cognate 70
Hsp70	heat shock protein 70
hVPS34	phosphatidylinositol 3-kinase, catalytic subunit type 3
lqf	liquid facets
Munc18	mammalian uncoordinated-18
NSF	N-ethyl-maleimide-sensitive fusion protein
OCRL	oculocerebrorenal syndrome of Lowe
Pak1	p21 protein (Cdc42/Rac)-activated kinase 1
PI3K	phosphatidylinositol-4,5-bisphosphate 3-kinase
Rab	ras-related in brain
Rac1	ras-related C3 botulinum toxin substrate 1
Ras	rat sarcoma
Slam	slow as molasses
SNAP25	synaptosomal-associated protein 25
SNX5	sorting nexin 5
Src64	sarcoma oncogene at 64B
Tec29	tyrosine-protein kinase tec at 29A
Tub67C	alpha-Tubulin at 67C
VAMP	vesicle-associated membrane protein
w	white
Wg	wingless

Chapter 1 Introduction

In this introduction, I will first describe the initial steps of *Drosophila* embryogenesis and then discuss the general regulatory principles underlying endocytosis. In the last chapters I will summarize some of the key experiments illustrating how endocytosis controls development with a special focus on signalling and cellularization.

1.1 Early Drosophila development

Early *Drosophila* development is a complex, yet highly reproducible process that includes massive nuclei replication, formation of a polarized ephitelium, and morphogenic movements. After fertilization, *Drosophila* embryo undergoes 13 nuclear divisions without cytokinesis (Foe and Alberts 1983; Turner and Mahowald 1976). All the nuclei are confided in a single cytoplasmic sack called syncytium, where astral microtubules organize the uniform distribution of the nuclei (Karr and Alberts 1986). At the division cycle 9 the first nuclei that progressively migrate towards the embryo cortex appear at the posterior pole, giving rise to the germ line (pole cells). At the cycle 10 all the remaining somatic nuclei anchor at the plasma membrane and formation of membrane pseudocleavage furrows can be observed (Foe and Alberts 1983; Turner and Mahowald 1976). The next three nuclear divisions are progressively longer until cycle 14, when all the nuclei pause in interphase (Foe and Alberts 1983). At this point, a step that is common to all embryonic developmental programs occurs (both animal and plants), that is maternal to zygotic transition (Schier 2007; Tadros and Lipshitz 2009). During this transition many mRNAs provided in the egg by the mother are rapidly degraded and the transcription of new zygotic genes starts. The mechanisms underlying this transition are not completely understood. In zebra fish microRNAs control the degradation of the maternal mRNAs (Mathavan et al. 2005; Giraldez et al. 2006), while in mouse DNA methylation controls the switching of genes on or off at this time (Reik and Walter 2001). In *Drosophila*, recently the early transcription factor Zelda has been shown to regulate the robust expression of many zygotic genes (Nien et al. 2011). In particular, Zelda has been shown to control the expression of genes involved in cellularization, the transformation of the syncytial embryo in 6000 mononucleated polarized cells (Nien et al. 2011; Liang et al. 2008).

1.2 Cellularization

During cellularization around 6000 polarized cells are formed by the invagination of the plasma membrane between single nuclei in close proximity to the embryo cortex (Foe and Alberts 1983; Turner and Mahowald 1976). A close interplay between cytoskeleton reorganization and membrane dynamics is necessary for the progression of the invaginating membranes (Warn and Warn 1986; Warn and Robert-Nicoud 1990). Cellularization lasts approximately 60-70 minutes and has been divided in four stages according to the organization of the furrow canals.

Furrow canals are present at the bottom of the invaginating membranes and have similar function and protein composition to the cleavage furrows present during the standard cytokinesis (Crawford et al. 1998). Furrows are assembled in close proximity to the apical plasma membrane during the first 10 minutes of cellularization. At the end of cellularization the contraction of furrow canals will drive basal closure of the cells (Crawford et al. 1998; Young, Pesacreta, and Kiehart 1991) (Figure 1.1 a). At the molecular level, the plasma membrane domains of the furrows are enriched in actin and myosin II (Crawford et al. 1998; Young, Pesacreta, and Kiehart 1991). The initial assembly of actin/myosin II at the furrow canal is dependent on the activity of a RhoGEF2 (Rho guanine nucleotide exchange factor 2) and the formin Dia (Diaphanous) (Grosshans et al. 2005). Mutants of any of these two genes result in a decrease in the levels of actin and the myosin II at the base of the furrow and defects in cellularization. In addition, ultrastructural analysis revealed a disorganization and blebbing of the furrow canals (Grosshans et al. 2005). Similarly, inhibition of actin polymerization using cytochalasin abolishes assembly of the furrow canal, but surprisingly does not have a noticeable effect on later stages of cellularization (Royou, Field, and Sisson 2004). These results show that actin is responsible for the initial stabilization and assembly of the furrows, but not for completing cellularization.

The assembly of furrow canals is controlled by the expression of slam (slow as molasses) (Thomas Lecuit, Samanta, and Wieschaus 2002; Stein et al. 2002). Slam protein localizes to the invaginating furrows and has been shown to associate with the RhoGEF2 (Rho guanine nucleotide exchange factor 2) (Wenzl et al. 2010). Hence the

slam/RhoGEF2 assembly regulates the Rho1 (ras homolog family member 1) activity at the leading membrane. However, slam mutants display phenotypes that are more severe from Rho mutants, therefore arguing that slam must have additional function. Indeed, in slam mutants the speed of membrane invagination does not increase and the furrows show irregular morphology with abnormal basal adherens junctions (BAJ) (Thomas Lecuit, Samanta, and Wieschaus 2002). BAJs are formed just above the furrow canals (Mazumdar and Mazumdar 2002; Thomas Lecuit 2004) and are composed of E-cadherin, alpha-catenin and Armadillo (the *Drosophila* homologue of beta-catenin). Furthermore, proper localization of BAJ is regulated by zygotic expression of the gene nullo (Hunter and Wieschaus 2000; Postner and Wieschaus 1994; Simpson and Wieschaus 1990). Removing nullo results in diffusion of Armadillo (Arm) into lateral membranes, destabilization of the furrow canals and regression of the lateral plasma membranes (Sokac and Wieschaus 2008b). As a consequence, many cells become multinucleated. Since Arm mutants show normal invagination, there must be a different mechanism for stabilization of the basal compartment. This function is provided by the gene nullo that organizes actin cytoskeleton at the furrow canal, and thus prevents destabilization of the basal membranes (Sokac and Wieschaus 2008b; Simpson and Wieschaus 1990; Postner and Wieschaus 1994). Another gene that has been shown to stabilize furrows is serendipity-alpha (Schweisguth, Lepesant, and Vincent 1990). This gene codes for a small peptide of unknown function.

In the second phase of cellularization plasma membrane invaginates towards the base of the nuclei (Figure 1.1 a-b). This process is blocked by the colchicine and therefore is dependent on microtubules (Royou, Field, and Sisson 2004). In parallel to membrane growth, nuclei start to change shape by elongating along the apical-basal axis (Schweisguth, Lepesant, and Vincent 1990; Brandt et al. 2006; Turner and Mahowald 1976). This process is also microtubule dependent and in addition requires reorganization of the nuclear envelope (Schweisguth, Lepesant, and Vincent 1990; Brandt et al. 2006). The change of the nuclear morphology might reflect a massive transcription initiation during cellularization but there is no evidence so far to prove this hypothesis.

The third phase of cellularization starts when the furrow canal reaches the base of the nuclei (Figure 1.1 b-c). At this step apical adherens junctions (AAJ) are formed.

Simillar to BAJ, AAJ are not necessary during cellularization, but rather for the subsequent morphogenic movement (Thomas Lecuit 2004; Kölsch et al. 2007; Müller and Wieschaus 1996; Hunter and Wieschaus 2000). This phase of celullarization is also referred as the fast phase, since plasma membrane growth increases three times, from ~0,3 to ~0,8 μm/min (Mazumdar and Mazumdar 2002).

The last step of cellularization is characterized by the constriction of the furrow canals and formation of the basal membranes (Figure 1.1 c). This process is dependent on contractile actin-myosin rings present at the base of each cell (Royou, Field, and Sisson 2004; Mazumdar and Mazumdar 2002). Similar to classical cytokinesis, furrow constriction is dependent on the Rho1 activity (Crawford et al. 1998). As mentioned before, Rho1 is recruited to the furrow by RhoGEF2 and activates Rho kinase that phosphorylates myosin II (Grosshans et al. 2005; Padash Barmchi, Rogers, and Häcker 2005). Therefore disruption of the RhoGEF2 function or the myosin II activity prevents basal constriction. Furthermore, two non-receptor kinases Src64 (sarcoma oncogene at 64B) and Tec29 (tyrosine-protein kinase tec at 29A) are needed for the proper closure (Roulier, Panzer, and Beckendorf 1998; Thomas and Wieschaus 2004).

Although RhoGEF2, myosin II, and kinases are present at the furrow canal through cellularization, their activity must be precisely controlled to ensure proper cell growth. The timing of basal closure is controlled by bottleneck (bnk) (Schejter and Wieschaus 1993). Bnk is expressed only early during cellularization and localizes to the furrow. Bnk is then degraded during the last phase of cellularization. In bnk mutants, the premature contraction of the furrows and trapping of the nuclei can be observed (Schejter and Wieschaus 1993). However, despite of activation of myosin II, the furrows are not constricting completely at the end of cellularization. There is still a connection between the cytoplasm and the yolk called the ‘yolk plug’ that is stabilized by the formin peanut (Adam, Pringle, and Peifer 2000). This connection persists till the next stage of the embryonic development called gastrulation.

During cellularization in addition to the lateral membranes, also the apical surface undergoes morphological changes. Scanning EM analysis of the different stages of cellularization revealed a dramatic reorganization of the apical plasma membrane (Turner and Mahowald 1976). During stages I to III of cellularization apical plasma membrane is

covered with microvillar-like protrusions. These protrusions disappear during the last stage of cellularization (Turner and Mahowald 1976). Formation of apical protrusions and plasma membrane flattening is associated with actin dynamics driven by its regulator Abl (Abl tyrosine kinase) (Grevengoed et al. 2003). In Abl mutants, there is an excessive polymerization of actin at the apical surface of cellularizing embryos. This leads to massive formation villous protrusions and interferes with membrane flattening (Grevengoed et al. 2003). There is no detailed information about the dynamics of apical flattening during cellularization.

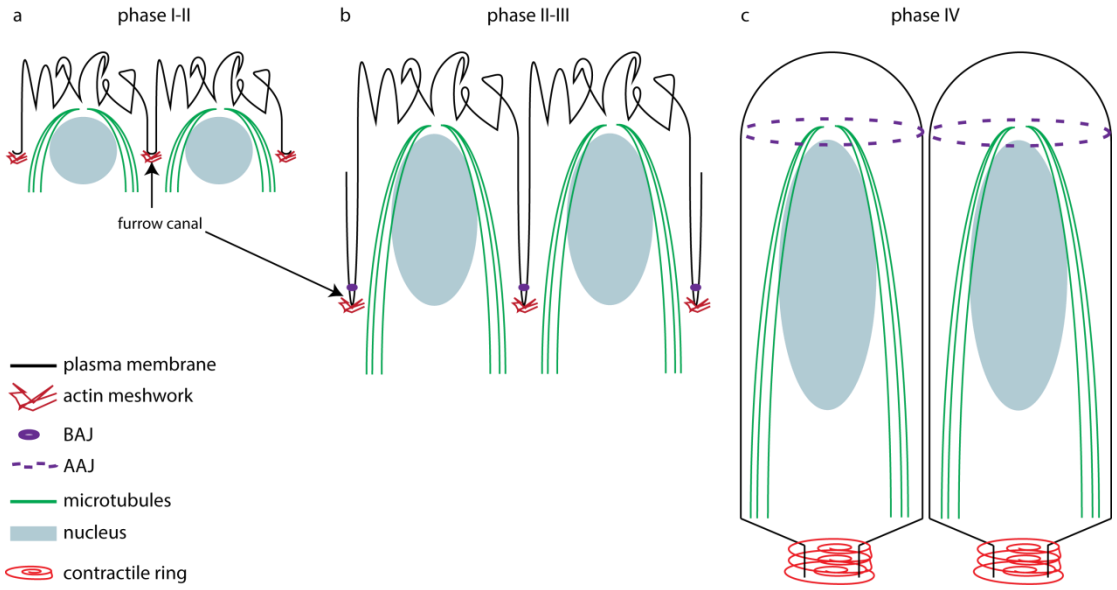

Figure 1.1 Four phases of cellularization.
Schematic view of cell morphology during cellularization. This process is divided into four stages that represent different points of membrane invagination and junction assembly. For more details see Chapter 1.2

1.3 Mechanisms of endocytosis

In a developing organism every eukaryotic cell is in contact with the environment through the plasma membrane bilayer. Although some small molecules are able to cross this barrier simply by diffusion, many nutrients, signalling proteins and other substrates are uptaken by specialized vesicles in the process called endocytosis (Mellman 1996). At the basic level, endocytosis maintains cellular homeostasis by re-internalizing proteins and lipids inserted in the plasma membrane by ongoing secretion. Living organisms have developed many different forms of endocytosis, specific for different functions. Reuptake of synaptic contents by neurons (von Gersdorff 1994), engulfing pathogens by macrophages (Kinchen and Ravichandran 2008) and regulation of extracellular matrix (Shi and Sottile 2011) are only few examples that describe the many different endocytic functions. Moreover, in recent years it became evident a key role of endocytosis in mitosis (Fürthauer and González-Gaitán 2009), as well as in cell migration (Caswell and Norman 2008). Although, many basic regulators of endocytosis have been identified, the spatial-temporal regulation of endocytosis is less clear. In the next chapters I will present a general overview of the endocytic compartments and endocytic pathways.

1.3.1 Endocytic compartments

1.3.1.1 Early endosomes

Internalized vesicles are targeted to form a distinct intracellular compartment called early endosome (EE) (Mellman 1996). This slightly acidic organelle receives material from different internalization routs and serves as a central point for sorting (Gruenberg et al. 1989). EEs show a complex morphology. They are composed of big vacuolar structures (~400 nm diameter) with many tubulated membranes extending from them (~60 nm diameter) (Gruenberg 2001). While the material in the vesicular compartment will be targeted for degradation, tubulation of EE is associated with protein and lipid recycling back to the plasma membrane (Jean

Gruenberg 2001; Mellman 1996). This sorting mechanism is very important for internalized receptors bound to their ligands. Most of the ligands undergo degradation, while receptors are recycled back to the plasma membrane for the next round of signalling and endocytosis (Bleil and Bretscher 1982). The acidic part of EEs facilitate the dissociation of receptor-ligand complexes (Dautry-Varsat, Ciechanover, and Lodish 1983).

1.3.1.2 Recycling endosomes

Detailed morphological and kinetic analysis argues that there are two major recycling pathways acting in mammalian cell culture. Recycling can take place either directly from the early endosomes (fast route) or through the recycling endosomes (slow route) (van der Sluijs et al. 1992; Sönnichsen et al. 2000). Recycling endosome (RE) is a tubulated organelle associated with microtubules (Yamashiro et al. 1984) . Similar to the EEs, the sorting mechanism targeting cargo to the PM is based on the geometry of the compartment rather than specific sorting proteins. Nevertheless, sorting proteins are present on the RE, but their function is to target the cargo through the retrograde transport to the trans-Golgi network (Seaman 2004; Arighi et al. 2004). In addition, RE has higher pH comparing to the EE (~6.5) (Yamashiro et al. 1984).

1.3.1.3 Late endosomes and lysosomes

Late endosomes (LE) are derived from the vesicular domain of EEs. The lumen of LEs contains ligands decoupled from their receptors as well as proteins and solutes internalized with the fluid phase. LEs have a distinct morphological and biochemical composition from EEs (reviewed in Huotari & Helenius 2011). This leads to a robust degradation of their content. Prior to degradation, receptors targeted to the LE are modified on their cytoplasmic tail by an addition of a small protein called ubiquitin (Hicke and Riezman 1996; Hershkos et al. 1983; Kölling and Hollenberg 1994). Ubiquitinated transmembrane proteins induce formation of

intraluminal vesicles (Levkowitz et al. 1998; P. S. Lee et al. 1999). This process is required to down-regulate receptor signalling by cutting off the access for the receptor to the cytoplasm (Felder et al. 1990). An additional role for the formation of the intraluminal vesicles is to expose the receptors to the acidic hydrolases present in the lumen (Futter et al. 1996). Activity of these degradative enzymes is dependent on a low pH (~4.9 - 6.0) that is maintained within LE.

Degradative endocytic pathway ends in the lysosomes. While most of the components of LEs will be degraded by fusion with lysosomes, some will contribute to the generation and maintenance of the new lysosomes (reviewed in Luzio et al. 2007).

It is worth noting that polarized cells have developed a system to segregate apical and basal endocytic machineries. Such separation of endocytic machineries has been studied in the polarized MDCK (Madin-Darby Canine Kidney) cells. The apical surface of MDCK cells is in contact with lumen, while the basolateral membrane interacts with the basement membrane. For this reason the polarized epithelium requires proper sorting and positioning of different apical and basal membrane components. In MDCK cells endocytic compartments originating from the apical and the basolateral PM are segregated and are not prone to heterotypic fusion (S. M. Leung et al. 2000; Bucci et al. 1994). Rather they reside close to the source of internalization. Endocytosed materials from the apical and the basolatral compartments can transcytose, be recycled back to the apical PM or be degraded (Leonid and Mostov 1994; Casanova, Apodaca, and Mostov 1991). This way endocytosis can be fine tuned to the requirements of the cell to sort properly its cargo and adds another level of complexity to the endocytic routes.

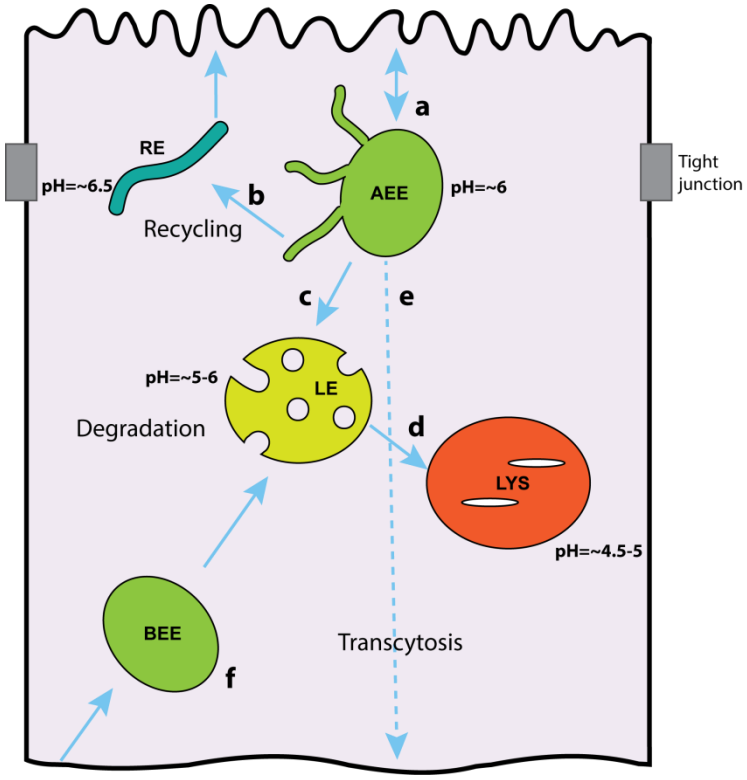

Figure 1.2 Organization of endocytic pathways in polarized cells.
In polarized cells such as MDCK cells the early endocytic machinery is divided into the apical and the basolateral groups that do not intermix. Apically internalized cargo (a) can be recycled through recycling endosomes (b), undergo degradation (c-d) or be transcytosed to the basolateral membrane (d). Fluid uptaken from the basolateral membrane (f) usually is targeted for degradation.
AEE = apical early endosome; BEE = basolateral early endosome; RE = recycling endosome; LE = late endosome; LYS = lysosome.

1.3.2 Pathways of endocytic entry

As mentioned in the previous chapter, endocytosis is characterized by de novo formation of intracellular vesicles from the plasma membrane. There are numerous forms of endocytosis that can be schematically divided in two groups: a clathrin-mediated and non clathrin-mediated endocytosis. The second group is composed of many pathways including caveolae-mediated endocytosis, macropinocytosis, phagocytosis and others. Although clathrin-mediated endocytosis is the best understood pathway, it accounts for less than 50 percent of ingested fluid

by the cell (Schnatwinkel et al. 2004; Lundmark et al. 2008). In next chapters I will describe the molecular mechanisms of different endocytic pathways that operate at the plasma membrane.

1.3.2.1 Clathrin-mediated endocytosis

Most of the work has focused on clathrin-mediated endocytosis (CME), therefore it is one of the most understood pathways. CME is present in every eukaryotic cell and is defined by uptake of extracellular material by clathrin-coated vesicles (CCV) (Y.-W. Liu, Su, and Schmid 2012). Formation of CCV can be described in five stages based on ultrastructural and live-imaging studies (Kukulski et al. 2012; Taylor et al. 2011; reviewed in Harvey T McMahon & Emmanuel Boucrot 2011)

In the first step of CME a membrane invagination is formed (Figure 1.3 a). This involves assembly of the protein complex (so called nucleation module) at the plasma membrane. The protein complex is composed of the FCH domain only (FCHO) proteins, the EGFR pathway substrate 15 (EPS15) and the intersectins (Henne and Boucrot 2010; Reider et al. 2009; Stimpson and Toret 2009). A common feature of these proteins is their affinity to the lipid phosphatidylinositol-4,5-bisphosphate (PtdIns(4,5)P2) present at the plasma membrane (Stimpson and Toret 2009; Henne and Boucrot 2010).

In the next step, this nucleation module recruits a conserved Adaptor Protein 2 (AP2) to the membrane (Figure 1.3 b). AP2 binds both to PtdIns(4,5)P2 and the cargo (Collins et al. 2002; Kelly et al. 2008). In fact AP2 interacts with the cargo by directly binding to the cytoplasmic residues of the receptors or indirectly through additional accessory adaptor proteins (reviewed in Traub 2009). Cargo packaging is a highly redundant system operating with high fidelity. This is ensured by the overlapping functions of many of adaptor and accessory proteins. These protein interactions are also responsible for the generation of membrane curvature during vesicle formation irrespective of the cargo type (M. G. Ford et al. 2001; M. G. Ford et al. 2002). The function of AP2 at the PM is to recruit clathrin triskeleta from the cytoplasm to the vesicle assembly site (Ehrlich et al. 2004; Boucrot et al. 2010) (Figure 1.3 c). This step is necessary for the stabilization of the forming vesicle and recruitment of curvature

generators like epsin and EPS15 (epidermal growth factor receptor pathway substrate 15) at the neck of the invaginating membrane (H. Chen et al. 1999; H. Chen et al. 1998; Ehrlich et al. 2004). Once the clathrin cage is assembled, dynamin is recruited by the endophilin and the SNX9 (sortin nexin 9) at the base of the pinching vesicle (Sundborger et al. 2011; Lundmark and Carlsson 2003). Dynamin is a mechanochemical GTP-ase that changes its conformation upon nucleotide hydrolysis, that results in vesicle fission (Figure 1.3 d) (the function of dynamin is discussed in Chapter 1.3.3.4) (Sweitzer and Hinshaw 1998). Impairing dynamin activity causes an arrest in vesicle formation at either the clathrin assembly stage or scission (Kosaka and Ikeda 1983).

Once the vesicle pinches off, the clathrin coat is disassembled by the ATP-ase HSC70 (heatshock cognate 70), and its cofactor, auxilin (Figure 1.3 e) (Ungewickell and Ungewickell 1995; Schlossman et al. 1984). This step is necessary for the fusion of vesicles with early endosomes. The clathrin complex is then reused to form new vesicles. A schematic view of the CCV formation is presented on the Figure 1.3, and the key proteins involved in the vesicle formation are listed in the Table 1.1

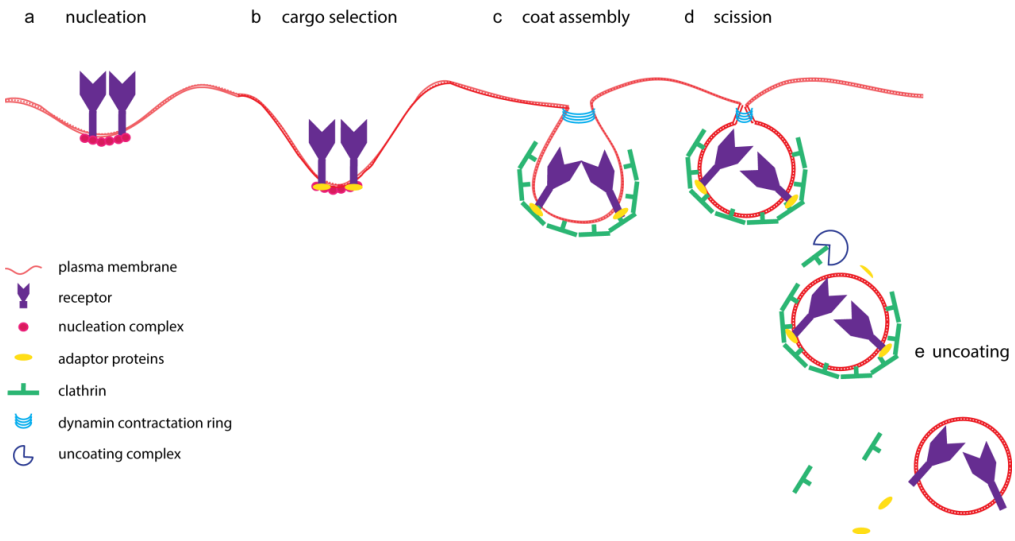

Figure 1.3 Clathrin-mediated endocytosis.

The five steps underlying the formation of clathrin coated vesicles are illustrated. See Chapter 1.3.2.1 for detailed information

Protein	*Drosophila* homologue	Function
Clathrin	Chc, Clc	composed of three heavy and three light chains that form the clathrin triskelion
FCHO	CG8176	nucleates clathrin-coated pits and generates the initial membrane curvature
AP2	α-Adaptin, Bap, AP-50, AP-2σ	a heterotetrameric adaptor complex (α-, β2, μ2 and σ2 subunits) that links membrane cargo to clathrin and accessory proteins
EPS15	Eps-15	AP2 clustering and scaffolding protein
Intersectin	Dap160	links various components of the clathrin machinery
Epsin	lqf	a cargo-specific adaptor for monoubiquitylated receptors
Amphiphysin	Amph	bends the membrane and recruits dynamin to clathrin-coated pits
Sorting nexin 9	SH3PX1	binds AP2 and dynamin
Dynamin	shi	triggers vesicle scission upon GTP hydrolysis
Auxillin	aux	recruits HSC70 to clathrin cages for uncoating
HSC70	HSC70-4	ATPase triggering uncoating of clathrin cages

Table 1.1 Major components of the CME and their function.

Table was adapted and modified from (McMahon and Boucrot 2011).

1.3.2.2 Caveolae- and lipid raft mediated endocytosis

Caveolae-mediated endocytosis involves the formation of large vacuolar carrier at the apical surface of epithelial cells (Yamada 1955). This endocytic process is dependent on lipid rafts, low-density detergent insoluble membrane domains that are enriched in cholesterol and sphingolipids (reviewed in Lingwood & Simons 2010). These endocytic sites are marked by the presence of a protein named Caveolin (Cav) (Rothberg et al. 1992). Although many cell types do not express Cav, ultrastructural studies have shown that caveolar-like structures can also form in the absence of Caveolin (Mirre and Monlauzeur 1996). Thus it seems that Caveolin plays a facilitating role in formation of 30-70 nm flask-shaped membrane invaginations that are then budding from the PM in a dynamin dependant manner (Henley et al. 1998; Oh, McIntosh, and Schnitzer 1998). Caveolae formation is initiated by local disruption of the actin cytoskeleton in response to

either extracellular cues (e.g. SV40 virus internalization) or by endogenous regulators (albumin internalization) (Pelkmans, Kartenbeck, and Helenius 2001; Bento-Abreu et al. 2009; Y. Chen and Norkin 1999). Caveolae-mediated endocytosis might be important for regulation of signalling events by sequestering receptors or by promoting distinct signalling cascades than CME (Kong, Hasbi, and Mattocks 2007; Saldanha et al. 2012).

So far there is no evidence for caveolae formation in *Drosophila*. Although caveolae-mediated endocytosis received much attention in the recent years, many details regarding this process are still lacking solid experimental proofs.

1.3.2.3 CLIC/GEEC mediated endocytosis

Electron microscopy studies have shown the existence of tubulo-vesicular pinocytic structures that do not contain clathrin, and have been named clathrin independent carriers (CLIC). These intracellular tubes are also not associated with Caveolin (Kirkham et al. 2005; Lundmark et al. 2008). It has been shown that CLICs are required for the internalization of bulk fluid, bacterial exotoxins as well as Glycosyl-phosphatidylinositol (GPI)-anchored proteins (GPI-AP) (Kirkham et al. 2005). GPI-AP are enriched within cholesterol domains of the PM and their internalization leads to the formation of distinct GPI-enriched endosomal compartments (GEEC) (Kirkham et al. 2005). This endocytic pathway accounts for almost 50% of all fluid phase internalization in cultured mammalian cells (Lundmark et al. 2008). Moreover, recent studies suggest an important role of CLIC/GEEC endocytic pathway in turnover of adhesion components and regulation of cell migration (G. J. Doherty et al. 2011; Howes et al. 2010). In addition, this endocytic pathway has been linked to the proper myoblast differentiation and fusion in the Xenopus embryo (J. T. Doherty et al. 2011).

A major regulator of this pathway is the Cdc42 (cell division control protein 42 homolog), a small GTP-ase that controls actin polymerization (Nobes and Hall 1995). Indeed, disruption of Cdc42 activity results in the depletion of CLICs (Sabharanjak et al. 2002). Actin polymerization by Cdc42 is directly linked with formation of tubular vesicles through GRAF1 (GTPase regulator associated with focal adhesion kinase 1). The N-terminal BAR (Bin–Amphipysin–Rvs) domain of GRAF1 generates membrane

curvature, the GAP (GTP-ase Activating Protein) domain exhibits GAP activity on Cdc42 (Lundmark et al. 2008). Moreover, GRAF1 can directly bind to dynamin, although scission CLIC tubes from the plasma membrane seems dynamin independent (Lundmark et al. 2008). It has been proposed that the activity of the dynamin might be important for the post-processing of the CLICs. CLIC/GEEC pathway has been also shown to be present in *Drosophila* (Gupta et al. 2009).

1.3.2.4 Phagocytosis

Phagocytosis and macropinocytosis represent endocytic pathways that are internalizing large volume of cargo (reviewed in Groves et al. 2008). Particles larger than 1 μm, like microbes and apoptotic cells are uptaken by the cells through phagocytosis. This process is conserved from amoeba to vertebrate and in single cell organisms it is the major pathway to internalize nutrients from the extracellular environment. Multicellular organisms adapted this pathway for clearance of apoptotic cells during development as well as to protect the organism from invading pathogens (Franc et. al 1999).

Phagocytosis begins upon binding of large particles to specific receptor on the cell surface. The most conserved receptor initiating phagocytosis is the lectin receptor that binds carbohydrate residues present on the surface of bacteria. Cells of the immune system express a variety of other receptors that recognize opsonized microbes, like Fc (fragment crystallisable) complement or scavenger receptors. All of these receptors activate a signalling cascade leading to actin reorganization and particle engulfment (Sánchez-Mejorada and Rosales 1998; Caron and Hall 1998; Maniak et al. 1995; Zigmond and Hirsch 1972; Groves et al. 2008).

Formation of phagosomes require large surface of membrane. For example, macrophages are able to internalize membranes equivalent to their entire cell surface in only 30 minutes (Mellman, Plutner, and Ukkonen 1984; Michl and Unkeless 1983). This high rate of turnover is hallmarked by the delivery of new membranes via RE (Cox et al. 2000). Increased surface in combination with actin cytoskeleton reorganization leads to the internalization of microbes or apoptotic cells. Next, a fully formed phagosome fuses with early endosomes, and is finally delivered to lysosome (Duclos et al. 2000;

Blanchette et al. 2009). This maturation process is necessary for the degradation of the phagosomal content. Phagocytosis have also a crucial role in the generation of adaptive immunity reviewed in Jutras & Michel Desjardins 2005.

1.3.2.5 Macropinocytosis

Macropinocytosis is a nonselective route for the uptake of big amounts of solutes. It can be constitutive or induced by variety of growth factors. In fact little is known about the molecular mechanisms underlying macropinsome formation and maturation (Bar-Sagi et al. 1987; reviewed in Swanson 2008; Mercer & Helenius 2009). Macropinosomes are 200 nm - 3000 nm vacuoles internalized upon ruffling of the plasma membrane. This dynamic morphological change of the PM is induced by the receptor tyrosine kinsases, that activate the Rac1 (ras-related C3 botulinum toxin substrate 1) and the Cdc42 GTP-ases (Ridley et al. 1992; Garrett et al. 2000). Both the Rac1 and Cdc42 activate PAK1 (p21-activated Kinase-1), which in turn regulates actin dynamics and formation of ruffles at the plasma membrane (Edwards et al. 1999). PAK1 targets include also Dynein light chain, a component of microtubule motor complex (Vadlamudi et al. 2004). Dynein has been shown to be regulated during the first steps of pinosome formation (Yang, Vadlamudi, and Kumar 2005). Furthermore, up-regulation of Sorting nexin 5 (SNX5) stimulates macropinocytosis (Lim et al. 2008; Wang et al. 2010). SNX5 is a BAR domain and a PX domain containing protein, that is targeted to the endosomes through binding to the phosphatidylinositol 3-phosphate (PtdIns(3)P) (Worby and Dixon 2002). SNX5 localizes to the early endosomes and macropinosomes and is involved in the maturation of the macropinosomes by inducing early tubulation of the vacuolar membrane (Kerr 2006). Similar to the EE, tubulation might be involved in the segregation of the cargo into subcompartments. However, instead recycling to the PM it cargo is delivered to the TGN (trans-Golgi network) (Kerr 2006; Jing Zhang et al. 2012).

Maturation of macropinosomes is relatively fast. In the EGF (Epidermal Growth Factor) activated macrophages just 3-4 minutes after internalization vacuoles are enriched in late endosome and lysosomal markers (Racoosin and Swanson 1993; Kerr 2006).

1.3.3 Regulators of endocytosis

In next chapters I will describe major regulators of endocytosis. I will focus first on actin, and then I will describe some of the proteins involved in vesicle fusion and scission as well as general regulatory machineries present on endocytic membranes.

1.3.3.1 Actin

Actin is a necessary component of the endocytic process. For instance in yeast and plant cells CME sites are marked by an accumulation of actin and disruption of actin nucleation regulates in an immediate block of endocytosis (Kübler and Riezman 1993). Moreover, actin polymerization provides sufficient force for bending the plasma membrane. For example, after the initial deformation of a clathrin coated pit (check Chapter 1.3.2.1) actin drives its elongation and assists scission of the vesicle. This is crucial in both, yeast and plant cells as the intracellular pressure (turgor) in these cells is relatively high and exerts a constant tension at the PM (Aghamohammadzadeh and Ayscough 2009). Moreover, in yeast force generated on the PM by actin is sufficient for budding of CCVs (Kaksonen, Toret, and Drubin 2005; Chu, Pishvaee, and Payne 1996; Payne et al. 1988).

In mammalian cells actin is recruited to the sites of CCVs formation, however there are some differences. For instance, mammalian cells have relatively low turgor and the force generated by actin to form a vesicle is not obligatory (Fujimoto et al. 2000). However, actin was shown to be essential for CCV formation in the experiments where artificial increase of rigidity of the plasma membrane was generated (Boulant et al. 2011; Saffarian, Cocucci, and Kirchhausen 2009; A. P. Liu et al. 2009). Similarly to these experiments, mammalian cells do undergo increased PM tension during morphogenesis. For example, cortical accumulation of filamentous actin (F-actin) at focal adhesions and junctions generate force at the PM (reviewed in Lecuit et al. 2011). Although in these cellular domains CME is less abundant, vesicles that are formed are dependent on actin nucleation (Levayer, Pelissier-Monier, and Lecuit 2011). In contrast to yeast, force

generated by actin in mammalian cells is insufficient for the scission of the CCV and is generated by dynamin (Marks et al. 2001) (Chapter 1.3.3.4).

Actin dynamics is also involved in clathrin-independent endocytosis. Formation of large invaginations at the PM such as phagosomes and macropinosomes is dependent on actin remodelling (Mercer and Helenius 2009). For instance during the uptake of opsonized particles, actin surrounds the outer layer of the pinocytic cup (Coppolino et al. 2001). This allows the large cargo to be completely surrounded by the PM and to be subsequently internalized. Similar actin structures are formed during macropinosome formation. Actin branching close to the PM results in formation of membrane ruffles. Upon the collapse of the ruffle on itself a macropinocytic cup is formed, ingesting the extracellular material (Mercer and Helenius 2009).

In addition, studies on Shiga toxin internalization by the lipid raft dependent endocytosis (CLIC) demonstrated a role for actin in the scission of endocytic tubes (Römer et al. 2010). It has been shown that formation of intracellular tubes are stable in the presence of monomeric actin, while polymerization of F-actin drives pinching in a dynamin independent manner (Römer et al. 2010).

Taken together, these data suggest that actin plays an important role in many aspects of vesicle formation and cells are able to utilize the force generated by actin polymerization to counteract PM rigidity and thus facilitate vesicle formation.

1.3.3.2 Tethers and SNARE-s

Transport along endocytic pathways involves recognition and fusion of different endocytic organelles. The first step in this process is mediated by tethering proteins represented by two classes: the multisubunit tethering complexes and the coiled-coil tethers. Coiled-coil tethers are dimeric complexes with two globular head groups connected through a coiled-coil domain (Callaghan, Simonsen, and Gaullier 1999). This class forms long, rod-like structures connecting membranes up to 200 nm apart (Sapperstein et al. 1995; Barr and Short 2003). Coiled-coil tethers are recruited to the specific endocytic compartments via the Rab GTP-ases (Christoforidis, McBride, et al. 1999).

The second class of tethers is represented by the multi-subunit tethering complexes (MTC) bringing together endocytic structures in close proximity. For example, these complexes are important for the maturation of early endosomes into lysosomes (Markgraf, Ahnert, and Arlt 2009; Peplowska et al. 2007). Moreover, MTCs can interact directly with SNARE proteins (Siniossoglou and Pelham 2001; Conibear, Cleck, and Stevens 2003).

SNAREs (soluble NSF attachment protein receptor, where NSF stands for N-ethyl-maleimide-sensitive fusion protein) are the key players in vesicle fusion (reviewed in Ungar & Hughson 2003). Syntaxin-1, SNAP25 (synaptosomal-associated protein 25) and VAMP (vesicle-associated membrane protein) were identified as limiting factors for the fusion of synaptic vesicles (Trimble, Cowan, and Scheller 1988; Oyler et al. 1989; Bennett, Calakos, and Scheller 1992). These three proteins as well as their homologues gave rise to the SNARE hypothesis (Söllner et al. 1993). The hypothesis states that SNAREs are ubiquitous proteins that drive fusion of membranes. Furthermore, these proteins fall into two categories: v-SNAREs associated with vesicle and t-SNAREs present at the target membranes. More adequate classification of SNARE proteins is based on the conserved residues (R-, Qa-, Qb-, Qc-SNARE). In general the R-SNARE corresponds to the v-SNARE and the Q-SNARE to the t-SNARE (Fasshauer et al. 1998).

The function of SNAREs relies on its specific structure. Even though the individual SNARE proteins remain unfolded, when expressed together they are forming a stable four helix structure between two adjacent membranes (the trans-SNARE complex). Formation of the trans-SNARE complex generates an exergonic force responsible for bringing together and fusing two lipid bilayers. This fully zippered SNARE complex is called the cis-SNARE. Afterwards, SNARE proteins are retrieved from the cis- complex by the NSF ATP-ase in cooperation with the adaptor protein SNAP. SNARE proteins are then reused for another round of fusion (Clary, Griff, and Rothman 1990; Ungar and Hughson 2003).

SNAREs are regulated by the Sec1 (syntaxin binding protein 1)/Munc18 (mammalian uncoordinated-18) complex, which has a dual role. First, it binds and stabilizes the closed conformation of syntaxin-1, which inhibits formation of the SNARE

complexes. Second, SM (Sec1/Munc18) acts as a catalyst for the trans-SNARE complex (Carr and Rizo 2010). This dual function of SM proteins is still not fully understood.

In summary, tether molecules and SNAREs are the key regulators of membrane docking and membrane fusion in endocytic pathways.

1.3.3.3 Rab GTP-ases and their effectors

The high fidelity underlying membrane fusion and fission reactions implies that the activity of tethering proteins, SNAREs and actin must be spatially and temporally regulated. This spatial-temporal regulation is provided by guanidine triphosphate hydrolases (GTP-ases) of the Ras-super-family, including Ras (rat sarcoma), Rho, ARF (ADP-ribosylation factor), Sar (secretion-associated ras) and Rabs (ras-related in brain) (reviewed in Wennerberg et al. 2005).

Rab GTP-ases are the largest group of the Ras-like family and consist of over 60 members in human and 31 in *Drosophila* (Pereira-Leal and Seabra 2001; Jun Zhang et al. 2007). The different family members display a high degree of homology in their amino-acid sequence, especially in the region responsible for the GTP binding and hydrolysis (Pfeffer 2005). However, each member of this family localizes to specific intracellular compartment where it exerts its function (reviewed M Zerial & H. McBride 2001). Rab proteins function as a ‚molecular switches' meaning that they occupy two different conformational states, a GTP bound (referred as active) and a GDP bound (referred as inactive) (M.-T. G. Lee, Mishra, and Lambright 2009). Active Rabs act through their effectors (i.e. proteins preferentially binding to the active form), which control vesicle formation, motility, tethering and fusion. Importantly there is a distinct set of effectors for each Rab-pathway (Zerial and McBride 2001).

The life cycle of Rab proteins has been extensively studied. Upon translation, Rab proteins are bound by the Rab escort protein (REP) that transfers them to the Rab geranylgeranyl transferase (RabGGT) (Alexandrov et al. 1994) (Figure 1.4 a). RabGGT is an enzyme that adds a single or two geranylgeranyl lipid groups to the cysteins in the CAAX boxes close to the C-terminus of the Rab protein (Figure 1.4 b) (Farnsworth et al. 1994). Following this reaction, GDP bound Rab is delivered to its target organelle

(Figure 1.4 c). This targeting depends on approximately 40 amino acids (usually referred to as the hyper-variable region) upstream of the CAXX box (Chavrier, Gorvel, and Stelzer 1991). Upon binding to the membrane, GDP is exchanged to GTP by guanine nucleotide exchange factors (GEF) (Figure 1.4 d). GTP hydrolysis is catalysed by GTP-ase activating proteins (GAP) (GEFs and GAPs are reviewed in Bos et al. 2007). Following GTP hydrolysis, Rab is extracted from the membrane by RabGDI (GDP-dissociation inhibitor) (Figure 1.4 e) (Luan et al. 1999). This cascade is important for the maturation of endocytic compartments as Rab proteins are progressively exchanged one by the other along the pathway (Rink et al. 2005).

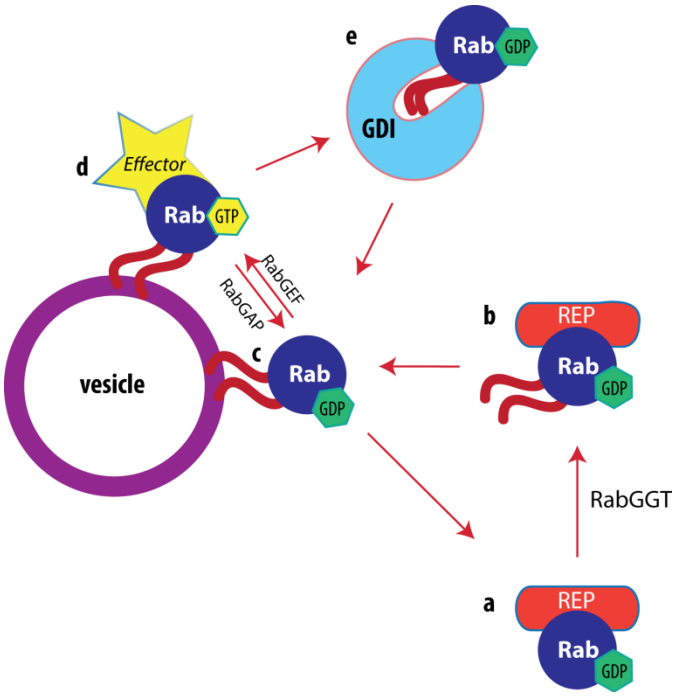

Figure 1.4 Rab GTP-ases membrane cycle.

Schematic view of the proteins that regulate the localization and activity of Rab. For detailed description, see Chapter 1.1.3.3

1.3.3.3a Rab5

One of the best-characterized GTP-ases in the endocytic pathway is Rab5. Rab5 controls both CCVs formation as well as early endosome biogenesis. It is involved in the uncoating of CCVs and their fusion with EEs. In addition, Rab5 controls EE motility, tethering, fusion and actin remodeling (Zerial and McBride 2001). Over-expression of the GTP-ase deficient Rab5 (active form) induces the formation of enlarged endosomes (Roberts et al. 1999), while knock-down of Rab5 results in loss of early and late endosomal compartments (Zeigerer et al. 2012).

Rab5 regulates a vast network of effectors and controls the production of PtdIns(3)P on early endosmal membranes. PtdIns(3)P is an important regulator of early endosome function and is generated by two Rab5 effectors, the hVps34 (vacuolar protein sorting 34) kinase and the PI3Kβ (phosphoinositide 3-kinase beta) (Christoforidis, Miaczynska, et al. 1999). hVps34 can directly generate PtdIns(3)P from PtdIns on the early endosome while PI3Kβ function is restricted to the PM (Simonsen, Lippe, and Christoforidis 1998; Christoforidis, Miaczynska, et al. 1999). Upon stimulation by signalling factors and in cooperation with a chain of phosphatases, PI3Kβ converts PtdIns(4,5)P2 into PtdIns(3)P (Shin et al. 2005). Local increase in PtdIns(3)P facilitates the recruitment of other Rab5 effectors containing a conserved protein motif (FYVE finger domain) that binds specifically to PtdIns(3)P (Kutateladze et al. 1999). For example, EEA1 and Rabenosin-5 are Rab5 effectors containing FYVE domain responsible for the homotypic fusion and maturation of the endocytic compartment (Nielsen et al. 2000; Gaullier et al. 2000). EEA1 (early endosome antigen 1) is a tethering protein that additionally binds to the syntaxin-6 (a SNARE), therefore enabling vesicle fusion (McBride et al. 1999). Another Rab5 effector is Rabaptin-5, a coiled-coil protein necessary for the homotypic fusion between early endosomes (Stenmark et al. 1995). In addition, Rabaptin-5 interacts also with Rab4, a GTP-ase presents on the tubular sub-domain of EEs and whose function has been linked to recycling back to the PM (Vitale et al. 1998; Sönnichsen et al. 2000). Thus Rabaptin-5 coordinates entry in and exit out of EEs.

As mentioned above, Rab5 is involved also in the removal of the AP2 coat from CCVs. AP2 is a multi-subunit adaptor protein linking clathrin with cargo and other adaptor proteins. While the clathrin coat is removed by the combined action of the Hsc70 and the auxilin, AP2 removal is controlled by the Rab5 GAP, RME-6 (Rab5-activating protein 6). RME-6 competes for the binding of the adaptor-associated protein kinase 1 (AAK1) with the μ2 subunit of the AP2 complex and thus facilitates μ2 dephosphorylation. In addition, Rab5 mediates also the reduction of PtdIns(4,5)P2 levels on the vesicle. This in turn facilitates uncoating as AP2 binding to membranes is PtdIns(4,5)P2-dependent (Sato et al. 2005; Semerdjieva et al. 2008).

Rab5 controls also the motility of EEs. Endosome motility is important for both their intracellular localization as well as for their maturation into late endosomes. Early endosomes move in two fashions, on long routs by binding to microtubules and on short routes by binding to actin. Microtubule movement of EEs is bidirectional with a preference for the minus-end direction. This movement is dependent on the function of the hVps34 that generates PtdIns(3)P and allows the recruitment of KIF16B (kinesin family member 16B), a plus end directed motor containing a FYVE finger domain (Hoepfner et al. 2005). To date there are no details about the Rab5 effectors regulating the minus end movement of endosomes on microtubules. A second type of movement of EEs is driven by actin. This type of endosome motility is regulated by the huntingtin/HAP40 (huntingtin-associated protein 40) complex that binds directly to Rab5. Huntingtin is responsible for the switch of the EE from the microtubule to the actin cytoskeletons, and over-expression of HAP40 leads do a significant decrease in movement of the Rab5-positive vesicles (Pal et al. 2006).

Rab5 is very important also for the regulation of clathrin independent pathways. For instance, Rab5 colocalizes and regulates membrane ruffles that are involved in the formation of macropinosome (Chapter 1.3.2.5). Membrane dynamics during macropinocytosis is regulated by RN-tre (USP6 N-terminal like protein), which acts both as a GAP and as an effector for Rab5. RN-tre interacts with actin and the actin cross-linker, actinin-4. Rab5, actin and actinin-4 together induce formation of membrane ruffles (Lanzetti et.al 2004).

1.3.3.3b Rabankyrin-5

Another Rab5 effector involved in apical endocytosis and macropinocytosis is Rabankyrin-5. Rabankyrin-5 was identified as a 130kDa effector of Rab5 and is expressed in many tissues throughout mouse development (Ito et al. 1999). It consists of a BTB (BR-C, ttk and bab) domain responsible for homo- and heterodimerization, 21 ankyrin repeats and a C-terminal FYVE finger domain (Schnatwinkel et al. 2004; Ito et al. 1999). Endogenous Rabankyrin-5 binds to the EEA1 positive endosomes and associates to newly formed macropinosomes. Association to these organelles is dependent on the FYVE domain as well as on other unidentified part of the protein. Importantly, knock down of Rabankyrin-5 reduces fluid phase uptake in NIH3T3 cells while its over-expression has a positive stimulus on this process. In addition, over-expression of Rabankyrin-5 in polarized MDCK cells induces specifically apical endocytosis. Moreover, Rabankyrin-5 is necessary for the homotypic fusion between EEs but not for the fusion between CCVs and the EEs (Schnatwinkel et al. 2004). In summary, Rabankyrin-5 is a Rab5 effector that controls both apical endocytosis and macropinocytosis and its function will be further described in the results section.

1.3.3.4 Dynamin

Dynamin is a large GTP-ase involved in vesicle fission and was first identified in *Drosophila* as the gene coding for shibire, a gene whose temperature sensitive allele resulted in muscle paralysis (Suzuki et. al 1971; Kosaka and Ikeda 1983). In *Drosophila* and *C. elegans* dynamin is coded by a single gene while in mammals there are 3 isoforms that have distinct tissue expression patterns (Cao, Garcia, and McNiven 1998; Raimondi et al. 2011). This differential localization suggests that in mammals specific isoforms have evolved to fulfil the needs of different tissues. Structurally dynamin is composed of an N-terminal GTP-ase domain, an effector binding domain, a PH (pleckstrin homology) domain with affinity for PtdIns(4,5)P2, and a C-terminal SH3 (src homology 3) domain binding to actin regulatory partners (Muhlberg, Warnock, and Schmid 1997).

As oppose to the other GTP-ases like Rab proteins, dynamin has low affinity for nucleotide binding. Therefore GAPs and GEFs are not necessary for the stability of the GTP in its binding pocket (Sever, Muhlberg, and Schmid 1999). Upon binding to GTP, dynamin self-polymerizes instead of interacting with down-stream effectors as it is the case for Ras-like small GTP-ases (Hinshaw and Schmid 1995, Warnock et. al 1996). Dynamin polymers form a helix around the neck of the forming CCV and thus facilitate vesicle scission (Takei, Schmid, and Camilli 1995). In vitro dynamin can polymerize spontaneously around synthetic liposomes and other tubular matrix through its curvature-sensing domain (Roux et al. 2006; Hinshaw and Schmid 1995). However, in vivo membrane curvature is generated by BAR domain containing proteins like amphiphysin, which facilitates the recruitment of dynamin to the neck of the pinching vesicle (Ferguson et al. 2009; Grabs et al. 1997). The main function of dynamin (generation of force on the membrane) is dependent on GTP hydrolysis (Takei, Schmid, and Camilli 1995). Hydrolysis generates change in conformation of dynamin propagated along the helix that results in squeezing of the membrane and pinching of the vesicle (Chappie et al. 2011). Therefore, mutants of dynamin characterized by their inability to hydrolyze GTP, result in the arrest of clathrin dependent endocytosis. Ultrastructural analysis of such mutants shows elongated intracellular membranes covered with dynamin helix unable to pinch off from the PM (Kosaka and Ikeda 1983; Takei, Schmid, and Camilli 1995).

Initial studies on dynamin function in *Drosophila* showed that dynamin mutants are characterized by impaired axon growth (Murphey 2003). This led to the hypothesis that dynamin might be involved in the regulation of actin cytoskeleton. Indeed dynamin was shown to bind directly to actin bundles though its effector binding domain or indirectly through the association of its SH3 domain with other actin regulators (reviewed in S. M. Ferguson & Pietro De Camilli 2012). This association with actin might be important for the generation of actin driven plasma membrane morphological changes. For example, blocking dynamin activity alters formation of phagocytic cups, invadopodia and podosomes (Gold et al. 1999; Ochoa et al. 2000; Baldassarre et al. 2003). In T-cell, dynamin has been shown to interact with the RhoGEF, and this interaction contributes to the reorganization of actin at the immunological synapse (Miletic et al. 2009). The impact

of dynamin on actin organization suggests that this GTP-ase plays important in cell physiology in addition to endocytosis

1.4 Endocytosis-dependent regulation of developmental processes

Endocytosis regulates many developmental processes including tissue patterning (by regulating cell signaling), maintenance of cell adhesion and establishment of cell polarity. Below I will describe three examples of how endocytosis controls development at the tissue and organismal level. I will describe the impact of endocytosis on morphogen gradient formation, on the regulation of signalling between neighbouring cells (Notch pathway) and on cytokinesis. In the last chapter I will focus on endocytic events taking place during cellularization in *Drosophila* embryo.

1.4.1 Endocytosis in morphogen gradient formation

In a developing multicellular organism differentiating cells acquire positional information through secreted proteins called morphogens. Morphogen molecules are secreted from a group of signalling cells and form a concentration gradient, which is interpreted by receiving cells in a concentration-dependent manner. For example, Hedgehog (Hh), Wingless (Wg) and Decapentaplegic (Dpp) are three important morphogens controlling tissue patterning and whose gradient formation requires endocytosis (reviewed in Tabata & Y. Takei 2004). In general, there are two main hypotheses that attempt to explain the establishment and stability of these concentration gradients.

In the planar transcytosis hypothesis, morphogens are uptaken by the receptor-mediated endocytosis by cells close to the source and then secreted further. This would involve formation of endosomes able to transcytose their content across opposite lateral membranes. By multiple rounds of endocytosis and secretion a gradient would be formed. Support to this hypothesis came from studies aimed at understanding how the Dpp gradient forms in the imaginal wing disk of *Drosophila*. It has been shown that

blocking endocytosis in clone of cells limits the spreading of Dpp behind the clone (Entchev, Schwabedissen, and González-Gaitán 2000; Kicheva et al. 2007).

However, analysis of Wg distribution revealed that dynamin dependent endocytosis is not necessary to generate a stable gradient for this particular morphogen (Strigini and Cohen 2000). In contrast, ECM (extracellular matrix) components, especially heparan sulfate proteoglycans (HSPGs) and lipoproteins associated with them, are responsible for proper gradient formation (Esko and Selleck 2002; Nakato, Futch, and Selleck 1995; Baeg et al. 2001). This led to the restricted diffusion hypothesis, where morphogens are immobilized by binding to the HSPGs. According to this hypothesis, endocytosis controls only the internalization and degradation of the morphogen and contributes only indirectly to the formation of the gradient. For example, endocytosis and lysosomal degradation of Hh, via binding to its receptor Patched, limits the spreading of this morphogen (Callejo, Culi, and Guerrero 2008; Torroja, Gorfinkiel, and Guerrero 2004). It is very likely that these two hypotheses are not mutually exclusive and that both endocytosis and ECM components together shape morphogen gradients during tissue patterning.

1.4.2 Endocytic-regulation of Notch signaling

Another example showing the importance of endocytosis in cell signalling during development is represented by the Delta/Notch signalling pathway. The Notch pathway is involved in developmental processes such as limb formation in mammals, wing patterning in *Drosophila*, specification of mesoectoderm and neurons in the early *Drosophila* embryo (Pan et al. 2005; Baonza and Garcia-Bellido 2000; De Renzis et al. 2006). This signalling pathway is initiated by the interaction between two transmembrane proteins, the Notch receptor and its ligand Delta/Serrate/Lag2 . In contrast to morphogen gradient this interaction occurs between two neighboring cells and is therefore a short-distance signalling system (reviewed in Bray 2006).

After the initial interaction with the transmembrane ligand, Notch undergoes two sequential cleavage events. First, an extracellular part of the receptor NECD (Notch extracellular domain) bound to the DSL is digested and subsequently an intracellular part

of Notch (NICD) is cleaved off. NICD then shuttles to the nucleus and acts as a transcription factor (Bray 2006).

For proper signalling both the activated receptor and the ligand must undergo endocytosis (Parks et al. 2000). The second event is quite surprising since Delta endocytosis takes place in the signalling-sending cell. Recent studies in *Drosophila* proposed a new hypothesis that can explain this phenomenon. Because the interaction of Notch and Delta happens between two cells, it is possible that the internalization of Delta induces a pulling force on Notch (Parks et al. 2000; Meloty-Kapella et al. 2012). This would uncover the extracellular cleavage site of Notch leading to Notch processing and signalling in the receiving cell. In addition, Delta molecules might need to be activated in an endocytic compartment in order to interact with Notch. This hypothesis is based on the fact that Delta is ubiquitinated by the E3 ligase Neuralized (Deblandre et al. 2001; Emery et al. 2005). In general, ubiqiunated transmembrane proteins are internalized from the PM and delivered to endosomes (reviewed in Polo 2012). Trafficking of Delta through an endocytic compartment might lead to its activation. In addition, the amount of Delta at the PM might be important for a stoichiometric balance between ligand and receptor on the surface of signalling and receiving cells (Lyman and Yedvobnick 1995; Fanto and Mlodzik 1999).

As mentioned before internalization of Notch is necessary to complete signalling. So far it is not known whether the intracellular part of Notch is cleaved at the PM or in an endocytic compartment. Studies on ESCRTI/II (endosomal sorting complex required for transport) mutants suggest that cleavage might take place on the endosomal surface. Blocking the ESCRT complexes, a key component of multivesicular body formation, leads to the hyperactivation of Notch signalling (Vaccari et al. 2009). This result suggests that the internalization of Notch into multivesicular body limits the amount of Notch molecules that can be processed on the limiting membrane of endosomes.

The mechanisms controlling Notch and Delta internalization have been extensively studied in the early *Drosophila* embryo. During cellularization, Delta and Notch are specifically internalized in presumptive mesodermal cells. This trafficking pathway is regulated by Neuralized whose activity is restricted to mesodermal cells by a family of small peptides, the bearded proteins that are specifically expressed outside of

the mesodermal primordium (De Renzis et al. 2006; Bardin and Schweisguth 2006). Given that Bearded proteins inhibit Neuralized they also block Delta endocytosis (De Renzis et al. 2006; Bardin and Schweisguth 2006). As a result, signalling between Notch and Delta can occur only between the cells at the mesoderm border that act as a donor for the ligand and the cells adjacent to the mesoderm that receive the signal. This leads to the activation of Notch in a single stripe of cells, the mesoectoderm that will give rise to the nervous system at the later stages of development (Martín-Bermudo, Carmena, and Jiménez 1995; De Renzis et al. 2006; Bardin and Schweisguth 2006).

In summary, formation of morphogen gradients and Notch signaling clearly demonstrate the importance of endocytosis in controlling tissue patterning.

1.4.3 Endocytosis during cytokinesis

The first experimental observation suggesting that endocytosis plays a role in cytokinesis comes from the discovery that the cell volume is rapidly decreasing before cell division (Boucrot and Kirchhausen 2007). This is due to an increase in chlorine ion efflux from the cells (Russell 2000). At the same time the surface of the PM is reduced leading to an accumulation of endocytic vesicles that are then redistributed to the cleavage furrow (Horgan et al. 2004). Indeed, during cytokinesis the site of new membrane insertion is at the cleavage furrow (Shuster and Burgess 2002; Goss and Toomre 2008). This membrane redistribution requires trafficking through recycling endosomes. In fact, studies on spermatocyte division in *Drosophila* revealed a role of Arf6, Rab11 and Rab4, three regulators of the endocytic-recycling pathway in this process (Giansanti et al. 2007; Dyer et al. 2007). Arf6 belongs to the same super-family of small GTP-ases as Rab proteins and it has been shown to be important for the rapid addition of membranes to the cleavage furrow in dividing spermatocytes (Dyer et al. 2007; Schweitzer, Sedgwick, and D'Souza-Schorey 2011). Furthermore, mutations in this gene result in the formation of multinucleated cells. Additionally, *Drosophila* Rab11 mutants show a similar phenotype to Arf6 mutant flies, suggesting that membrane recycling is necessary for the addition of new membrane to the cleavage furrow (Giansanti et al. 2007). Another recycling pathway required for cytokinesis is the one

regulated by Rab35. Indeed, genetic screens performed in Schneider 2 (S2) cells have shown that Rab35 is required for cytokinesis (Yu, Prekeris, and Gould 2007). Rab35 acts through its effector, OCRL (oculocerebrorenal syndrome of Lowe) phosophatase. OCRL accumulates at the cleavage furrow in late cytokinesis in a Rab35 dependent manner. The phosphatase activity of OCRL regulates the amount of Ptd(4,5)P2 at the furrow that is important for proper actin cytoskeleton assembly at the division plane (Kouranti et al. 2006; Dambournet et al. 2011; Chesneau et al. 2012). Dynamin has also been shown to be important for cell division. During cytokinesis dynamin accumulates preferentially at the ingressing furrow, probably on recycling endosomes (Wienke et al. 1999; Thompson et al. 2002). Because dynamin has also been shown to regulate actin cytoskeleton the possibility exists that the assembly of the contractile ring is also dynamin dependent (Schafer 2004).

As mentioned before, the activity of the early endosome regulator Rab5 is also required for cell division. For instance, Rab5 knockdown results in formation of multinucleated cells (Yu, Prekeris, and Gould 2007). Moreover, Rab5 is tightly regulated during the cell cycle by the Cdc14 and the Cdk1 (cyclin-dependent kinase 1) kinases. During early mitosis Cdk1 phosphorylates RN-tre (see Chapter 1.3.3.3) leading to the down-regulation of Rab5 activity. During cytokinesis Cdc14 inactivates Cdk1 and as a consequence reactivates Rab5 (Lanzetti et al. 2007).

Taken together these data demonstrate that trafficking along the endocytic-recycling pathway plays an important role during cytokinesis. However, we still do not know much about the specific routes responsible for the initial changes in PM organization during cytokinesis.

1.4.4 Membrane trafficking and endocytosis during cellularization

During cellularization the plasma membrane area increases of over 20 fold in one hour. As a result a polarized epithelium composed of approximately 6000 cells is established (Mazumdar and Mazumdar 2002). Therefore cellularization represents a good model system to study the mechanisms underlying plasma membrane remodeling during morphogenesis.

Injection of WGA (a lipid binding molecule) coupled to a fluorescent dye revealed that the addition of new membranes occurs in two different areas. During the slow phase of cellularization membranes are added to the apical domain of the growing cells. In contrast, the furrow canal seems to be devoted from new membrane materials. This situation changes during the fast phase when new membranes are delivered to the lateral PM. This result indicates that there are different two routs or two targeting mechanisms to the PM (T Lecuit and Wieschaus 2000). One important question relates with the source of the new membranes. Injection of Brefeldin A, a drug that inhibits Golgi function, results in the arrest of furrow ingression. Similar effects were obtained by inhibiting golgin Lava lamp, a protein responsible for the movement of the Golgi apparatus (Sisson et al. 2000; Papoulas, Hays, and Sisson 2005). Additional evidence for the role of the secretory pathway in membrane addition comes from the analysis of Sec5 mutants. Sec5 is part of the exocyst complex and is responsible for the fusion of exocytic vesicles with the PM (He and Guo 2009). Experiments that took advantage of a temperature sensitive allele of Sec5 demonstrated that newly synthesized proteins accumulate in the Golgi complex and cellularization did not proceed (Murthy et al. 2010). Surprisingly, in contrast to the WGA injection experiments, Sec5 localizes mostly apically and sub-apically during fast-phase without the expected strong localization to the basolateral surface. It is possible that exocyst controls only one of the two routs that are specific for the addition of new membranes.

Research done in recent years demonstrated also that the endocytic-recycling pathway plays an important role during cellularization. As mentioned in Chapter 1.4.3, recycling endosomes positive for Rab11 are an important source for the addition of new membranes during cytokinesis. Indeed injection of recombinant dominant negative form of Rab11 into cellularizing embryos results in the arrest of cellularization. Moreover, accumulation of the neurotactin in intracellular vesicles could also be observed (Pelissier, Chauvin, and Lecuit 2003). However, it is hard to distinguish whether this cellularization phenotype is solely due to a defect in new membrane addition or is rather mediated by the miss-regulation of some other Rab11-dependent pathways, such as the regulation of actin dynamics at the furrow canal.

Rab5 regulates another pathway that is important for cellularization. Injection of the recombinant dominant negative mutant of Rab5 results in arrest of cellularization and furrow disassembly. Detailed analysis of the membranes in early cellularizing embryo labelled with WGA, revealed that endocytosis takes place at the furrow canal during the slow phase. Also, it was shown that in cellularizing embryos endocytosis at the furrow is dependent on actin. Disruption of actin at the furrow canal results in formation of long intracellular tubes. These structures originate from the bottom of the furrow canal (Sokac and Wieschaus 2008a). Similar to Rab5 phenotype can be also obtained in dynamin mutants (Pelissier, Chauvin, and Lecuit 2003).

Taken together, understanding the mechanisms that control membrane delivery and removal at the specific domains of the cellularizing embryo might bring us closer to understand a detailed role of endocytosis in controlling many aspects of cell and tissue morphogenesis.

Chapter 2 Materials and methods

2.1 Materials

2.1.1 Equipment

100x oil objective	Zeiss
60x oil objective APO N	Olympus
60x water objective LSM 780 NLO	Zeiss
ABI PRISM 7500	Applied Biosystems
Agarose gels electrophoresis chambers	Thermo Scientific
Analytical scale TE412	Satorius
Block thermostate	Grant
Cell^R, multi-color TIRF	Olympus Biosystems
Dissection microscope	Zeiss
Heraeus Multifuge	Thermo Scientific
Improvision Ultraview VoX Spinning disk confocal	Perkin Elmer
Incubator B15	Thermo Scientific
Microcentrifuge 5415 and 5424	Eppendorf
Microfluidizer M-110L	Microfluidics
Microinjector	Eppendorf
MicroPulser Electroporation Apparatus	Bio-Rad
Nanodrop Spectrophotometer ND-1000	Nanodrop Tech.
Optima L-100 XP Centrifuge	Beckman Coulter
P-97 Flaming/Brown puller	Sutter Instrument
PCR machine S1000	Bio-Rad
Pipettes	Gilson
Potter S Homogeniser	Satorius
Power supply PowerPac HC	Bio-Rad
Rotator with wheel SB3	Stuart
SDS-PAGE chamber	Life Technologies
Sorvall RC 6 Plus Superspeed Centrifuge	Thermo Scientific
Trans-blot system	Bio-Rad
Transilluminator	Life Technologies
Two photon microscope LSM 780 NLO	Zeiss

Vortex	Neolab
Water bath thermostate	Julabo
Water bath WNB7	Memmert

2.1.2 Consumables

Amicon Ultra-0.5 Centrifugal Filter Unit	Millipore
Borosilicate glass capillaries	Harvard Apparatus
Electroporation cuvettes	Bio-Rad
Filter paper	Whatmann
Glass bottom microscopy dishes	MatTek
Kodak Biomax MR film	Kodak
Microscopy coverslips	Warner Instruments
Microscopy slides	Thermo Scientific
NuPAGE Novex 4-12% Bis-Tris Gel	Life Technologies
PCR tubes	Bio-Rad
PVDF membrane	Bio-Rad
Tubes 1.5 mL, 2 mL	Eppendorf
Tubes 15 mL, 50 mL	Falcon
Vivaspin	GE Healthcare

2.1.3 Chemicals

2-mercaptoethanol 98%	Sigma-Aldrich
Agarose	Life Technologies
Ampicilin sodium salt	Applichem
Aqua-Poly/Mount	Polysciences
Bovine serum albumin	Sigma-Aldrich
Bromophenol Blue	Sigma-Aldrich
Chloramphenicol	Karl Roth
Coomassie Brilliant Blue G250	Fluka
Dextran, Alexa Fluor 647	Life Technologies
DTT	Biomol
EasyTag L-[^{35}S]-Methionine	Perkin Elmer
GDP sodium salt	Sigma-Aldrich

GTPγS lithium salt	Sigma-Aldrich
Halocarbon oil 27	Sigma-Aldrich
Halocarbon oil 700	Sigma-Aldrich
IPTG	Biomol
Kanamycin sulfate	Karl Roth
Orange G	Sigma-Aldrich
Paraformaldehyde 20% solution	Electron Microscopy Sciences
pHrodo Red Dextran 10 000 MW	Life Technologies
SDS	Life Technologies
Sodium hypochlorite	Merck
SYBR Safe	Life Technologies
Triton X-100	Sigma-Aldrich
Tween 20	Sigma-Aldrich

All other common chemicals were obtained from Sigma-Aldrich and Merck.

2.1.4 Reagents and Kits

Complete protease inhibitor coctail	Roche
GeneJET Purification Kit	Thermo Scientific
Glutathione Sepharose 4B	GE Healthcare
Ni-NTA	QIAGEN
QIAfilter Plasmid Midi Kit	QIAGEN
QIAprep Spin Miniprep Kit	QIAGEN
QIAquick Gel Extraction Kit	QIAGEN
QIAquick PCR Purification Kit	QIAGEN
RNeasy Mini Kit	QIAGEN
Western Lightning Plus ECL	Perkin Elmer

2.1.5 Enzymes

Crimson Taq DNA polymerase	New England Biolabs
DNase I	Roche
Gateway LR Clonase II	Life Technologies
GoTaq Green PCR Master Mix	Promega

pENTR™/D-TOPO® Cloning Kit	Life Technlologies
Phusion Flash PCR Master Mix	Thermo Scientific
Proteinase K	Thermo Scientific
Restriction endonucleases	New England Biolabs
RNase A	Roche
SuperScript III First-Strand	Life Technologies
SYBR Green PCR Master Mix	Life Technologies
T4 DNA Ligase	New England Biolabs
TNT Quick Coupled Translation System	Promega

2.1.6 DNA and protein markers

1 Kb Plus DNA Ladder	Life Technologies
Precision Plus Protein Dual Color	Bio-Rad

2.1.7 Plasmids and vectors

pENTR/D-TOPO	Life Technologies
pPGW	T. Murphy
pPHW	T. Murphy
D277M	A. Brand
pCa4G2B	DGRC
pEOC	This study
pGEX-4T	GE Healthcare
pET32	Novagen
pCR2.1-TOPO TA	Life Technologies
pCR-XL-TOPO	Life Technologies

2.1.8 Bacterial strains

Rosetta (DE3)	Novagen
Top10	Life Technologies
XL1-Blue	Stratagene

2.1.9 Primers

To generate transgenic flies:

α-adaptin

sfGFP F	**CACCATGTCCAAGGGCGAGGAGCTG**	**directional TOPO**
sfGFP R	TCCCCCCGCACCGGCGCCATGGAGCCCTTGTACAGC	overhang with α-adaptin
Adaptin F	GCTGTACAAGGGCTCCATGGCGCCGGTGCGGGGGGA	overhang with sfGFP
Adaptin R	TTAGAATTGATCCGTCAACAGATCGCAGAT	

Rab11

Rab11 F	**CACCATGGGT GCAAGAGAAGACGAGTACGAT TA**	**directional TOPO**
Rab11 R	TCACTGACAGCACTGTTTGCGC	

CG41099-PC

CG41099 F	**CACCATGAAAACAGGTAGTAATGAGACGTTCTCC**	**directional TOPO**
CG41099 R	CTATGACAAGGAGCCATTTCC	

bcd-secYFP

FOGYFP F	**ATGTCTCCGCCCAATTGTCTGCTGGCTGTTCTGGCGCT CACGGTTTTCATAGGGGCCAACAACGCCGTGAGCAAGG GCGAGG**	**FOG signal peptide**
YFP R	CTACTTGTACAGCTCGTCCATGCCGAG	
5' bcd F	CACACACCGAAACCGAACGAAAGAG	
5' bcd R	CAATTGGGCGGAGACATTTTCCCCAAACACTCCGCCGC	FOG overhang
FOG F	GCGGCG GAGTGTTTGGGGAAAATGTCTCCGCCCAAT TG	5' bcd overhang
FOGYFP R	CTCTCTAACACGCCTCTCATCCAGGTCACTTGTACAGCTCG TCCATGCC	3'UTR bcd overhang
3'UTR bcd F	GGCATGGACGAGCTGTACAAGTGACCTGGATGAGAGGCGT GTTAGAGAG	YFP overhang
3'UTR bcd R	ACTAGTGTTAA CTAGGTGTGATGAAGGGCACAGG	

αTub67C-secYFP

Fog BamHI F	**GGATCCATGTCTCCGCCCAATTGTC**	**BamHI**
YFP XhoI R	CTCGAGCTACTTGTACAGCTCGTCCATGCCGAG	XhoI

secGFP and secmCherry

Fog GFP F	**CACCATGTCTCCGCCCAATTGTCTGCTGGCTGTTCT GGCGCTCACGGTTTTCATAGGGGCCAACAACGCCGT GAGCAAGGGCGAGG**	**directional TOPO, FOG signal peptide**
FOG Cherry F	CACCATGTCTCCGCCCAATTGTCTGCTGGCTGTTCTGGC GCTCACGGTTTTCATAGGGGCCAACAACGCCGTGAGCA	directional TOPO, FOG signal peptide

	AGGGCGAGGAGG	
mCherry R	CTACTTGTACAGCTCGTCCATGCCG	

Rab5 DN

Rab5 F Fly	**CACCATGGCAACCACTCCACGCAG**	**directional TOPO**
Rab5 R Fly	TCACTTGCAGCAGT GTTCGTCGG	
QC Rab5DN 1	TCCGCTGTGGGCAAGAATTCACTGGTGCTGCGC	Directional mutagenesis TTC to AAT
QC Rab5DN 2	GCGCAGCACCAGTGAATTCTTGCCCACAGCGGA	Directional mutagenesis TTC to AAT

For GFP::Rab5 homologous recombination:

Rab5 5'Arm F	**GCCGGCATAACTTCGTATAGCATACATTATACGAAG TTATGCCGTCGACAAGCCCAGTTCAA**	**NgoMIV, loxP**
Rab5 5'Arm R	TGTTCCGCTCACTTGTATGTTCGC	
Rab5 3'Arm F	GTACATATTGAACTGGGCTTGTCGACGGC	
Rab5 3'Arm R	TGGGGAGCCTCCTTCGCCGGA	
Rab5 500 F	GGGCAGCATGTTTTCAAGGG	primer pair to test transgenic lines for insertion
Rab5 500 R	TCTGTGTCAGAAAGGCCGCA	

For recombinant protein expression:

Rab5

Rab5 F	**GAATTCATGGCAACCACTCCACGCAG**	**EcoRI**
Rab5 R	CTCGAG TCACTTGCAGCAGT GTTCGTCGG	XhoI

CG41099 (660-920 aa)

Rabank5 Ab F	**CCATGGATGAAAACAGGTAGTAATGAGACGTTCTCC GTAC**	**NcoI**
Rabank5 Ab R	GGATCCCTATGACAAGGAGCCATTTCCACATTGTAGTA C	BamHI

2.1.10 Antibodies

Name	Host	Dilution	Source
anti-CG41099	Rabbit	1:1000 (WB) 1:500 (IF)	This study
anti-α-Tubulin, B-5-1-2	Mouse monoclonal	1:10000 (WB)	Sigma Aldrich
anti-rabbit IgG,	Goat	1:500 (IF)	Life

AlexaFluor 488			Technologies
anti-rabbit IgG, HRP	Donkey	1:5000 (WB)	GE Healthcare

2.1.11 Fly stocks

Genotype	Source
OregonR	Bloomington #5
w, *shi*^{1}	Bloomington #7068
w;; P{UAS-GFP::Clc}/TM6B, Tb	Bloomington #7109
w; P{UAS-GFP::Rab11}	Bloomington #8506
y, w; P{αTub67C>Gal4}; {αTub67C>Gal4}	E. Wieschaus
y, w^{1118}	Bloomington #6598
y,w, P{UASp-secGFP}	This study
y,w; P{bcd>secYFP}attP40/CyO	This study
y,w;; P{sqh>GAP43-mCherry}attP2/TM3, Sb	E. Wieschaus
y,w; P{sqh>GAP43-mCherry}attP40/CyO	E. Wieschaus
y,w; GFP::Rab5 (endogenous locus)	This study
y,w; P{SuperFolderGFP::α-adaptin}/CyO	This study
y,w; P{UASp-GFP::CG41099-PC}/CyO	This study
y,w;; P{UASp-GFP::CG41099-PC}/TM3, Sb	This study
y,w; P{UASp-GFP::Rab11}/CyO	This study
y,w;; P{UASp-secGFP}/TM3, Ser	This study
y,w;; P{UASp-secmCherry}/TM3, Ser	This study
y,w; P{UASp-YFP::Rab5}	Bloomington #9775
y,w; P{αTub67C>secGFP}	This study
y, sc, v;; P{CG41099 shRNA}attP2/TM3, Sb	Bloomington #34883
y, sc, v;; P{GFP shRNA}attP2/TM3, Sb	Transgenic RNAi project
y, w; If/CyO	Bloomington #2
y, w/P{hs-hid} Y;; P{hs-FLP}, {hs-SceI}/CyO, P{hs-hid}	Bloomington #25680
y, w;; P{loxP(w^{+})loxP-GFP::Rab5, 3xP3>mCherry}(donor)	This study
y, w/ P{Crey}; sco/CyO	Bloomington #766

2.1.12 Software

Name	Purpose	Source
CellProfiler	Microscopy data quantification	Broad Institute
Illustrator	Data presentation	Adobe
ImageJ	Microscopy data analysis	NIH
Imaris	3D rendering and data visualization	Bitplane
MacVector	DNA sequence analysis	MacVector
Photoshop	Data presentation	Adobe

2.1.13 Buffers and solutions

Bacteria lysis buffer	5 mM	β-mercaptoethanol
	2 mM	$MgCl_2$
	10 µg/ml	DNase
	10 µg/ml	RNase
	2x	Protease Inhibitor Cocktail
	1x	PBS
Column buffer	5 mM	β-mercaptoethanol
	2 mM	$MgCl_2$
	1x	PBS
DNA loading buffer 10x	50%	Glycerol
	0.5x	TAE
	0.2%	Orange G
Elution buffer for affinity chromatography	100 mM	HEPES pH=7.4
	1.5 M	NaCl
	20 mM	EDTA
	1 mM	DTT

Embryo fixative solution	5 mL	Heptane
	4 mL	PBS
	1 mL	20% paraformaldehyde
LB 1x	10 g	Bactotryptone
pH=7.2	5 g	Yeast extract
	5 g	NaCl
	ad 1 L	dd H_2O
LB agar 1x	10 g	Bactotryptone
	5 g	Yeast extract
	5 g	NaCl
	15 g	Agar-Agar
	ad 1 L	dd H_2O
Nucleotide exchange buffer	20 mM	HEPES pH=7.4
	5 mM	$MgCl_2$
	10 mM	EDTA
	1 mM	DTT
	100 mM	NaCl
Nucleotide stabilization buffer	20 mM	HEPES pH=7.4
	2 mM	$MgCl_2$
	100 mM	NaCl
	1 mM	DTT
PBS 1X	137 mM	NaCl

pH=7.4	2.7 mM	KCl
	10 mM	Na2HPO4
	2 mM	KH2PO4
PBST	1x	PBS
	0.1%	Tween 20
PBSTX	1x	PBS
	0.1%	TritonX-100
Protein loading buffer 5x	313 mM	TRIS pH=6.8
	500 mM	DTT
	10%	SDS
	0.05%	Bromophenol blue
	50%	Glycerol
SOC 1x	5 g	Yeast extract
	20 g	Bactotryptone
	20 g	Dextrose
	10 mM	NaCl
	2.5 mM	KCl
	10 mM	$MgSO_4$
	ad 1 L	dd H2O
TAE 50x	2 M	TRIS
pH=8.4	1 M	Acetic acid
	50 mM	EDTA
TE 1x	1 mM	TRIS pH=8.0

pH=8.0	1 mM	EDTA
Transfer buffer	25 mM	TRIS
	192 mM	Glycine
	0.01%	SDS
	20%	Methanol

2.2 Methods

2.2.1 Standard molecular biology methods

2.2.1.1 Isolation, purification and concentration measurements of plasmid DNA

In order to extract small quantities of plasmid DNA (up to 20 μg) from bacterial culture a QIAprep Spin Miniprep Kit was used according to the manufacturer's protocol. For quantities above 20 μg QIAfilter Plasmid Midi Kit was used. DNA concentration was measured by UV spectroscopy (260 nm) using NanoDrop spectrophotometer.

2.2.1.2 Agarose gel electrophoresis

This method was used to separate and purify DNA fragments. Typically 1% agarose gels in TE buffer were casted with addition of SYBIR safe DNA gel stain (1x). DNA solution was diluted with 10x DNA loading buffer and separated at 100 V for 30 minutes. Gels were analysed using UV- or blue-light transilluminator. When needed, DNA fragments were extracted and purified using QIAquick Gel Extraction Kit or MinElute Gel Extraction Kit.

2.2.1.3 Polymerase chain reaction

For preparative PCR, Phusion Flash DNA polymerase was used and for analytical PCR GoTaq DNA polymerase was used. Typically 20 μL reaction was performed using Phusion Flash polymerase. The reaction was performed with 10 μL polymerase master mix, 0.5 μM of each primer, and 10 – 50 pg of plasmid DNA or 1 - 5 μL of *Drosophila* genomic DNA. Typical amplification protocol using Phusion Flash DNA polymerase is presented in Table 2.1.

Cycle step	Temperature	Plasmid DNA	Genomic DNA	N of cycles
		Time	Time	
Initial denaturation	98°C	10 s	20 s	1
Denaturation	98°C	1 s	2 s	30
Annealing	60°C	5 s	15 s	
Extension	72°C	15 s/1 kb	15 s/1 kb	
Final extension	72°C	1 min	5 min	1
Incubation	4°C	hold	hold	

Table 2.1 PCR protocol for the plasmid and genomic DNA templates.

2.2.1.4 Restriction digest and ligation of DNA fragments

Preparative restriction digests were performed in 30 μL volume using typically 1 μg of DNA and 10 U of appropriate enzyme. The reaction was incubated at 37°C (55°C for BsiWI) for 30 minutes. DNA fragments were separated and purified as described in the previous chapter. Purified fragments were ligated using T7 DNA ligase according to the manufacturer's protocol. Typically a 10 μL reaction was performed using 2 μL of digested plasmid DNA, 6 μL of insert DNA, 1 μL of 10x ligation buffer and 1 μL of T4 ligase (3000 U). The ligation reaction was performed for 15 minutes at room temperature. Finally, 1 μL of the ligation reaction was used to transform bacteria.

2.2.1.5 TOPO TA cloning

TOPO TA method was used for constructs amplified from genomic DNA or from cDNA library. Prior to the cloning reaction, PCR fragments were separated and purified form agarose gels. 3´ A-overhangs were added to the purified DNA fragments by incubation with Crimson Taq DNA polymerase. Typically 40 μL reaction was performed with 5 U of Crimson Taq polymerase, 1x amplification buffer, 0.2 mM dNTPs and 30 μL of purified PCR product. The TOPO cloning reaction was performed according to the manufacturer's protocol. For PCR fragments < 4 kb the TOPO TA kit was used and for

larger fragments the TOPO XL kit was used. One Shot TOP10 bacteria were transformed with 1 μL of the reaction.

2.2.1.6 Gateway cloning

Constructs to generate transgenic fly lines were constructed with Gateway cloning method. This method is divided into two steps: the Gateway TOPO cloning reaction and the LR reaction.

2.2.1.6.a Gateway TOPO cloning

The directional pENTR⁄D-TOPO Cloning Kit was used to generate donor vectors for the LR reaction. In order to do that, 5' PCR primers were designed with a CACC overhang in front of an open reading frame. PCR was performed as described in Chapter 2.2.1.3 and purified as described in Chapter 2.2.1.2. Gateway TOPO cloning was performed according to the manufacturer's protocol. One Shot TOP10 bacteria were transformed and DNA from single colonies was sequenced in order to check the fidelity of PCR. Plasmids were purified as described in Chapter 2.2.1.1.

2.2.1.6.b Gateway LR reaction

For the LR reaction 25 ng of DNA purified from pENTR clone and 75 ng of proper destination vector were used. Plasmids were diluted in TE buffer and 1 μL of the LR Clonase II enzyme mix was added. Total volume of the cloning reaction was 5 μL. The mixture was incubated at 25°C for 1 hour and then stopped by adding of 1 μL of Proteinase K and then incubated at 37°C for 10 minutes. One Shot TOP10 bacteria were transformed with 1 μL of the LR cloning reaction. DNA from single colonies was sequenced.

2.2.1.7 Transformation of bacteria

Transformation of bacteria with plasmid DNA was performed using either electro-competent or chemically-competent cells. 50 μL of chemically-competent bacteria were mixed with 1 μL of ligation reaction followed by 30 minutes incubation on ice. Afterwards, bacteria were heat shocked at 42°C for 45 seconds, and recovered in SOC medium for 1 hour at 37°C. Solution was spread on LB agar plates supplemented with appropriate antibiotic. Electro-competent cells were transformed using MicroPulser electroporation apparatus using standard protocol.

2.2.2 *Drosophila* methods

2.2.2.1 Fly husbandry

Flies were maintained at room temperature unless specified otherwise and kept in vials supplied with standard fly food. Flies crossed to αTub67c:Gal4 were kept at 18°C for higher expression efficiency.

2.2.2.2 Isolation of genomic DNA from adult flies

Genomic DNA was prepared using the Fermentas GeneJET kit. The manufacturer's protocol was modified. Five to ten adult flies were collected into an Eppendorf tube and frozen at -80°C for 30 minutes. 180 μL of digestion solution provided with the kit was added and samples were homogenized with a hand grinder for 10 seconds. 20 μL of Proteinase K was added and samples were incubated at 56°C over night. Next day, digestion solution was cooled to room temperature and incubated with 20 μL of RNase A for 10 minutes. Next steps were performed according to the manufacturer's protocol. Genomic DNA was eluted from the column with 50 μL of preheated to 60°C elution buffer provided with the kit.

2.2.2.3 Generation of cDNA library from *Drosophila* embryos

To generate DNA template for standard PCR, a small volume of 0-4 hour embryos were used. Alternatively, one or ten cellularizing embryos were used for qPCR purposes. Collected embryos were frozen in liquid nitrogen and stored at -80°C until processed. Total RNA was isolated with the RNeasy Mini Kit. Embryos were homogenized in 100 µL of RTL buffer provided with the kit and the grinding pestle was washed with additional 250 µL of the buffer. Samples were treated according to the manufacturer's protocol including DNA digest on the column. cDNA was synthesised using the SuperScript III First-Strand Synthesis System according to the manufacturer's protocol. cDNA concentration was measured with a NanoDrop spectrophotometer.

2.2.2.4 Cloning strategies

2.2.2.4a UASp-GFP:α-Adaptin

This construct was generated by the overlap extension polymerase chain reaction. In order to ensure fast maturation of the fluorophore, a GFP variant (SuperFolder GFP) was used. α-Adaptin-PA was amplified from *Drosophila* cDNA library (Chapter 2.2.2.3). Ligated GPF::α-Adaptin was cloned into the pENTR plasmid and recombined with the pPW vector.

2.2.2.4b UASp-GFP:CG41099-PC and UASp::GFP:Rab11

CG41099-PC and Rab11 were amplified from *Drosophila* cDNA library and cloned into the pENTR vector. In order to add an N-terminal GFP tag, constructs were recombined with the pPGW vector using the Gateway cloning system.

2.2.2.4c UASt-HA:Rab5DN

Rab5 sequence was amplified from the cDNA library and cloned into pENTR vector. The S43N mutation was introduced by site directed mutagenesis method. The TCC codon was replaced by the AAT. In the next step construct was recombined with pTHW vector using the Gateway system.

2.2.2.4d UASp-secGFP and UASp-secmCherry

A long 5' primer was designed with sequence corresponding to the signalling peptide of Fog protein (MSPPNCLLAVLALTVFIGANNA). With this primer either GFP (amplified from the pPGW vector) or mCherry (Clontech) was amplified. Constructs were cloned into the pENTR plasmid and recombined with the pPW vector.

2.2.2.4e αTub67c-secYFP

This construct was designed analogously to the secGFP and the secmCherry. secYFP was cloned between BamHI and XhoI sites into the D277M vector containing αTub67c promoter.

2.2.2.4f bcd-secYFP

In order to drive expression of secYFP only in the anterior of embryos, the construct was fused with the bcd promoter. In addition, to ensure proper localization of RNA, the 5'UTR and the 3'UTR sequences of bcd was added to the construct. These sequences were amplified from genomic DNA and fused together using an overlap extension polymerase chain reaction. Next, the construct was cloned into the pCa4G2B vector between the BamHI/SpeI restriction sites.

2.2.2.4g pEOC (pEndsOutmCherry)

This vector was designed for more efficient screening of flies after the 'ends out' homologous recombination. The vector was made on a backbone of the pP{EndsOut2} vector. Two markers expressed in flies were introduced into the sequence. The white gene under the GMR (Glass Multimer Reporter)/hsp70 promoter and the 3xP3:mCherry-SV40 construct. The white gene is a positive marker for recombinants and resides between two homologous arms of the construct. The 3xP3:mCherry-SV40 lies outside the recombination cassette and therefore is a negative marker for homologous recombination. In addition, the multiple cloning sites were replaced by the NotI/MluI/EcoRI/SphI/BglII/BsiWI and the AatII/NdeI/NaeI/NgoMIV sites. Detailed map of the vector can be found in the Appendix A.

2.2.2.4h pEOC GFP::Rab5 for homologous recombination

The 5' (3.2 kb) and the 3' (2 kb) homologous recombination arms were amplified from BACMID DNA containing the Rab5 locus (BACR22P10, BPRC). In addition, GFP with a Glycine-Alanine-Glycine-Alanine (GAGA) linker was inserted at the 5' end of the Rab5 coding sequence. Homologous arms were cloned in the AatII/NgoMIV and the SphI/MluI restriction sites. In addition, two loxP sequences were introduced in order to excise the white gene from the intron of Rab5.

2.2.2.5 Generation of transgenic flies

All transgenic lines except the bcd:secYFP were generated using the P-element based method .These lines were generated in the y,w^{1118} background. The bcd:secYFP lines were generated using the PhiC31 integrase-mediated site-specific transgenesis in the attP2 and the attP40 lines. Plasmid injections were performed by Sandra Mueller and BestGene.

2.2.2.6 Homologous recombination

In order to generate endogenously tagged Rab5 the 'ends-out' homologous recombination method was used. As a first step, a donor line was generated using the construct described in Chapter 2.2.2.4h. These lines were selected by screening for the white gene and for high expression of 3xP3>mCherry. Line with construct mapped to the third chromosome was taken for further consideration.

In order to induce homologous recombination, the donor element needs to be mobilized and double strand DNA breaks need to be generated. Therefore, the donor line was crossed with the line expressing the FLP recombinase and the restriction enzyme SceI under the heat shock promoter. Approximately 200 females from the donor line were crossed to 40 males carrying hsp>FLP and hsp>SceI. These crosses were separated into 40 vials and propagated into new tubes for 5 days. 24-hours-old embryos were heat shocked at 38°C for 120 minutes in the water bath. To maximize the efficiency of this procedure, heat shock was repeated on 48-hours-old embryos.

After hatching, positive selection for recombinants was performed. Virgin females hatched from the previous cross were mated with y,w^{1118} males. In the next generation, flies positive for the white gene were selected. At the same time a screen for false-positive recombinants was performed. These are the flies that carry the white gene, however, in their case the donor construct either did not mobilize or recombined in a locus different than Rab5. These flies carried the 3xP3>mCherry construct. Screening was performed under a dissecting microscope equipped with a fluorescent lamp.

Proper localization of GFP::Rab5 was confirmed by PCR. In addition, the region of recombination was sequenced. In a final step, the white gene was removed from the Rab5 intron by Cre recombination.

2.2.2.7 Quantitative PCR

qPCR was used to measure the efficiency of CG41099 knock-down with RNAi. As a control, embryos expressing GAL4 under the αTub67c promoter were used. Either single or ten cellularizing embryos were lysed and cDNA was generated as described in Chapter

2.2.2.3. qRT-PCR for CG41099 was performed with the SYBR Green PCR master mix using standard protocol and was normalised to the RPL32 gene. An Applied Biosystems 7500 Real-Time PCR System was used. All PCR reactions were performed in triplicates. To exclude the presence of non-specific products, a melting curve for each primer pair was analysed. To quantify the ratio between expression of CG41099 in control embryos and embryos expressing RNAi a comparative C_T method ($\Delta\Delta C_T$) was used.

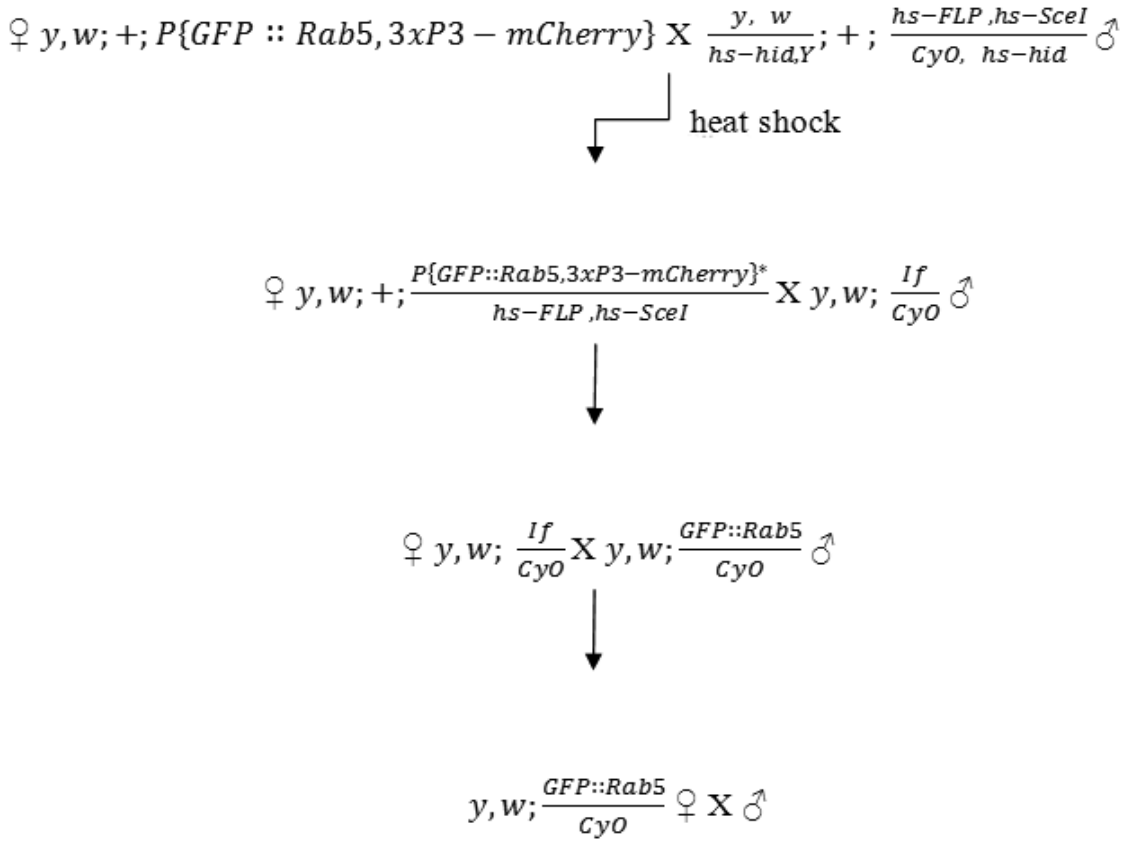

Figure 2.1 Crossing scheme for the Rab5 homologous recombination.

2.2.2.8 Immunostaining

Cellularizing embryos were dechorinated with 50% household bleach solution in water (2.5% sodium hypochlorite final) for three minutes and collected on a metal sieve. To

remove residual bleach, embryos were rinsed with water for few seconds and then blotted on a paper towel. Dechorinated embryos were transferred to a glass vial containing 10 mL of fixative solution and incubated for 20 minutes with shacking. For devitellization, the aqueous phase was discarded. Then, 5 mL of methanol was added followed by energetic shacking for 20 seconds. Devitellinized embryos were collected in Eppendorf tubes and washed three times in methanol. Fixed embryos were stored in methanol at -20°C.

Before immunostaining, embryos were briefly washed with PBS and then equilibrated with PBSTX solution for 20 minutes. Equilibrated embryos were blocked with 10% BSA solution in PBTX for 1 hour. Next, primary antibodies diluted in 5% BSA solution in PBSTX were added, and embryos were incubated over night at 4°C. Next day, embryos were washed three times for 10 minutes with PBSTX solution at room temperature. Secondary antibodies, diluted in 5% BSA in PBSTX were added followed by 45 minutes incubation at room temperature. After three times washing in PBSTX, embryos were fixed to microscopy slides using mounting medium.

2.2.2.9 Perivitelline dextran injection

10 000 MW Dextran labelled with Alexa647 or pHrodo Red were injected into the perivitelline space of cellularizing embryos as described previously (Levayer et al. 2011). Embryos were covered with a thin layer of halocarbon oil 700/27 (1:2). The coverslip was placed on a microscope slide platform and embryos were visualized using a standard 18 upright microscope equipped with a 10x objective (Zeiss). Microinjection was carried out with an Eppendorf 5242 microinjector.

Microinjection pipettes were pulled from borosilicate glass capillaries (1.2mm outer diamater x 0.94mm inner diamater), using a P-97 Flamming /brown puller. 20 mg/mL PBS solution of dextran was used.

2.2.3 Biochemical methods

2.2.3.1 Expression and purification of GST-Rab5

Drosophila Rab5 was amplified from cDNA library and cloned into the pGEX-4T vector in the EcoRI/XhoI sites. Rosetta (DE3) cells transformed with the pGEX-4T Rab5 were grown (5 L) to express GST-Rab5. Overnight bacterial culture was diluted 1:200 with fresh LB medium supplemented with an antibiotic. Bacteria were grown at 37°C until OD of 0.6. Cultures were induced by adding IPTG with final concentration of 1 mM. Bacteria were grown for 3 hours at 37°C and then sedimented. Pellet was resuspended 1:1 in lysis buffer and lysed using a microfluidizer under 7000 psi. In order to remove the insoluble fraction, lysate was pelleted by centrifugation at 2×10^5 g for 45 minutes. The soluble fraction was decanted into a Falcon tube and then Glutathione Sepharose 4B beads were added. Beads were incubated for 2 hours at 4°C with gentle rotation. Next, beads were washed four times with ten times beads volume of column buffer. Immobilized Rab5 protein was used in affinity chromatography in cellularizing embryos.

2.2.3.2 Affinity chromatography of Rab5 effectors from cellularizing *Drosophila* embryos

0-4 h old embryos were harvested, dechorionated for 2 minutes in 50% bleach solution in water, washed in PBS with addition of 0.1% Triton X-100. Embryos were frozen in liquid nitrogen and stored at -80°C until needed. Thirty grams of packed embryos were diluted in 60ml of embryo lysis buffer and homogenized in the Potter S tissue homogeniser at 4°C. In order to remove the insoluble fraction, lysate was pelleted by centrifugation at 5×10^5 g for 45 minutes. The supernatant was carefully decanted and used for the affinity chromatography.

Next, GST-Rab5 was loaded with a proper nucleotide. Purified GST-Rab5 immobilized on Gluthathione Sepharose resin (250 μL for each nucleotide) was washed twice with 1.5 mL of nucleotide exchange buffer containing 100 μM GTPγS or 100 μM GDP for

5 minutes followed by incubation in exchange buffer containing 1 mM GTPγS or 1 mM GDP for 20 minutes. The wash was repeated and the nucleotide binding was stabilized by incubation with stabilization buffer supplemented with 2 mM of appropriate nucleotide for 20 minutes.

Resin with nucleotide bound Rab5 was transferred to 10 mL of embryo lysate and incubated for 2 h at 4°C with gentle rotation. Next, resin was washed twice in stabilisation buffer for 5 minutes. In order to decrease unspecific binding, next wash was performed with stabilization buffer supplemented with 250 mM NaCl. Proteins bound to Rab5 were eluted for 20 minutes with 250 μL of elution buffer preheated to 37°C. Eluted proteins were concentrated using the Amicon Ultra-0.5 column and resolved on the 4-12% SDS-PAGE gel. Proteins bound to the GTPγS loaded Rab5 were selected and analyzed by mass spectrometry. The specificity of binding was confirmed in the in vitro binding assay.

2.2.3.3 In vitro affinity chromatography assay

To confirm specific binding between active Rab5 and CG41099 the TNT T7 Quick coupled Transcription/Translation System was used. GST-Rab5 was prepared as described in Chapter 2.2.3.1 and loaded with nucleotide as described in Chapter 2.2.3.2. CG41099-PA protein was expressed and radiolabeled using the TNT-Rabbit Reticulocyte lysate. 50 μL reaction was performed. 40 μL of the TNT-Rabbit Reticulocyte lysate was diluted with 1 μg of DNA template (pOT CG41099-PA, DGRC) solution and 20 μCi of ^{35}S-Methionine. Reaction was incubated for 90 minutes at 30°C. In the next step, the TNT reaction was mixed with 25 μL of 20% BSA solution, 20 μL of 50 mM nucleotide, 50 μL of Glutathione Sepharose 4B beads bound to GST-Rab5 and filled to 500 μL with stabilization buffer. Next steps are identical to described in Chapter 2.2.3.2. Eluted proteins were resolved on the 4-12% SDS-PAGE gel. Detection was performed overnight by autoradiography on MR KODAK film.

2.2.3.4 Production of CG41099 antibody

Fragment corresponding to amino acids 660 to 920 of CG41099-PC was cloned to the pET32 vector in the NcoI/BamHI sites. Rosetta (DE3) bacteria were transformed and overnight bacterial culture was diluted 1:200 with fresh LB medium supplemented with antibiotic. Bacteria (10 L) were grown at 37°C until OD of 0.6. Cultures were induced by adding IPTG with final concentration of 1 mM. Bacteria were grown for 16 hours at 18°C and then sedimented. Pellet was resuspended 1:1 in lysis buffer and lysed using a microfluidizer under 7000 psi. In order to remove the insoluble fraction, lysate was pelleted by centrifugation at 2×10^5 g for 45 minutes. Protein was purified using Ni-NTA agarose according to the manufacturer's protocol. Protein was concentrated on the Vivaspin 15 columns and buffer was exchanged to PBS on the column. In order to check the purity of eluate, protein samples were resolved on SDS-PAGE and stained with Coomassie Brilliant Blue. Protein samples were frozen and sent to Eurogentec for antibody generation in rabbits. Antibodies were purified from serum by affinity chromatography.

2.2.3.5 Protein gel electrophoresis and immunodetection

To separate proteins, SDS polyacrylamide gel electrophoresis (SDS-PAGE) was used. Protein solution was diluted with protein loading buffer, boiled for 5 minutes and loaded on commercially available 4%-12% Novex gradient gels. Electrophoresis was performed with constant voltage (125 V) for 90 minutes. To detect the total amount of proteins, gels were stained with Coomassie Brilliant Blue solution for 15 minutes followed by incubation in destaining solution for 1 hour.

For immunodetection, gels were washed briefly in ddH_2O and incubated in transfer buffer for 15 minutes. Immobilon-P transfer PVDF membrane was activated by incubation in methanol for 15 seconds. Methanol was removed by washing in ddH_2O and membrane was equilibrated in transfer buffer for 15 minutes. To transfer proteins to the PVDF membrane a semi-dry setup was used. The transfer was performed at 15 V for 45 minutes. Next, membrane was blocked with 5% milk solution in PBST buffer for 1 hour

at room temperature. Incubation with primary antibody diluted in 5% milk solution (in PBST) was performed overnight at 4°C. The membrane was washed three times in PBST for 10 minutes at room temperature. Washes were followed by incubation with secondary antibody conjugated with HRP. Antibody was diluted in 5% milk solution in PBST and incubated with the membrane for 30 minutes at room temperature. The membrane was washed three times in PBST for 10 minutes at room temperature. For signal detection, membrane was incubated in ECL solution for 1 minute and exposed in dark on MR KODAK film.

2.2.4 Microscopy methods

2.2.4.1 Confocal and two-photon microscopy

For time-lapse imaging, embryos were dechorionated with 20% sodium hypochlorite solution in water. To ensure the close proximity to the coverslip, dishes were covered with thin silicon layer (Sigmacoat). Dechorinated embryos were positioned on glass-bottom culture dishes (MatTek) in a drop of PBS solution. Imaging was performed on a PerkinElmer Improvision Ultraview VoX Spinning disk confocal using a 100x NA 1.3 oil immersion objective (Zeiss).
Two photon imaging was performed using Zeiss LSM 780 NLO system using a 63x NA 1.2 water immersion objective (Zeiss). Images were processed in ImageJ (NIH).

2.2.4.2 TIRF microscopy

Embryos were dechorionated with 20% sodium hypochlorite solution and positioned on glass-bottom culture dishes in a drop of PBS solution. In order to produce a uniform interface between the vitelline membrane and the coverslip, a thin slab (~ 5mm) of 2% agar was placed on top of embryos prior to imaging. Time-lapse TIRF imaging was performed on an Olympus Biosystems Cell^R TIRF system using an Olympus APO N 60x oil objective (NA 1.49). The incident angle was set at the critical angle for total internal reflection with subsequent small, manual angular adjustments used to optimize

signal from the apical membrane. All imaging was performed at room temperature unless stated otherwise. For experiments involving the temperature sensitive *shibire* mutant, either cold (18 ºC) or pre-warmed (32 ºC) PBS and agar were used for embryo mounting and live TIRF-M imaging was subsequently conducted in a temperature control chamber at either 18 ºC or 32 ºC.

2.2.5 Quantification and statistics

2.2.5.1 Quantification of GFP::Rab5 signal

GFP::RAB5 signal at the apical plasma membrane was imaged over the course of cellularization using TIRF microscopy and subsequently quantified using CellProfiler Image analysis software. Briefly, 3 independent data sets were obtained each for both ectopically expressed YFP::RAB5 and for endogenous GFP::RAB5. Identification and segmentation of RAB5-positive puncta was accomplished using Cell Profiler, registration was verified manually, and the number and integrated intensity of puncta were quantified. Both the number and integrated intensity of puncta were normalized by expressing their value over cellularization as a ratio to the mean value of the first 20 frames in each sequence.

2.2.5.2 Quantification of internalization assay

Quantification of intracellular signal in UAS::secGFP/+; Tub67::GAL4/+; Tub67::GAL4/+ embryos was performed manually. Intracellular tubes and vesicles positive for GFP were counted from the Z-stack corresponding to the volume between 4 to 5 microns under the apical membrane over the course of cellularization. Quantification was performed on 3 areas of 25 micron x 25 micron each in three different embryos. j

2.2.5.3 Quantification of the rate of apical surface flattening

This method was developed by Sebastian Streichan. First the images were corrected for

bleaching by fixing the mean intensity at each time point to that of the initial image. Then the images where filtered using a mexican hat filter with values sigmax = 7, sigmay = 1, which was rotated according to angles in an interval from 0 to pi. The response images form a stack, where each planecorresponds to an angle from the interval, enhancing protrusions along the given angle. The maximum intensity projection of that stack was then segmented using Ilastik (Ilastik: Interactive Learning and Segmentation Toolkit, Christoph Sommer,Christoph Straehle, Ullrich Koethe and Fred A. Hamprecht. 8th IEEE International Symposium on Biomedical Imaging, ISBI 2011) to yield a segmentation of the image. The skeleton of the image was then taken to compute the area in the image covered by protrusions.

Chapter 3 Aim of the thesis

3.1 Aim of the thesis

The aim of this thesis was to address the contribution of membrane trafficking in controlling plasma membrane remodelling during cell and tissue morphogenesis. In particular, I focused on the role of endocytosis in regulating the re-structuring of the apical plasma membrane during cellularization, the transformation of the syncyitial *Drosophila* embryo in 6000 mononucleated epithelial cells. Early during cellularization the apical surface is covered with highly dynamic membrane protrusions that retract towards the end of cellularization. This morphogenetic process is commonly referred to as surface flattening and immediately precedes gastrulation.

The mechanisms underlying surface flattening are still poorly understood and have been mainly linked to changes in actin organization. However, the reduction in apical surface area and changes in membrane organization accompanying surface flattening suggest that additional endocytic mechanisms might control this membrane remodelling process. To test this hypothesis, I developed multiple assays that allowed me to visualize, to quantify and to manipulate at the molecular level apical endocytosis during surface flattening. The molecular tools that I used are the large GTPase dynamin, which regulates vesicle formation at the plasma membrane, and the small GTPase Rab5, which regulates the biogenesis of early endosomes.

In summary, my data demonstrate that apical surface flattening is a dynamin-dependent morphogenetic process associated with the up-regulation of several endocytic events. Taken together my results are consistent with a model in which surface flattening is an endocytosis dependent morphogenetic process driven by the rapid removal of large quantities of tubular membranes. This tubular endocytic pathway is dynamin-dependent and leads to the *de novo* formation of apical Rab5 endosomes.

Chapter 4 Results

4.1 The localization of Rab5 endosomes is developmentally modulated during cellularization

Endocytosis has been shown to be crucial for cellularization. Blocking endocytosis at the early stage of cellularization by inhibiting dynamin and Rab5 activity results in the arrest of furrow progression (Pelissier, Chauvin, and Lecuit 2003). However, so far there is no information about the dynamics of endocytosis during cellularization. Therefore, I decided to closely analyze the spatial-temporal organization of endocytosis over the course of cellularization. To start with, I decided to follow Rab5 dynamics during cellularization using live imaging. I took advantage of a UAS-Rab5 line tagged with an N-terminal YFP that was available from the Bloomington Stock Center. To drive expression of this construct I used a line expressing the GAL4 in the pattern of the αTub67C gene. The αTub67C promoter is active throughout oogenesis and therefore early embryos are loaded with GAL4 protein. YFP::Rab5 expressing embryos were imaged at one minute interval using a spinning disk confocal microscope with a 40x water objective. Rab5 signal was first detected at the invaginating furrow (Fig. 4.1 b-c) early during cellularization. Towards the end of cellularization, a second pool of Rab5 endosomes appeared at the subapical plane (Fig 4.1 d). In order to overcome the limitation of the penetration depth of the spinning-disk confocal microscope, these observations were confirmed using two-photon microscopy (Fig. 4.1 e-g). Using this technique I could also observe that upon forming these large Rab5 vacuoles moved towards the base of the cells (Fig. 4.1 h-k). This result suggests that apical Rab5 endocytosis is temporally regulated during development peaking during the fast phase of cellularization. Furthermore, this result prompted me to further investigate the role of apical endocytosis during this step of morphogenesis.

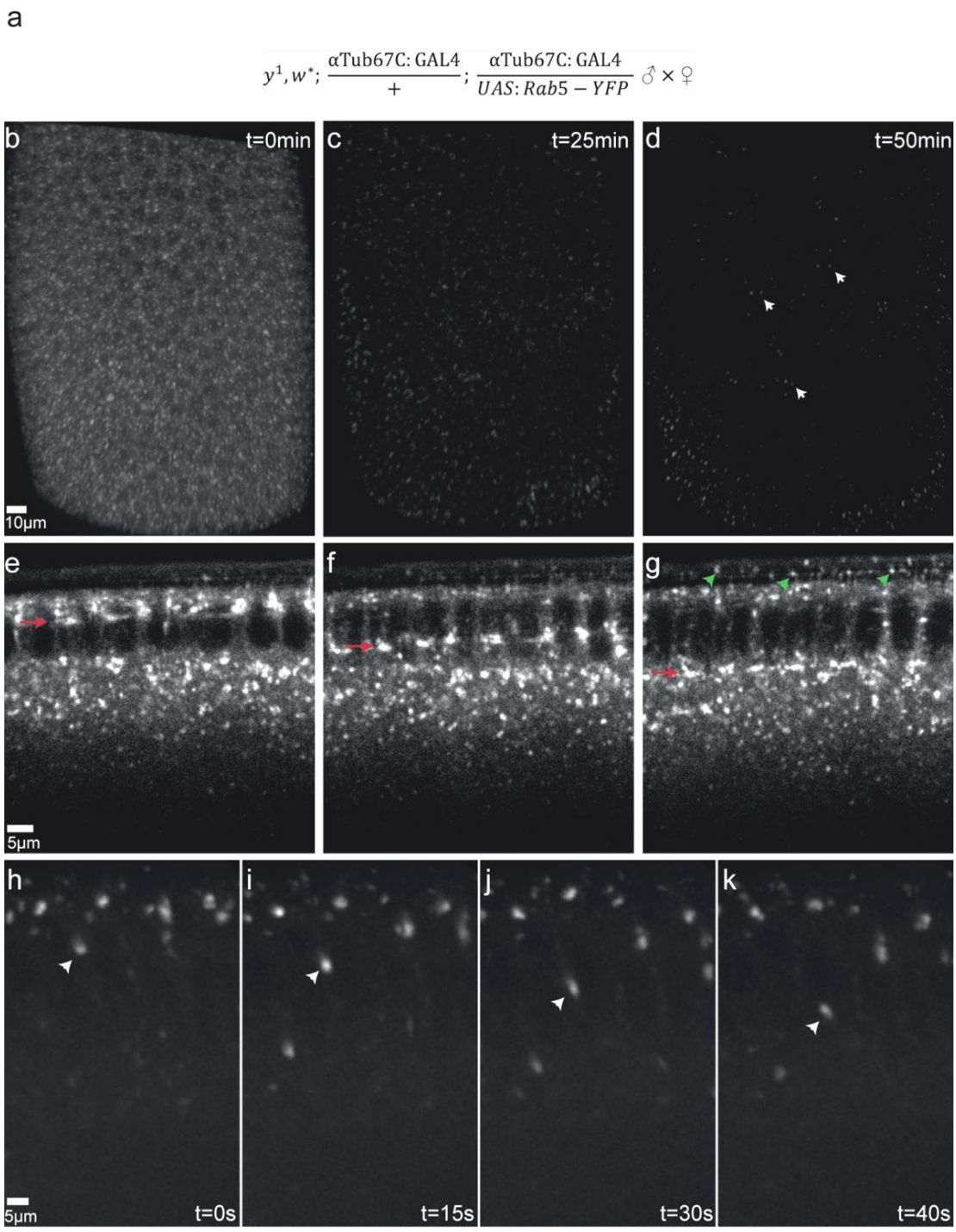

Figure 4.1 Rab5-mediated endocytosis is regulated in a spatial and temporal manner.

(a) The corresponding genotype of the parental cross that gives rise to embryos maternally loaded with YFP::Rab5 protein. (b-d) Apical view of a 15 µm z-stack over the course of cellularization. During the slow phase of cellularization Rab5 signal accumulates at the furrow canal and travels towards the base of the nuclei (b-c). Towards the end of cellularization, additional

YFP::Rab5-positive structures appear at the apical surface of the embryo (d). (e-g) An optical section of a cellularizing embryo that expresses the YFP::Rab5 obtained by two-photon microscopy. The YFP::Rab5 signal travels with the furrow (red arrows). During the fast phase of cellularization a clear YFP::Rab5 signal can be detected at the apical surface of the embryo (g, green arrows). Notice that most of the signal accumulates at the basal side of the embryo. A single plane was imaged. (h-k) Snapshots from a timecourse showing the apical Rab5 signal travelling to the base of the cell. Embryo was imaged 5 min prior to the gastrulation. White arrow marks a Rab5 positive signal moving down. A 3.5 μm z-stack is presented.

4.2 Developing TIRFM (Total Internal Reflection Fluorescence Microscopy) for imaging the apical endocytic dynamics in cellularizing embryo

To further investigate the role of apical endocytosis during cellularization I decided to apply TIRF microscopy to the early embryo in order to overcome two major limitations of confocal microscopy, namely the low time resolution and the high rate of photobleaching. TIRF microscopy allows the generation of a very narrow illumination plane that is created close to the coverslip (~ 100 nm). Using this technique, only a thin plane is illuminated at the time, so the photobleaching is reduced and at the same time temporal resolution is limited only by the acquisition speed of the camera. TIRFM is based on the principle that if there are two media of different optical density (n1 > n2) and the incident angle of the light path is greater or equal to the critical angle ($\alpha c = \arcsin(n2/n1)$), light does not go through the optically less dense medium, but is reflected at the interphase. This creates an evanescent wave that propagates in the n2 medium. In the TIRFM setup evanescent wave is created between a glass coverslip and water media, therefore only fluorophores close to the plasma membrane are illuminated. For this reason TIRM is commonly used in cell culture to study endocytic and exocytic events at the plasma membrane. To adapt this method for imaging the apical surface of the early *Drosophila* embryo several factors had to be taken under consideration:

- The *Drosophila* embryo is enclosed in the vitelline membrane, a lipid reach layer that protects the embryo from the extra-cellular environment.
- The *Drosophila* embryo has an ellipsoidal shape that limits the surface that can be illuminated by TIRF;
- The apical plasma membrane of the embryo is highly convoluted.

Because of these three majors constrains at the calculated critical angle only the surface of the vitelline membrane could be observed. Surprisingly by changing the angle of the laser beam, the signal of YFP::Rab5 was registered in a single illumination plane similar to the TIRF plane, arguing that an additional evanescent wave can be produced at the interphase between the vitelline membrane and the perivitelline fluid. To ensure proper attachment of the embryo to the coverslip and to increase the illuminated area I tried to immobilize the embryos using siliconized coverslips and glue. This method is commonly used for imaging embryos using confocal microscopy, but it was unsuitable for TIRFM as both glue and silicon interfere with the optical properties of the coverslip and prevents imaging. In a second attempt I decided to carefully place a thin slice of 2% agarose on the top of the specimen. This manipulation did not affect embryonic development or TIRF illumination. As a result a larger area of the embryo was touching the coverslip and therefore allowed to image more cells in a single embryo. Thus, this setup was ideal for high temporal resolution imaging of the surface of the *Drosophila* embryo.

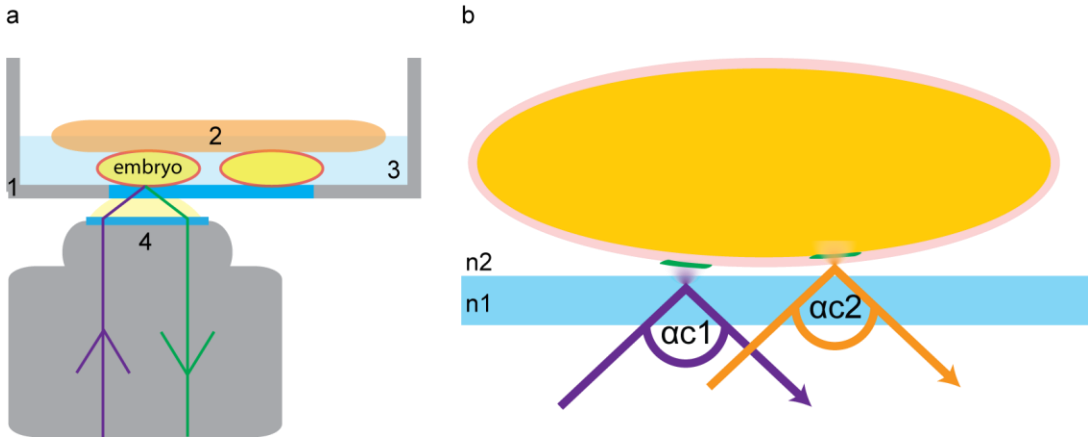

Figure 4.2 The experimental setup for the TIRF imaging of the *Drosophila* embryo.

(a) Embryos are positioned in a glass bottom dish (1) and carefully covered with a small block of 2% agarose (2). The specimen is submerged in PBS buffer (3) and imaged with an inverted TIRF objective (4). (b) An evanescent wave is generated at the coverslip incident light is reflected at the interphase between two media with different optical densities (n1 and n2). This occurs when the incident angle of the light path is greater than or equal to the critical angle αc =arcsin (n2/n1). Under normal conditions, the calculated angle for the glass (n1) and buffer (n2) results in a

situation in which only the surface of the vitelline membrane is illuminated (αc1). However, by manually increasing the light angle a condition can be found in which the surface of the apical plasma membrane is illuminated (αc2).

4.3 Apical Rab5 signal increases with the progress of cellularization

In order to closely analyze the dynamics of apical endocytosis during cellularization, embryos expressing YFP::Rab5 were imaged using the TIRFM. At the beginning of cellularization Rab5 localized to the forming furrow (Fig. 4.3 a). During the following 30 minutes only a few apical puncta appeared at the surface of the embryo (Fig. 4.3 b). From this point on, Rab5 signal increased gradually reaching towards the end of cellularization approximately a four-fold increase (Fig. 4.3 c and Fig. 4.3 g). This increase was observed along both the dorsal-ventral and anterior-posterior axes.

To test whether this increase is specific for the inward arm of endocytosis, I decided to analyze recycling endosome dynamics by following YFP tagged Rab11. To this end, I generated a transgenic Rab11 line tagged with GFP under the UASp promoter. I isolated two individual transgenic lines with detectable expression level and proceeded with the analysis. The Rab11 signal showed a significantly different pattern from that of Rab5. Most of the Rab11 positive recycling endosomes were concentrated around the nuclei and appeared only sporadically at the apical surface. Importantly the apical pool of Rab11 was constant during cellularization (Fig. 4.3 d-f). Therefore the up-regulation of endosomes at the apical surface during cellularization is specific for the Rab5 positive machinery.

In summary, these results demonstrate that Rab5 endosome dynamics are spatially and temporally regulated during cellularization. In particular the biogenesis of apical Rab5 endosomes is specifically up-regulated during the fast phase of cellularization. Interestingly, this up-regulation of Rab5 endosomes coincides with the morphological remodelling of the apical surface. Therefore I decided to further investigate whether there is any functional link between surface remodelling and up-regulation of Rab5 endosomes.

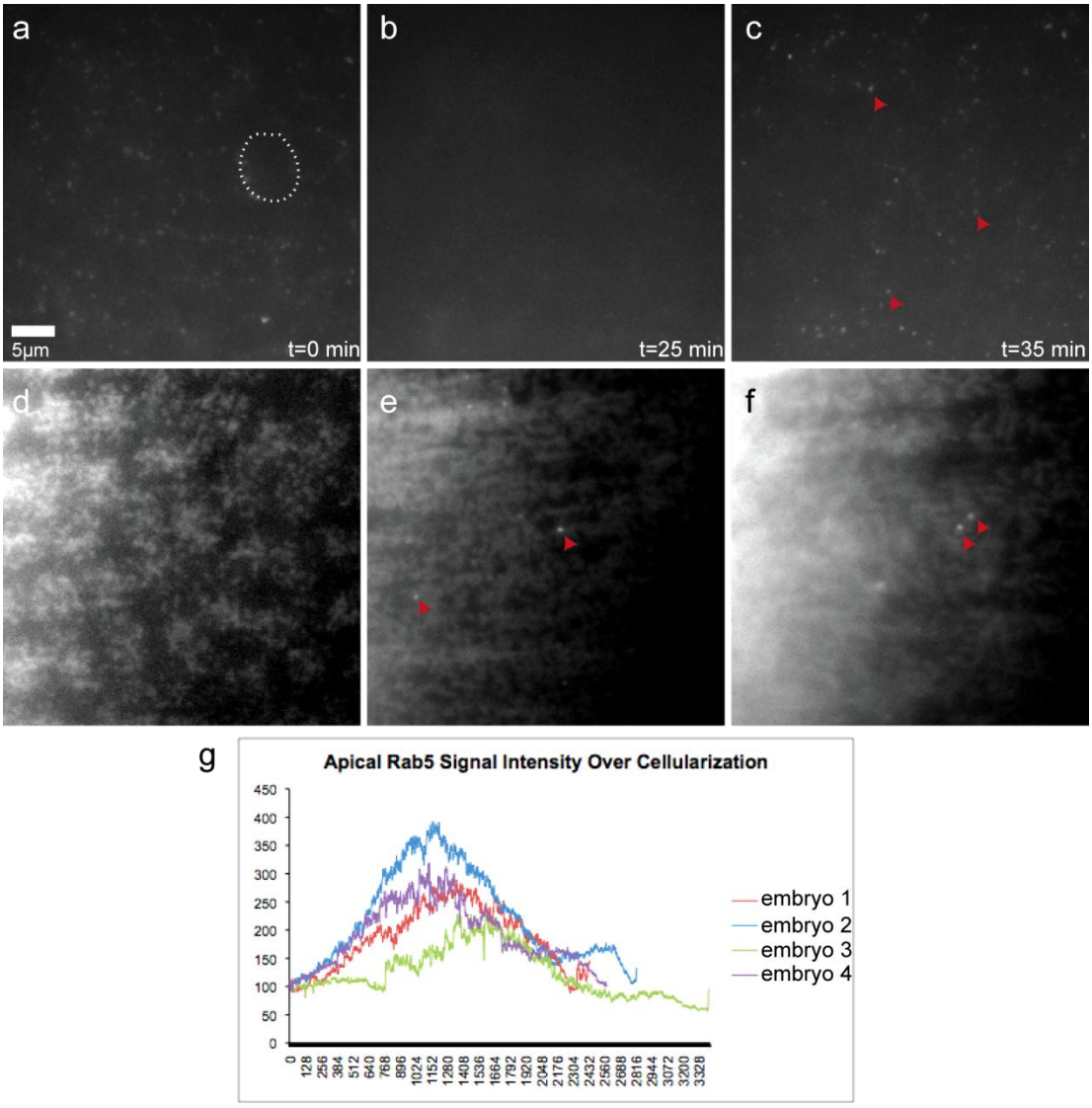

Figure 4.3 Rab5 but not Rab11 is apically upregulated during the fast phase of cellularization.

(a-c) TIRF view of YFP::Rab5 at the apical surface during cellularization. (a) At the beginning of cycle 14, Rab5 structures accumulate at the furrow canal. The dotted line represents the size of a single cell. (b) During the slow phase of cellularization Rab5 structures are lost from the apical surface. (c) A massive increase in the Rab5 signal is observed during the fast phase of cellularization. Red arrowheads indicate a subset of YFP::Rab5 puncta. (d-f) YFP::Rab11 expressed in the early embryo does not increase at the apical surface during cellularization. Single frames representing sequential time points from a time-lapse sequence representing the early (d), mid (e) and late stage (f) of cellularization. Most of the Rab11 signal is cytoplasmic. Sporadic YFP::Rab11-positive puncta can be observed at the apical surface (red arrowheads). (g) Quantification of YFP::Rab5 signal intensity over the course of cellularization from 4 unique

replicates. Quantification of each sample is represented by a different color (red, blue, green, violet). Notice a four-fold increase of the Rab5 signal at the time point corresponding to the end of cellularization.

4.4 The apical surface of the embryo is highly dynamic and undergoes morphological remodeling during cellularization

Previous electron microscopy data have shown that the apical surface of the early embryo is covered with a dense matrix of microvilli-like protrusions that are re-absorbed at the onset of gastrulation (Turner and Mahowald 1976). These data prompted me to ask whether the shift in endocytosis I observed was related to or even responsible for this morphological transformation of the apical surface. So far there is no information about the dynamics underlying surface remodelling. Therefore, I first decided to follow surface dynamics using TIRFM. I characterized the dynamics of the apical plasma membrane by imaging the fluorescent protein mCherry fused to the myristoylated peptide of GAP43, a well-established plasma membrane marker (Mavrakis et. al 2009). The result of this analysis showed that the apical PM undergoes various changes over the course of cellularization that can be classified in three stages. At the beginning of cycle 14 the apical membrane was covered with small, thin and highly dynamic protrusions (Stage 1, Fig. 4.4 a). These membrane protrusions first elongate and thicken at the beginning of fast phase (stage 2, Fig. 4.4 c) and then retracted at the onset of gastrulation (Stage 3, Fig 4.4 c). This massive retraction of apical plasma membrane protrusions resulted in flattening of the apical surface, in all cells of the embryonic epithelium. However, a few small differences between the dorsal and the ventral side of the embryo could be observed. On the dorsal side flattening was not complete and few long protrusions persisted especially in the inter-cellular space (Fig 4.4 d). The apical surface of ventral cells appeared instead completely flat. This dorso-ventral difference in apical morphology might reflect the need of ventral cells to completely flatten their apical surface in preparation for the cell shape changes (apical constriction) driving gastrulation (ventral furrow formation). All of the above results were confirmed in embryos expressing the trans-membrane protein spider (gish) tagged with the GFP as an independent membrane marker (Morin et al. 2001).

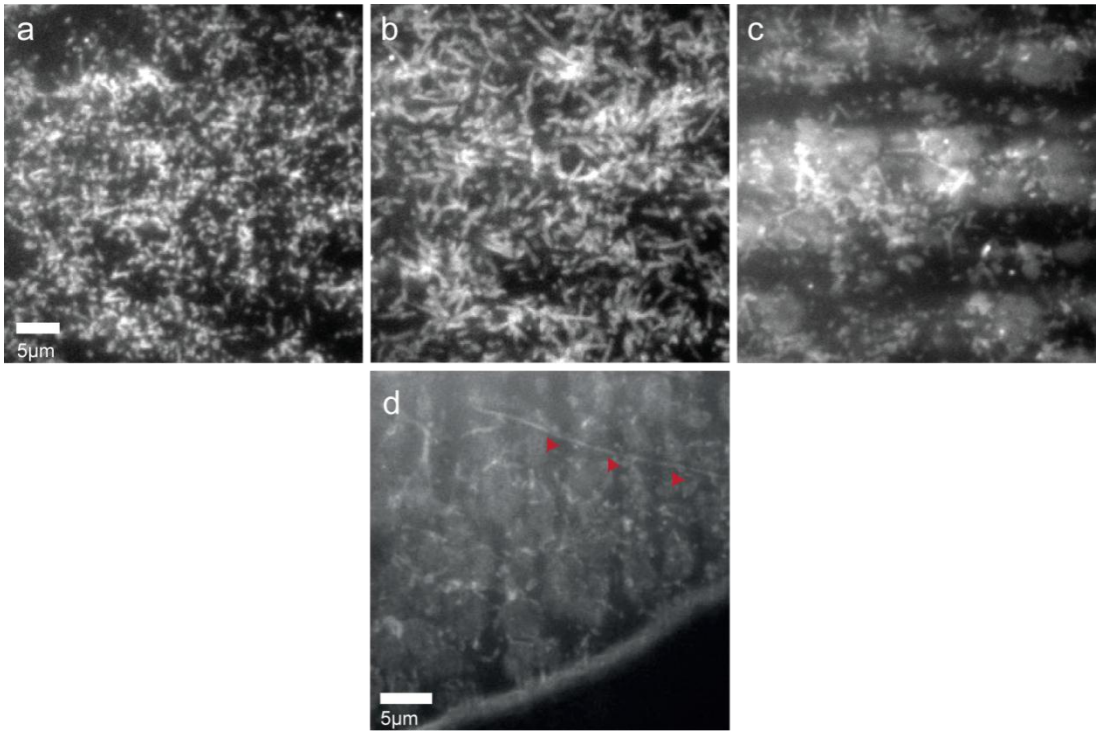

Figure 4.4 Apical surface of the embryo is covered with microvilli-like protrusions that undergo a stereotypical morphological change.

(a-c) Single frames from a timelapse TIRF acquisition of the apical plasma membrane (marked by GAP43::mCherry) over cellularization. (a) At the beginning of cycle 14, the apical surface is covered with small microvilli-like protrusions. (b) With time, apical protrusions elongate and thicken with some protrusions reaching a length of 5 µm (comparison to early cellularization). (c) At the onset of gastrulation, all of the cells flatten as a result of the retraction of protrusions. y,w*; sqh>GAP43::mCherry/+ flies were imaged on the lateral side. (d) View of the dorsal side of the embryo expressing spider::GFP. Following cell flattening some leftover protrusions can be observed (red arrowheads).

4.5 The up-regulation of apical Rab5 endosomes immediately precedes surface flattening

Since the increase in apical Rab5 endosomes and changes in apical membrane dynamics occur during the fast phase of cellularization, I decided to test if there was a correlation between these two processes. To analyze Rab5 and apical PM dynamics

together, the GAP43::mCherry and the Rab5::YFP were expressed at the same time. TIRFM imaging revealed that, during early cellularization, relatively few Rab5-positive endosomes exist at the apical plasma membrane (Fig. 4.5 a). In contrast, and consistent with a role for endocytosis in apical flattening, both the size and number of these Rab5-positive endosomes increased dramatically over the course of cellularization, reaching a peak immediately prior to apical flattening (Fig. 4.5 b). Furthermore, we could observe dynamic trafficking of Rab5-positive endosomes inside of individual protrusions prior to their retraction (Fig. 4.5 d). Importantly, over-expression of YFP::Rab5 did not alter the normal series of events observed in embryos expressing the plasma membrane marker alone.

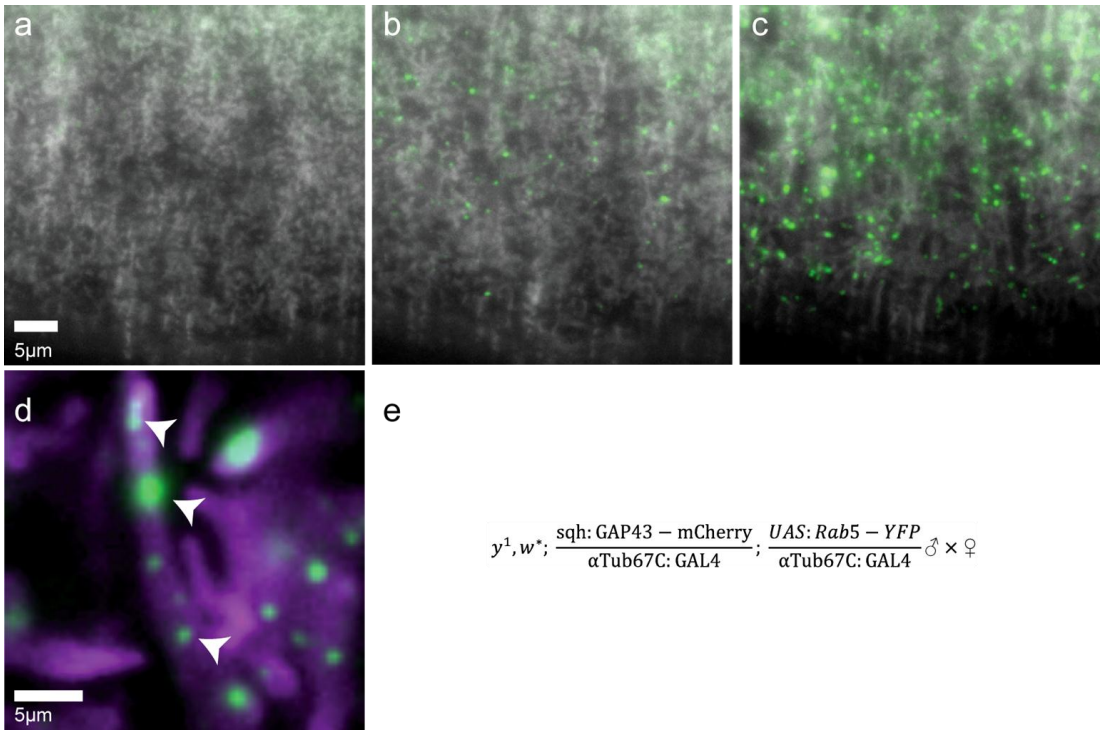

Figure 4.5 Increase of Rab5 at the apical surface of the embryo correlates with the elongation of protrusions.

(a-c) TIRF view of embryos that express YFP::Rab5 (green) and a membrane marker - GAP43::mCherry (grey). Single frames from a timelapse acquisition representing the early (a), the mid (b) and the late stage (c) of cellularization. (d) Zoom in on one of the protrusions marked with GAP43::mCherry (purple). YFP::Rab5 puncta travel inside the protrusions (green dots marked with arrowheads). (e) The genotype of the parental cross.

4.6 Analysis of endosome dynamics in endogenously tagged GFP::Rab5 expressing embryos

The test whether the up-regulation of Rab5 apical endosomes was not the consequence of an over-expression artefact, I decided to follow Rab5 endogenous dynamics. To this end, I replaced the gene coding for Rab5 with a GFP tagged Rab5 allele using the 'ends-out' homologous recombination technique (Huang et al. 2008). To perform this genetic manipulation I constructed a new targeting vector that significantly reduces the time needed to isolate positive transgenic flies (see Methods). I screened approximately 15 000 flies and I found 14 transgenic lines which had potentially Rab5 GFP inserted in the correct locus. I screened 9 of these lines by PCR and 5 of them were positive for the insertion of GFP-Rab5 in the correct locus (Fig. 4.6 c). Sequencing of genomic DNA confirmed the correct insertion. Unfortunately only approximately 10% of flies develop to homozygous adults indicating that tagging Rab5 with GFP creates a hypomorphic allele. This is quite surprising as tagging Rab5 at its N-terminus with GFP is extensively used in cell culture experiments. Nonetheless, heterozygous flies were viable with no visible abnormalities and were therefore used for all the subsequent experiments. Live imaging demonstrated that the GFP::Rab5 labelled structures were very similar to the structures labelled by YFP::Rab5 (over-expressed using the UAS/Gal4 system) (Fig. 4.6 d-f). Importantly, the number of GFP::Rab5 apical endosomes increased approximately four-fold over the course of cellularization (Fig. 4.7 a-c), thus confirming that the biogenesis of Rab5 endosomes is temporally regulated during development.

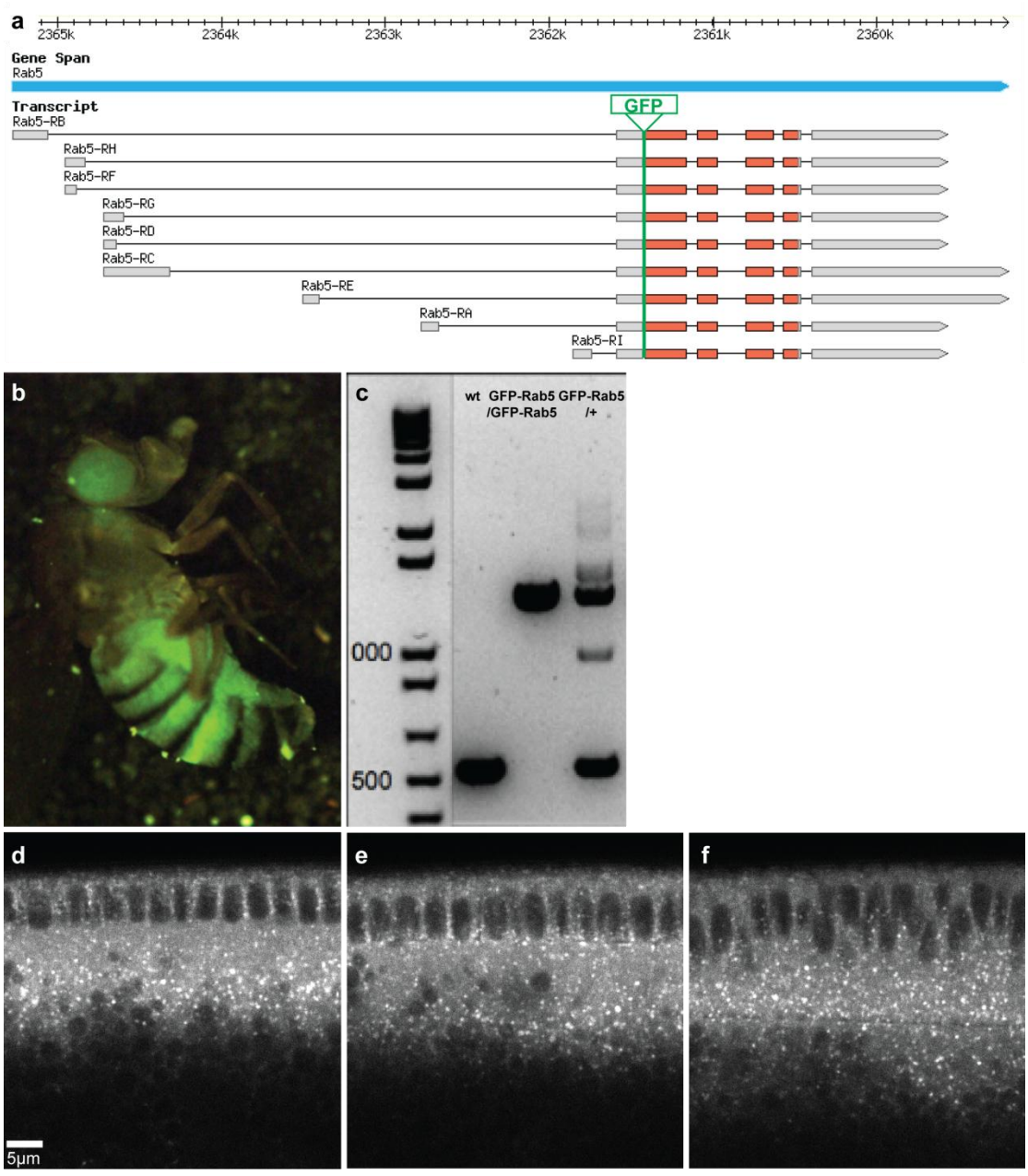

Figure 4.6 Generation of an endogenously tagged GFP::Rab5 transgenic fly line.

(a) Pictorial representation of the genomic region corresponding to the Rab5 locus. The Rab5 transcript has nine isoforms that have a common coding sequence (orange). A GFP tag was inserted in front of and in frame with the coding sequence the Rab5 (green line) by homologous recombination. (b) An image of a homozygous GFP::Rab5 adult female imaged under the fluorescent microscope showing GFP fluorescence. A particularly high level of GFP::Rab5 expression is present in the eye and the abdomen. (c) Potential recombination-positive flies positive were verified by PCR. Primers flanking the first codon were designed. These primers

give a 500 bp PCR product from the genomic DNA of the wild type flies (second lane). Recombinant flies homozygous for GFP::Rab5 give approximately 1200 bp PCR product as a result of the introduction of the GFP tag (third lane). As a control, heterozygous flies were used and show two products corresponding in size to the wild type allele and the GFP::Rab5 knock-in (right lane). (d-f) Expression pattern of the endogenously tagged Rab5 during cellularization. Single frames from a two photon timelapse over the course of cellularization.

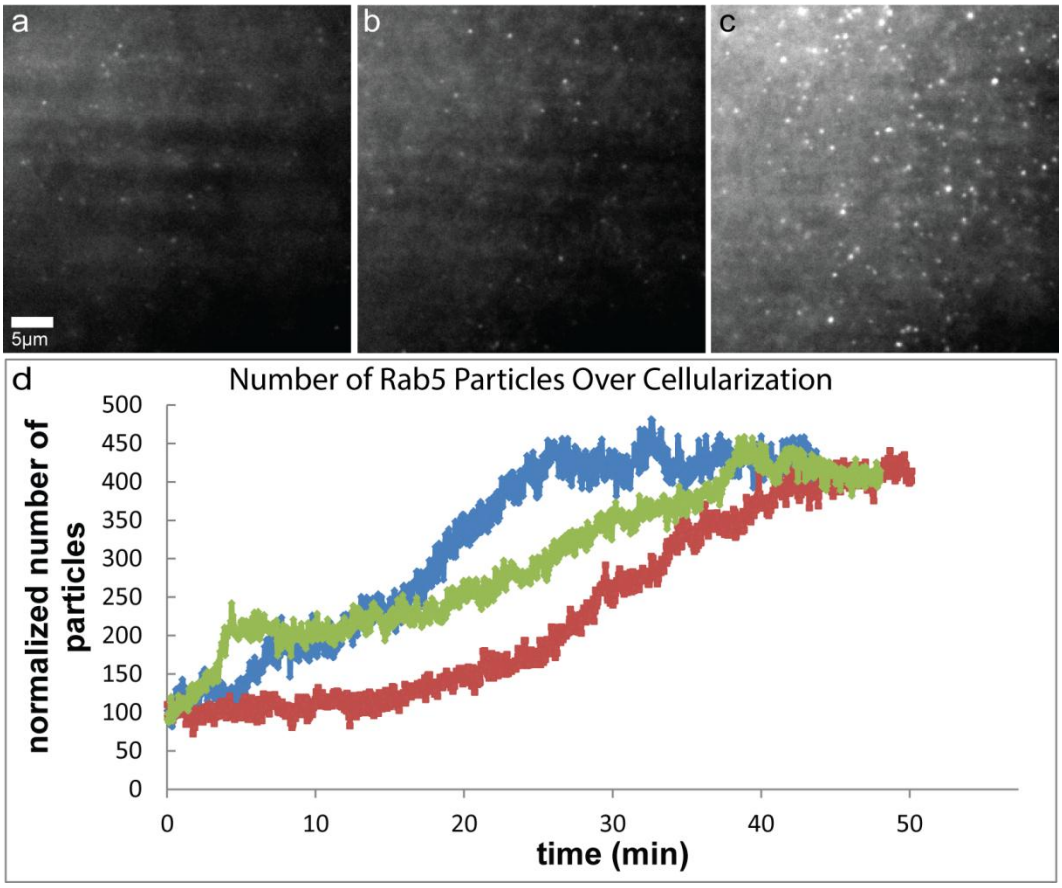

Figure 4.7 Endogenously tagged Rab5 displays a similar pattern of apical localization to the overexpressing line.

(a-c) Snapshots from the TIRF time course of the embryos expressing GFP::Rab5 under the endogenous promoter during early (a), mid (b) and late (c) stage of cellularization. Notice a significant increase in the GFP::Rab5 signal at the apical surface towards the end of cellularization. (d) Quantification of the number of the GFP::Rab5 particles over time. Quantification was performed for three different samples represented as three different colours (red, blue and green). At the end of cellularization a four to five fold increase in the number of GFP::Rab5 puncta can be observed.

4.8 Apically internalized fluid phase endocytic cargo localizes in apical Rab5 endosomes

Rab5 controls multiple steps along the endocytic pathway including endosome motility and fusion. To test whether the up-regulation of Rab5 endosomes corresponded to an actual endocytic event, the internalization of a fluid phase cargo was followed. To perform this experiment, I injected a solution of fluorescently labelled dextran into the perivitelline space. For technical reasons it was not possible to use TIRFM after injection, therefore, I used confocal microscopy. Upon injection, dextran diffused rapidly into the perivitelline space resulting in the counterstaining of the apical surface. Membrane protrusions appeared as dark non-fluorescent tubular extensions (Fig. 4.8 c). Internalized dextran was detected in vacuolar structures close to the apical plasma membrane (Fig. 4.8 a), as well as inside protrusions. To confirm that these structures represented *bona fide* endocytic events I performed two controls. First, I injected dextran into the embryo cytoplasm to check whether it can form aggregates that could appear as endosomes. This was clearly not the case. Second, I used pHrodo, a pH sensitive dextran that increases fluorescence in the acidic environment, and is therefore a suitable marker for acidified endocytic compartments. The fluorescence of the internalized pHrodo was clearly much higher than the non-internalized dextran residing in the perivitelline space (Fig. 4.8 b). In order to check if the internalized dextran localized to early endosomes I repeated this experiment in embryos expressing endogenously tagged GFP::Rab5. The result of this experiment clearly demonstrates that dextran was internalized into apical Rab5 positive vacuoles (Fig 4.8 d-f).

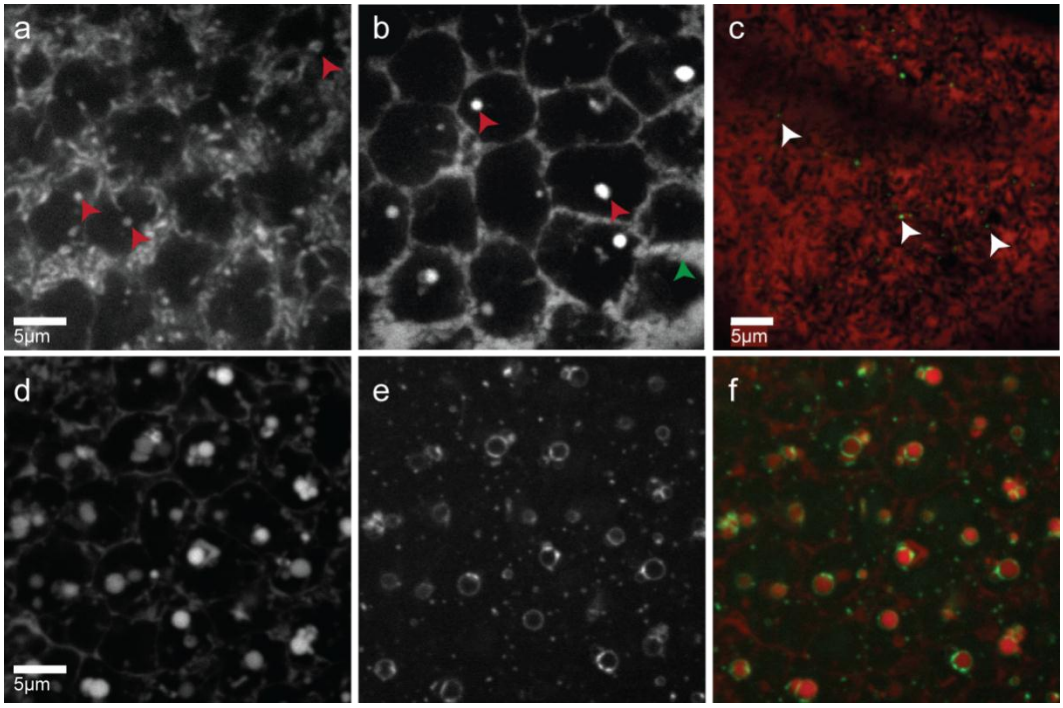

Figure 4.8 The shift in the apical GFP::Rab5 signal correlates with the uptake of the perivitelline fluid.

(a) Fluorescently labelled 10 000 MW dextran injected into the perivitelline space of a cellularizing embryo during the fast phase. Red arrowheads point to the internalized cargo. A single plane under the apical plasma membrane is presented. (b) pHrodo labelled 10 000 MW dextran injected into the perivitelline space of the wild type embryo. Internalized cargo is present in acidified compartments (red arrowheads) as the fluorescence is higher than in the perivitelline space (green arrowhead). (c-f) pHrodo dextran injected into endogenously tagged GFP::Rab5 embryos. (c) Rab5 positive structures (white arrowheads) are present in the apical protrusions counterstained with dextran. pHrodo accumulates under the plasma membrane (d) in GFP::Rab5-positive structures (e). (f) Merge of both channels. A single confocal plane was imaged.

The apical endocytic pathway described above has never been observed before. Previous studies attempting to visualize endocytosis in the early embryo were conducted using fluorescently labelled WGA. WGA binds to glycosylated residues of proteins present at the PM and therefore it may mark only a sub-set of endocytic pathways. To test whether WGA is internalized at the apical surface I tried to inject it in the perivitelline space. Unfortunately WGA clustered close to the injection site where the embryo is

damaged and the imaging conditions were poor. Therefore these experiments were not conclusive.

Next, I attempted to quantify the increase in apical endocytosis over time. Fluorescent labelled dextran was injected at the beginning of cellularization and embryos were imaged using confocal microscopy. This injection protocol turned out not to be suitable for long-term imaging and quantitative studies as a high number of embryos showed morphological abnormalities.

4.9 Apical endocytosis increases over the course of cellularization

In order to quantify apical endocytosis without damaging the embryo with perivitelline injection I thought of expressing a fluorescent secreted cargo in the embryo. I used both GFP and mCherry proteins fused to the signalling peptide of Fog (Fig. 4.9 a). Henceforth I will refer to this construct as secGFP. Fog is a signalling protein that is expressed and secreted during cellularization (Dawes-Hoang et al. 2005). Considering the fact that it might be difficult to distinguish fluorescent proteins that are undergoing secretion from the one that are being internalized I decided to spatially un-coupled secretion from endocytosis by using the 5' and 3' UTR of the bicoid gene to drive expression of secGFP. Bicoid is a transcription factor that is responsible for the determination of the anterior part of the embryo (Kilchherr et al. 1986). The mRNA of bcd is produced in the germline and is localized to the anterior of the oocyte. Moreover, the expression of the protein is suppressed until cycle 10 of nuclear division. This suppression is dependent on the 3' UTR of the bcd mRNA (Fig. 4.9 c-d) (Lasko 1999). I decided to drive the expression the secGFP–bcd 3'UTR construct under either the bcd or the αTub67C promoter (Fig 4.9 b). I generated transgenic flies and screened them for expression levels. The expression of the secreted GFP construct was detectable in the perivitelline space using two-photon microscopy (Fig. 4.9 e). The expression levels were however too low to perform time course experiments and no endocytic vesicles could be detected. Moreover, secGFP was often trapped intra-cellularly prior to cycle 14 (Fig. 4.9 f). In conclusion this approach was not suitable to perform time course internalization assays.

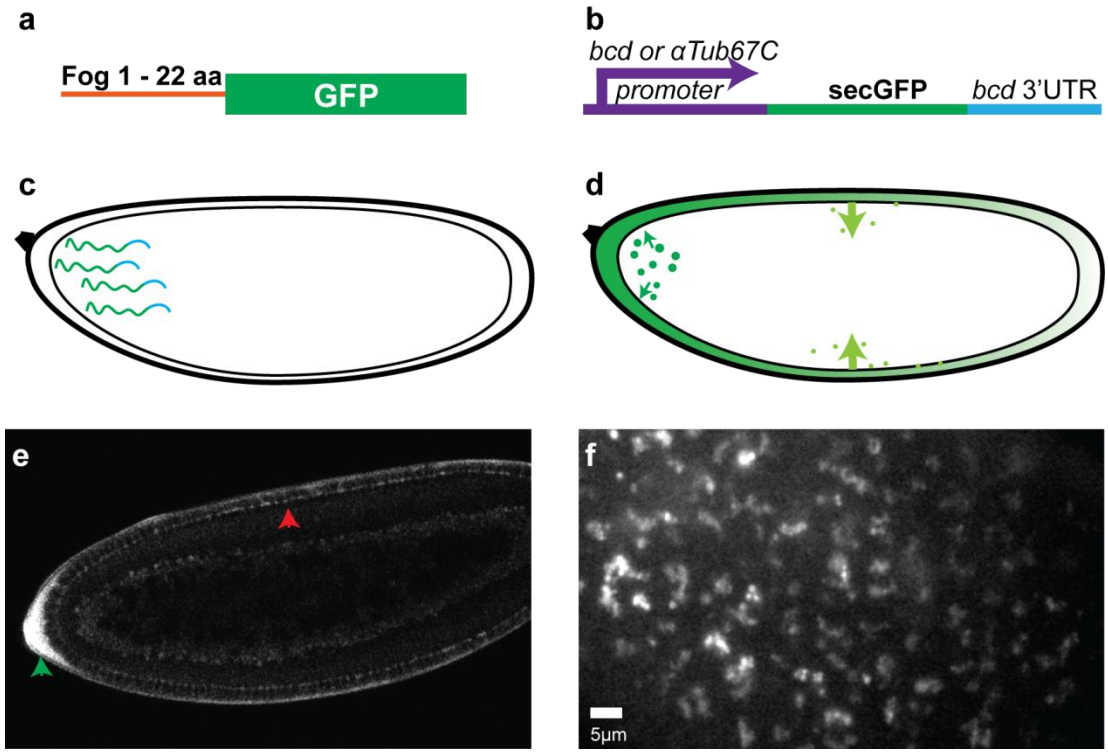

Figure 4.9 Design strategies for production of a genetically encoded cargo internalization assay.

(a) A cartoon representation of the secGFP protein. The fluorescent protein was fused to the first 22 amino acids of the Fog protein, which correspond to the Fog signal peptide. (b) secGFP was fused to the bcd 3'UTR and the bcd or the αTub67C promoter. The bcd 3'UTR is responsible for localization and anchoring of mRNA close to the anterior part of the embryo (c). The protein would be secreted into the perivitelline space in the anterior part of the embryo (d) (dark green). The assay would focus on the internalized signal far from the anterior pole (light green). (e) secGFP accumulates in the perivitelline fluid (green arrowhead) as well as in the furrows of the cellularizing embryo (red arrowhead). A single plane image taken with the two photon microscope. (f) During cycle of nuclear division 10, secmCherry surrounds the nuclei. No perivitelline signal can be detected at this point. Note that an intracellular signal can be detected in the whole embryo. A single plane Image is shown taken with the spinning disk confocal microscope.

The second approach I used was to express the same secreted GFP construct using the UAS/Gal4 system with the hope that maternally expressed proteins would accumulate in the perivitelline space prior to cellularization. Indeed using this approach, embryos secreted a sufficient amount of secGFP suitable for live imaging analysis. In addition,

most of the signal was detected in the perivitelline space at the beginning of cellularization and the signal in secretory compartments was below the detection limits. I therefore used this experimental condition to drive expression of secGFP and analyze apical endocytosis during cellularization. At the beginning of cycle 14, only few internalized structures positive for GFP signal could be detected (Fig 4.10 a'). As the embryo enters fast phase there was a dramatic increase in the number of internalized structures (Fig 4.10 b'-c'). Quantification of secGFP intracellular signal showed that apical endocytosis increased approximately five-fold from the beginning to the end of cellualrization. The timing of this increase perfectly correlated with the up-regulation of Rab5 apical endosomes (Fig 4.10 d).

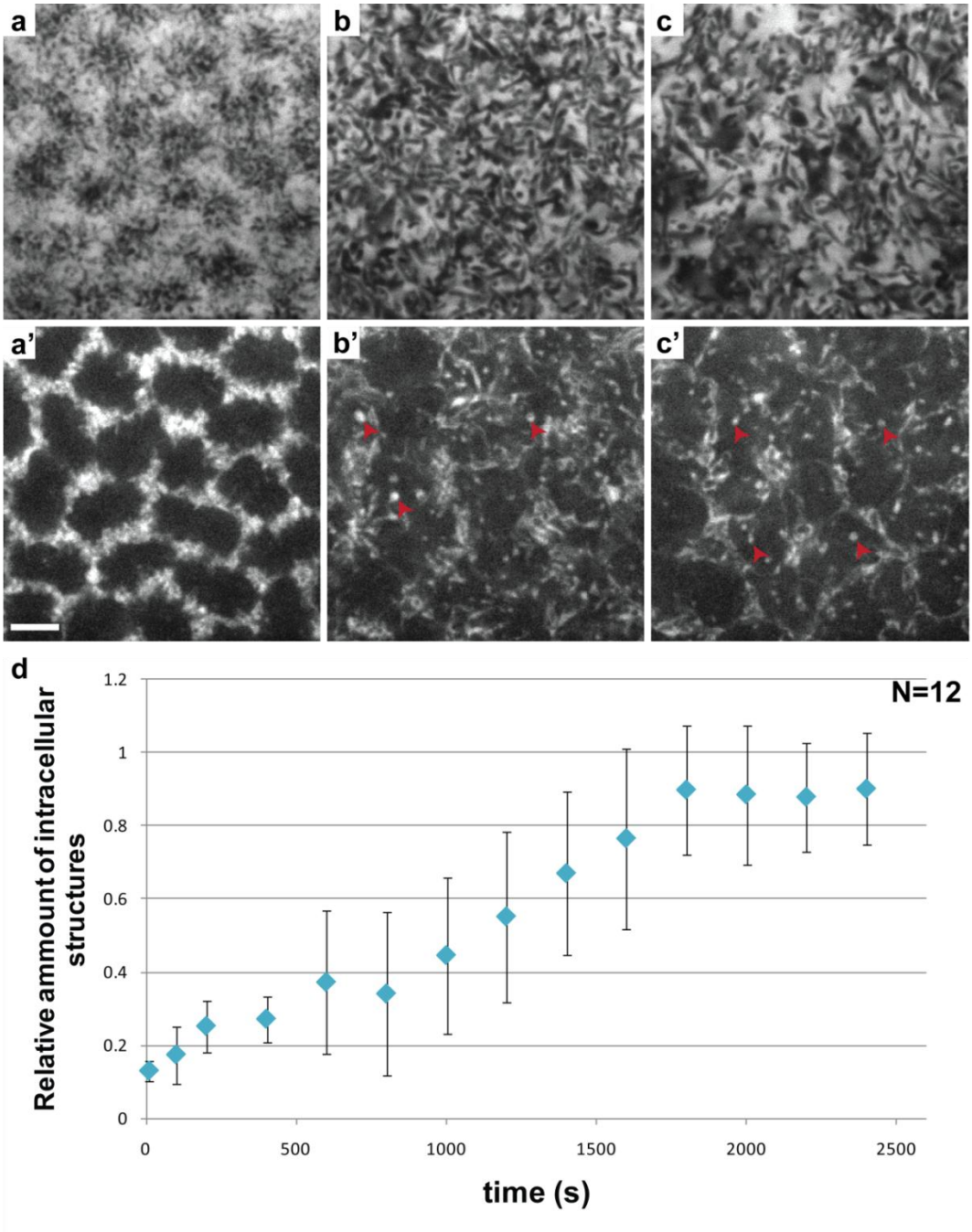

Figure 4.10 The rate of apical endocytosis increases during the fast phase of cellularization.

(a-c)(a'-c') Internalization the secGFP at the apical surface of the embryo during cellularization. y,w*,UAS-secGFP/Y/+; αTub67C>Gal4/+; αTub67C>Gal4/+ flies were imaged. Apical view of the apical protrusions counterstained with secGFP present in the perivitelline space during early (a), mid (b) and late (c) stage of cellularization. (a'-c') 1µm z maximum projection under the plasma membrane. At the beginning of cellularization no intracellular signal can be detected (a'). With the beginning of the fast phase intracellular vesicles can be detected (b'-c') marked with red arrowheads. (d) Internalization of cargo increases four-fold during cellularization. Relative

amount of internalized secGFP over time. Plot represents the intracellular structures counted at a given time point normalized to the time point with the highest amount of structures. (N=12). Error bars correspond to standard deviation.

This internalization assay also revealed that the major entrance route for soluble cargo is through tubular invagination of the plasma membrane (Fig. 4.11 a). Using 3D reconstruction I could show that these tubular invagination originate from the most apical surface of the PM (Fig 4.11 c-e) and in a single confocal plane they appeared as vacuoles rather than tubes (Fig 4.11 b). Importantly live imaging demonstrated that these tubular structures are pulled down from the PM and then pinch off forming vacuolar structures (Fig 4.11 d). Some of these vacuoles appeared as donut-like structures. Upon budding from the PM the GFP signal was very quickly quenched and it was therefore not possible to follow the fate of these vacuoles.

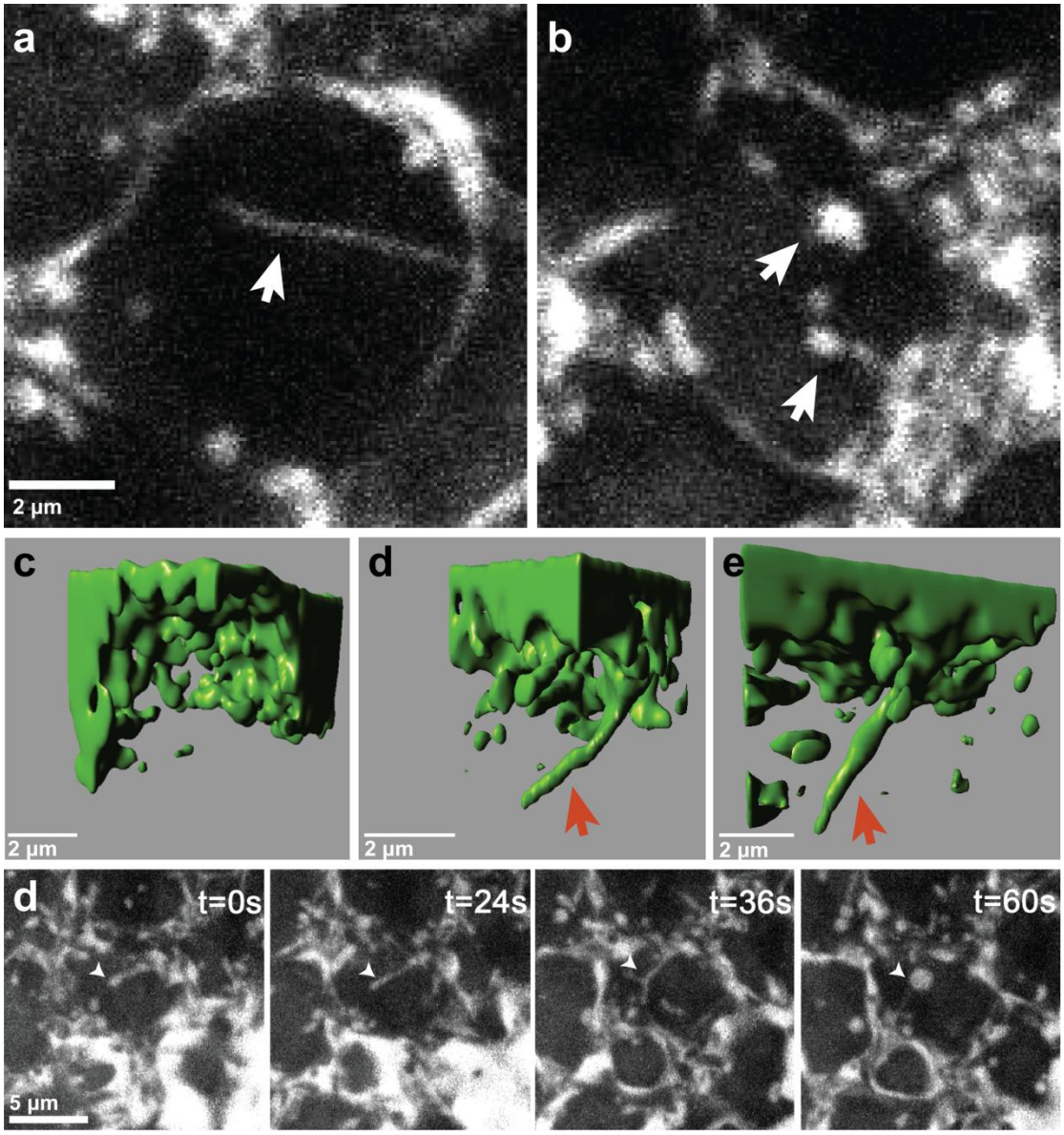

Figure 4.11 The main route for cargo internalization at the apical surface is through tubular endocytic intermediates.

(a-b) secGFP enters the cells by tubular intermediates as well as vacuolar structures. (a) A tubular intermediate originating from the plasma membrane (white arrow). (b) Example of vacuolar structure filled with secGFP close to the apical plasma membrane. A single confocal plane is shown (c-e) 3D reconstruction of the tubular structures originating from the most apical surface of the PM. secGFP is shown in green. The cell volume is transparent. (c) At the beginning of cellularization no intracellular tubes can be detected. During mid (d) and late stages (e) of cellularization 4-5 µm length intacellular tubes filled with GFP can be detected (orange arrows). (d) Snapshots illustrating pinching of the tubular intermediates. White arrowhead points on the

tube that is elongating. Between the t=36s and the t=60s a vacuole is formed. 2 µm z-stack under the apical plasma membrane is shown.

4.10 Dynamin activity is required for apical surface flattening

Since the observed increase in apical endocytosis coincides in time with changes in apical membrane dynamics I thought of testing whether endocytosis is directly involved in surface remodelling. To perform this experiment I used a mutant of dynamin (*shi*^{TS}) to block endocytosis. This well characterized temperature-sensitive mutation blocks dynamin activity at the non-permissive temperature (>29°C). Dynamin controls clathrin coated vesicles formation and it has been implicated also in other endocytic events including macropinocytosis (Chapter 1.3.3.4). Apical surface dynamics was analysed using TIRFM. Embryos carrying *shi*^{TS} and expressing GAP43::mCherry were covered with warm PBS (32°C) and transferred to a pre-heated microscopy chamber. Embryos that were heat shocked at the beginning of cellularization failed to form furrow canals and resulted in a rapid destruction of epithelial integrity. This result is consistent with previous reports (Pelissier, Chauvin, and Lecuit 2003). Embryos that were treated with warm PBS during the fast phase of cellularization still extended their lateral membranes. In this condition the growth of the cells was noticeably slower. Importantly, the apical surface of these embryos failed to flatten at the end of cellularization and the apical protrusions remained elongated (Fig. 4.13 d). These differences were quantified using a computational approach that was developed collaboration with Sebastian Streichan (Fig. 4.13 e-f).

To test whether the altered apical flattening was not the consequence of an artefact I performed two controls. First, I tested the influence of high temperature on apical flattening in wild type embryos. The result of this experiment showed that at 32°C plasma membrane flattening was not inhibited (Fig. 4.13 b). The second control I performed was to image shi mutant embryos at room temperature. Also in this case surface flattening occurred normally (Fig. 4.13 g-i). Thus, these experiments demonstrate that surface flattening is a dynamin-dependent morphogenetic process.

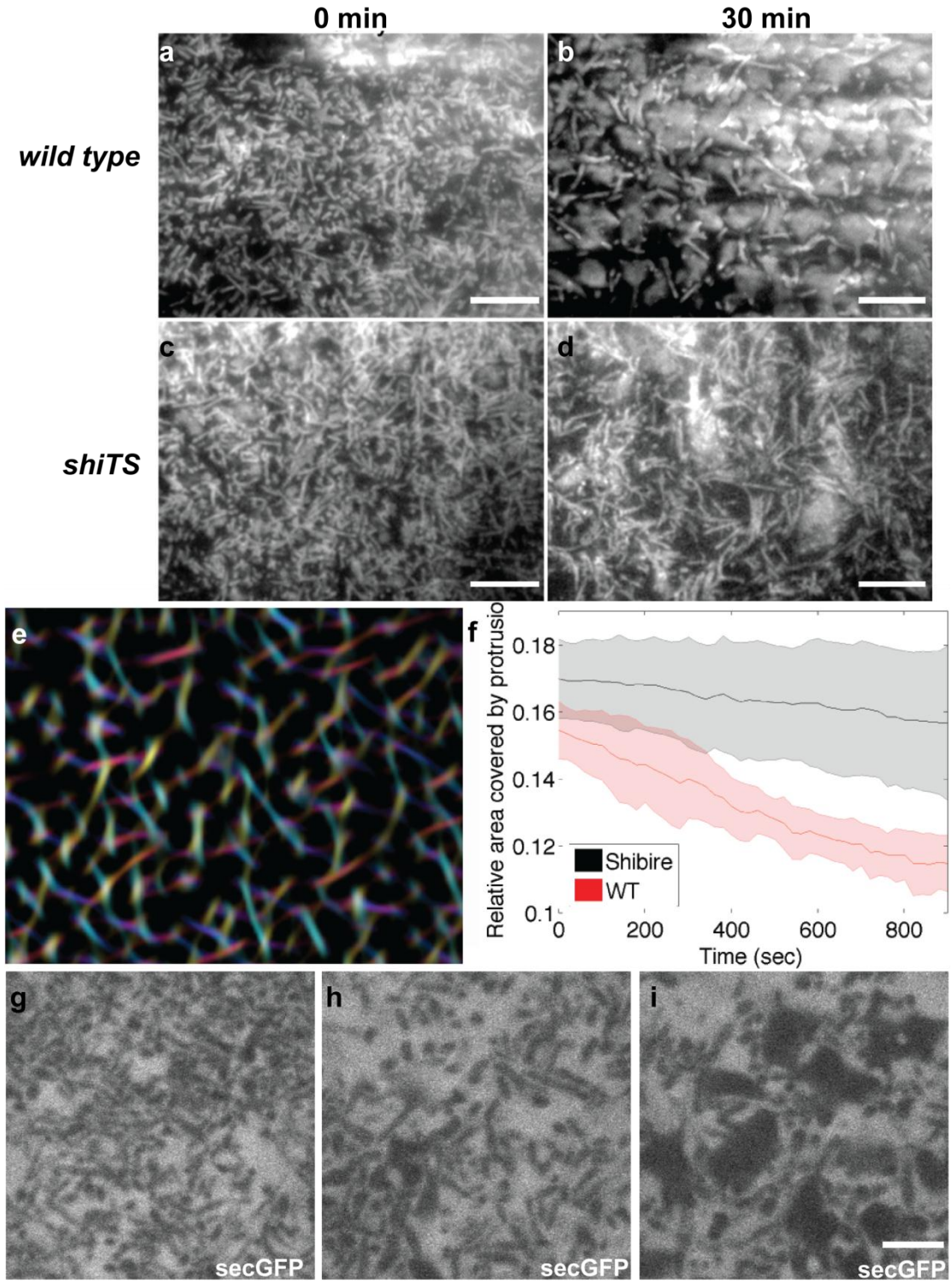

Figure 4.13 Endocytosis controls remodeling of the apical plasma membrane.

(a-b) TIRFM view of the apical surface of embryos expressing GAP43::mCherry imaged at 32°C. At the fast phase of cellularization the apical surface is covered with many protrusions (a) that

retract at the onset of gastrulation (b). (c-d) TIRFM view of the surface of *shi*^{TS} mutant embryos expressing GAP43::mCherry imaged at 32°C. (c) At the beginning of imaging at the non restrictive temperature the surface is covered with small protrusions. (d) In contrast, the apical surface of *shi*^{TS} mutant embryos remain covered with many protrusions at a time corresponding to when cells have flattened in wild type embryos. (e-f) Quantitative analysis of the apical protrusions in the wild type and *shi*^{TS} mutant embryos. (e) An example image of the apical protrusions detected by the 'mexican hat' filter (see Methods). (f) Relative area covered by protrusions over time. Notice that in *shi*^{TS} mutant the area covered by protrusions does not change over time. (g-i) Dynamin mutant embryos at room temperature do not show defect in apical flattening. View of the surface of *shi*^{TS} mutant embryos expressing secGFP imaged at room temperature. Mutant embryos imaged at early (g) mid (h) and late (i) stage of cellularization do not show defect in the morphology of apical plasma membrane.
(a-b) y,w*; sqh>GAP43::mCherry/CyO (c-d) *shi*TS; sqh>GAP43::mCherry/CyO
(g-i) *shi*^{TS}; αTub67C>Gal4/+; UAS>secGFP/ αTub67C>Gal4

4.11 Dynamin mediated endocytosis is responsible for apical upregulation of Rab5

In the next steps I tested the hypothesis whether observed increase in Rab5 signal and apical surface flattening are controlled by dynamin dependent endocytosis. In order to do that I generated flies expressing endogenously tagged Rab5 in the shibire mutant background. Using time course microscopy I followed GFP::Rab5 signal during fast phase of cellularization at non-permissive temperature.

Surprisingly, upon switching to non-permissive temperature almost instantaneously all Rab5 signal was lost from endosomal structures. Only cytoplasmic signal could be detected. (Fig. 4.14 b). To confirm that loss of endocytic Rab5 signal is due to the dynamin activity I performed two controls. First, I checked if co-expressing GFP::Rab5 and *shi*^{TS} can affect the localization of Rab5 by imaging mutant embryos at 18°C. As shown in Fig. 4.14, GFP::Rab5 was correctly localized. For my second control I checked if a temperature of 32°C has any effect on GFP::Rab5 localization. I imaged embryos expressing endogenously tagged Rab5 at 32°C and I could not detect any abnormality or difference compared to embryos imaged at room temperature or 18°C.

These results suggest that blocking dynamin function results in depletion of Rab5 positive endosomes. It also suggests that apical membrane flattening and increase in apical endocytosis are controlled by a single pathway dependent on dynamin.

Because tubular endocytic intermediates are the predominant form of apical endocytosis that can be detected, I asked whether dynamin controls budding of this type of vesicles and therefore controlled removal of apical plasma membrane.

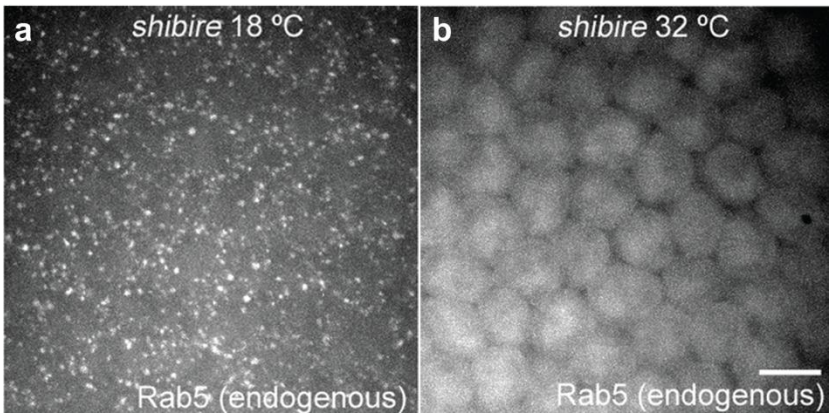

Figure 4.14 Dynamin controls biogenesis of Rab5 positive vesicles.

Live imaging of GFP::Rab5 expressed at endogenous levels in shibire mutant embryos reared at the permissive temperature (18 ºC, panel a) and at the non-permissive temperature (32 ºC, panel b) during mid-cellularization. The punctate distribution of Rab5-positive endosomes was lost upon inhibition of dynamin activity and exhibited a diffuse cytoplasmic distribution. Scale bar, 5 μm.

4.12 Blocking dynamin activity prevents the formation of intracellular tubes during the fast phase of cellularization

Having established that both surface flattening and apical endocytosis are dynamin-dependent, I next asked whether tubular endocytosis is also inhibited in shi^{TS} mutant embryos. For this experiment, I generated embryos expressing secGFP in a shi^{TS} background. Embryos were switched to 32°C during the fast phase of cellularization and imaged with the spinning-disk confocal microscope. Under these imaging conditions, membrane protrusions appeared as dark non-fluorescent elongated tubular extensions. Surprisingly no accumulation of vesicles could be observed upon switching to the non-permissive temperature (Fig 4.14 b). Moreover, no tubular structures were present inside the cells. This result demonstrates that dynamin activity is required for the

formation of tubular endocytic intermediates during surface flattening. The role of dynamin in tubular endocytosis must, however, be distinct from its role in vesicle fission. If dynamin were required for membrane fission, one would rather expect an elongation of tubular endocytic intermediates upon blocking dynamin.

In previous reports that analyzed the influence of *shi*^{TS} on endocytosis the incubation at the non-permissive temperature was performed for approximately 20-30 minutes. To reproduce these experiments, I performed time-course imaging and show that after approximately 15-20 min of incubation at 32°C small puncta did indeed accumulate under the apical plasma membrane (Fig 4.15 c). The size and the shape of these structures were compatible with that of CCVs. Thus, I conclude that in addition to its role in the formation of clathrin coated vesicle, dynamin controls also the activation of tubular endocytosis.

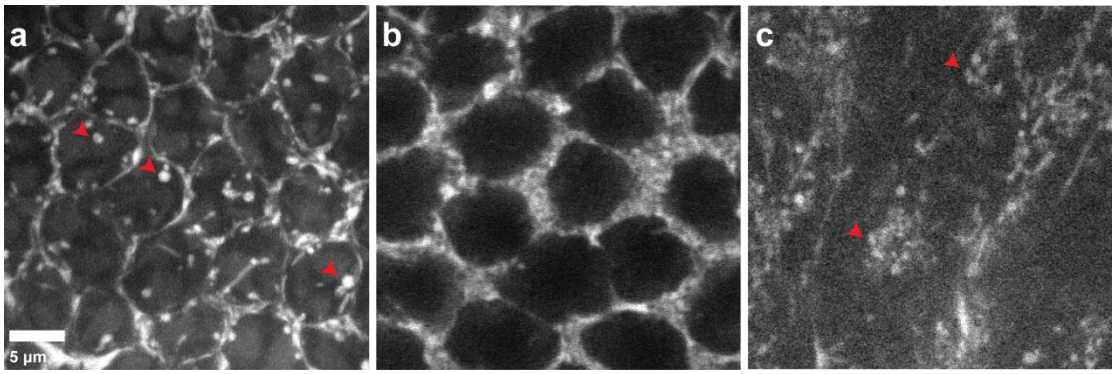

Figure 4.15 *shi*^{TS} inhibits the formation of intracellular tubes during the fast phase of cellularization.

(a) In the wild type embryos secGFP is detected in both tubular and vacuolar structures (red arrowheads) (b) In contrast, no intracellular structures are present at the non-permissive temperature in *shi*^{TS} mutant embryos. (c) 20 minutes after transfer to 32°C accumulation of small vesicles can be observed under the apical plasma membrane (red arrowheads). (a-c) 2 µm maximum intensity z-projection. (a) y,w*,UAS-secGFP/Y/+; αTub67C>Gal4/+; αTub67C>Gal4/+. (b-c) *shi*^{TS}; αTub67C>Gal4/+; UAS-secGFP/ αTub67C>Gal4.

4.13 Blocking dynamin function during the slow phase of cellularization does not prevent tube formation

Previous experiments had shown that blocking endocytosis at the beginning of cycle 14 resulted in the formation of long endocytic tubular structures originating from the invaginating furrows (Sokac and Wieschaus 2008a). This result suggests that there might be a similar mechanism controlling tube formation during the early stages at the furrow and during the late stage at the apical membrane. To test if shi controls formation of both endocytic structures I blocked dynamin in early cellularizing embryos. As readout for endocytosis I used secreted GFP. In agreement with previous reports, blocking shi activity at the beginning of cellularization resulted in the retraction of lateral membranes and arrest of cellularization (Fig. 4.16 a). Differently from the behaviour of apical endocytic tubes, intracellular tubes emerging from the furrow could still be observed upon blocking dynamin activity. These structures formed and then rapidly retracted back without budding (Fig 4.16 b-d). Therefore, the effect of dynamin inhibition on tubular endosomes emerging from the apical PM and the furrows is different. The activity of dynamin at the furrow is compatible with its role in vesicle scission as blocking its activity resulted in the elongation of tubular structures and delay in budding. The activity of dynamin at the apical plasma membrane is instead required for the initiation of membrane tubulation suggesting the presence of different endocytic mechanisms operating at the apical plasma membrane (see next chapters).

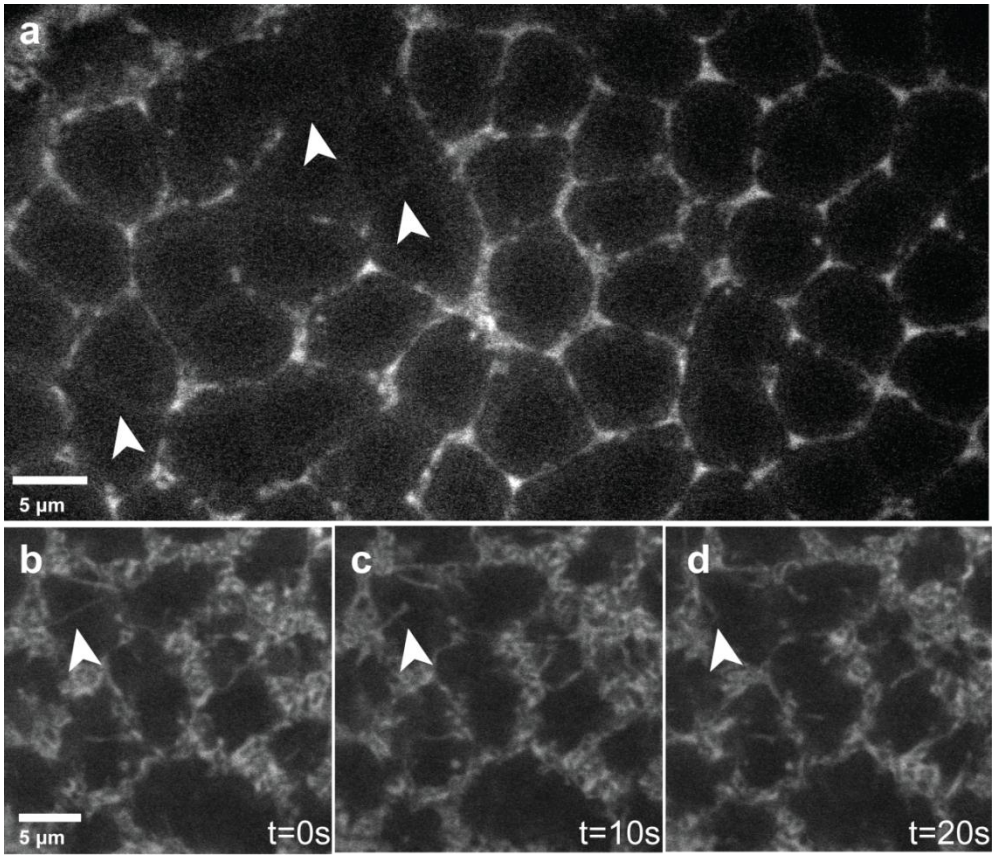

Figure 4.15 *shi*^{TS} inhibits the budding of endocytic tubes during the slow phase of cellularization.

(a) Blocking shibire function at the beginning of cellularization results in furrow regression. *shi*^{TS} embryos (b-d) Snapshots from the time-course analysis of tube formation during the slow phase of cellularization. Intracellular tubes formed (b) retract back to the PM (c) and disappear (d). No pinching could be observed. Images from a single plane acquisition are shown.

4.14 Rab5 localizes to tubular endocytic plasma membrane invagination

The injection of fluorescent dextran into the perivitelline space showed that apically internalized cargo is promptly delivered to Rab5 positive endosomes (see Chapter 4.8)**.** However, in this experiment I did not address the association between intracellular tubes and Rab5. One possibility is that the increase in Rab5 signal at the apical plasma membrane results from the budding off directly from the tubular intermediates. To test this hypothesis, I performed time-course analysis of tube formation

filled with secreted mCherry in embryos expressing endogenously tagged Rab5. This experiment revealed that intracellular tubes originating from the PM are marked with Rab5 (Fig. 4.16 a-c), which localizes to the distal part of the tubes (Fig. 4.16 b-c). At the beginning of the endocytic process, Rab5 signal accumulates at the apical plasma membrane (Fig. 4.16 d, t=0 min). Afterwards, only a distal part of the forming tube is marked with Rab5 (Fig. 4.16 d, t=1 min). In the next minute Rab5 positive vacuoles are formed (Fig. 4.16 d, t=2 min). Afterwards these vacuoles travel towards the base of nuclei (Fig. 4.16 d t=3 min). These results complement the data obtained with the dextran injection experiments and suggest that Rab5 associates and might function directly at the plasma membrane during surface flattening.

In summary, the data collected so far demonstrates that apical endocytosis controls flattening of the apical membrane during the late stages of cellularization. This process is dynamin dependent. Dynamin controls the formation of tubular intermediates and tubular intermediates are the main route for the internalization of apical cargo. The formation of tubular endocytic intermediates coincides in time with the up-regulation of Rab5 endosomes and Rab5 itself localizes to the tip of this tubular invaginations. In order to address the role for Rab5 in regulating intracellular tubes it would be advantageous to block specifically Rab5 function at the apical PM during the fast phase of cellularization.

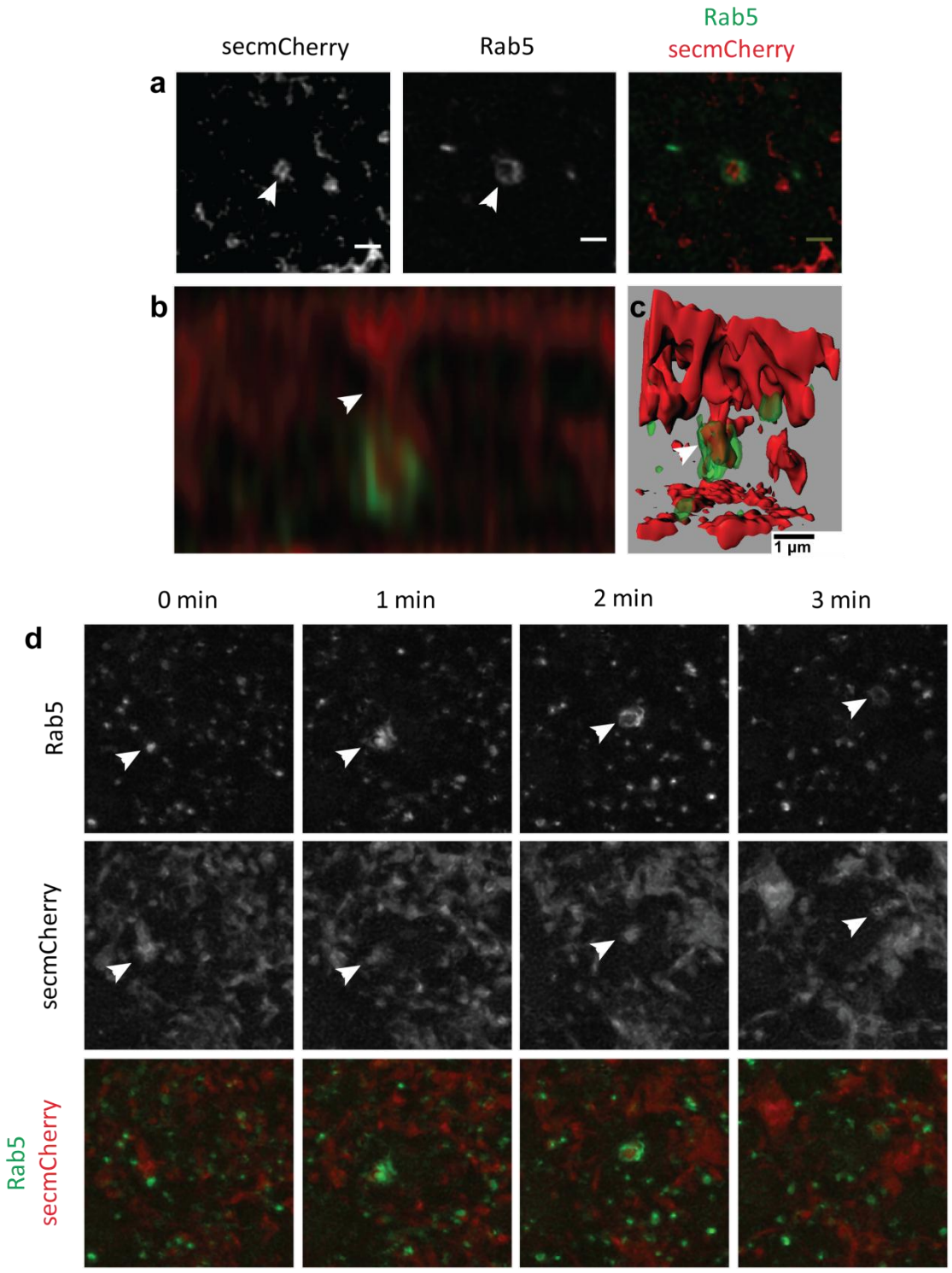

Figure 4.16 Rab5 associates with both tubular intermediates and nascent vacuoles.
GFP::Rab5 is associated with apical tubulo-vacuolar structures. secCherry cargo is surrounded by GFP::Rab5 signal (arrowheads). A single confocal plane is presented (b) GFP::Rab5 signal is

present at the distal part of the pinching tube. White arrowhead points on the part of the tube that is not marked by GFP::Rab5. (c) 3D reconstruction of a representative GFP::Rab5-positive tube. A secCherry filled tube originating from the apical PM is surrounded by GFP::Rab5 signal (white arrowhead). (d) Time-course analysis of the association of GFP::Rab5 with a budding tubular intermediate. A 4 µm confocal z-projection under the apical PM is shown. At the time point t=0 min only a small GFP::Rab5-positive domain is localized to the the apically formed tube. At time (t=1 min) this GFP::Rab5-positive domain expands on the tube and persists on the nascent/budded vacuole that moves towards the base of the nuclei (t= 2 min and t=3 min). Embryos were obtained from the following parental cross: (a-d) y,w*; GFP-Rab5/ αTub67C>Gal4; UAS-secmCherry/αTub67C>Gal4.

4.15 Approaches to inactivate Rab5 during surface flattening

To investigate the role of Rab5 on formation of endocytic tubes and flattening of apical PM I tried two different approaches. First, I tried to over-express Rab5S43N mutant during the fast phase of cellularization. The Rab5S43N mutation mimics the GDP bound conformation of Rab5 (see Chapter 1.3.3.3). Injection of recombinant Rab5S43N blocks cellularization and therefore it could be a useful tool to modulate Rab5 activity (Pelissier, Chauvin, and Lecuit 2003). To avoid any possible artefacts caused by injection into embryos, I decided to ectopically express Rab5 mutant during cellularization. Transgenic Rab5S43N lines available from the Bloomington Stock Center do not yield necessary level of expression for this experiment; therefore I generated and tested eight new transgenic lines. Unfortunately, none of these lines expressed the construct, which was confirmed by western blot analysis.

In the second approach I wanted to take advantage of endogenously GFP-tagged Rab5 line that I generated (see Chapter 4.6). I tried to develop chromophore-assisted light inactivation (CALI) in cellularizing embryo. This method is based on the principle that illumination of the fluorophore generates high amount of oxidative species. These are able to destroy proteins in close proximity to the illuminated fluorophore (McLean et al. 2009). In this case illumination of GFP would generate oxidative species that would affect Rab5 function. I used a two photon microscope to perform this experiment in embryos homozygous for GFP::Rab5. The main objective of the experiment was to find an appropriate laser power that would generate high amount oxidative species. Because previous reports (Pelissier, Chauvin, and Lecuit 2003) shown that Rab5 is necessary for

the furrow progression I tested different laser settings focusing on the furrow marked with Rab5. The laser power setting tested in cell culture resulted in embryos lysis, probably due to the high thermal energy released in the focal plane. Therefore, I gradually lowered the laser power to the point when lysis was not observed. At this setup photobleaching of the Rab5 was prominent. Unfortunately, Rab5 signal recovered to the endocytic structures almost immediately. This suggests that Rab5 is exchanged very fast on endocytic structures. It also suggests that Rab5 is not a suitable target for CALI.

4.16 The *Drosophila* homolog of human Rabankyrin-5 is an abundant Rab5 effector in the early developing embryo

To gain further insight about the Rab5 specific function at the apical membrane, I decided to search for Rab5 effectors using affinity chromatography on a large pool of cellularizing embryos. For this experiment I collected 20 g of 0–4 hours old embryos and prepared a soluble cytoplasmic extract. This extract was incubated with recombinant GST-Rab5 loaded with either GTP-γ-S or with GDP as a control. Proteins that were bound specifically to the GTP form of Rab5 were sequenced by mass spectrometry Fig. 4.17 a). Using this approach I found that the Drosophila homolog (CG41099) of human Rabankyrin-5 is the main binding factor of Rab5 during early embryonic development. Rabankyrin-5 localizes to different types of vacuolar structures that originate from the apical membrane in epithelial cells and fibroblasts (Chapter 1.3.3.3b). Little is known about the underlying molecular mechanism of Rabankyrin-5 function in endocytosis.

CG41099 transcripts have four isoforms. PA is the shortest one and does not contain the BTB domain. The isoforms PC and PD differ of only two amino acids at the N-terminus, while PB is 11 amino acids shorter than PC. In the Rab5 chromatography experiment an approximately 120 kDa protein was identified that correspond to one of the longer isoforms. I chose CG41099-PC for further investigation (Fig. 4.17 b). I confirmed the direct interaction between Rab5-GTP and CG41099. Unfortunately, I was unable to express the long isoform with the in vitro translation protocol (see Methods). Instead I used CG41099-PA construct for this experiment (Fig. 4.17 c).

In the next steps I tested the hypothesis that Rabankyrin-5 control apical endocytosis during surface flattening.

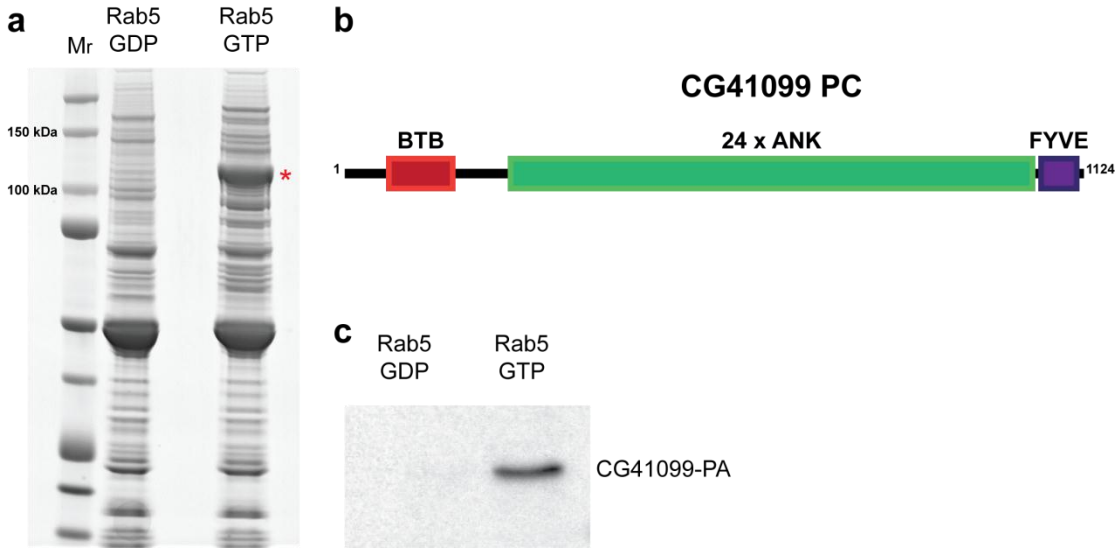

Figure 4.17 CG41099 is an abundant Rab5 effector expressed during the early *Drosophila* development.

(a) Identification of Rab5 effectors expressed during early *Drosophila* development. Rab5 affinity chromatography on a soluble fraction from 0-4 h old embryos. A picture of an acrylamide gel with resolved proteins stained with coomasie brilliant blue. The first lane represents a protein molecular weight marker. The second lane represents proteins bound to Rab5 loaded with the GDP. The last lane represents proteins bound to Rab5 loaded with the GTP-γ-S. The red asterisk points to the band identified by mass spectrometry as CG41099. (b) A graphical representation of the CG41099-PC domains. (see chapter 1.3.3.3b) (c) CG41099 interacts directly with Rab5. Direct interaction between Rab5-GTP-γ-S and the CG41099-PA was confirmed using an in vitro translation protocol. In the first lane no binding can be observed between the CG41099-PA and GDP-bound Rab5. In the second lane a clear binding between the CG41099-PA and GTP-γ-S-bound Rab5 was detected.

4.17 CG41099 localizes to apical vacuolar structures in the early embryo

Because there was no information available on the *Drosophila* homolog of human Rabankyrin-5, I decided to closely characterize both protein localization and its role in endocytosis during cellularization. To do that I generated transgenic flies expressing

CG41099-PC tagged with GFP on the N-terminus. I used the UASp promoter to express the transgene during oogenesis.

First, I investigated if *Drosophila* Rabankyrin-5 can be detected close to the apical plasma membrane. I performed time course imaging with TIRFM and spinning disk confocal microscope. In the result, I could observe a clear CG41099 signal in apical protrusions (Fig. 4.18 a-c). In addition, a more prominent signal could be observed on big vacuolar structures close to the apical plasma membrane (Fig. 4.18 d-f).

Interestingly, GFP::CG41099 signal does not localize uniformly on vacuolar membranes. The pattern resembles a diamond ring, where a bright domain is present on an otherwise uniformly stained vacuole. This pattern probably represents either accumulation of Rab5 or localization of PI3P domains on endosome. Moreover, detected signal persisted on vacuoles for short time. Additionally, homotypic fusion between Rabankyrin-5 positive vacuoles could be easily observed (Fig. 4.18 d-f). This result is in line with previous reports which showed that one role of human Rabankyrin-5 is to promote homotypic fusion between endosomes (Schnatwinkel et. al 2006)

In next step I decided to investigate whether CG41099 is involved in apical endocytosis. In this experiment I followed secreted mCherry in the GFP::CG41099-PC expressing flies (Fig 4.18 g-i). During the slow phase of cellularization no CG41099-positive structures containing secreted mCherry could be observed. Just before cell flattening big vacuoles containing cargo appeared in the sub-apical region (Fig 4.18 g-i).

To analyze the behavior of these endocytic structures I focused on the region between 2 and 4 microns below the apical membrane. I could observe formation of Rabankyrin-5-positive structures originating from intracellular tubular structures. Because time resolution was a limiting factor in this experiment, it is not clear whether Rabankyrin-5 appears on tubes just before or immediately after the budding event.

Studies performed in MDCK cells suggest that over-expression of Rabankyrin-5 can induce apical endocytosis (Schnatwinkel et al. 2004). The test whether formation of Rabankyrin-5 positive structures was not the consequence of an over-expression artefact I generated a polyclonal antibody against the *Drosophila* Rabankyrin-5 and I performed immunochemistry on fixed wild-type embryos (Fig 4.18 k). I could confirm that vacuolar

structures positive for Rabankyrin-5 were present in the cellularizing embryos. These structures were present both at the apical and basal part of the cell. However, in general, only one or two vacuoles per cell could be detected. This is probably due to transient occupancy of Rabankyrin-5 on endosomes.

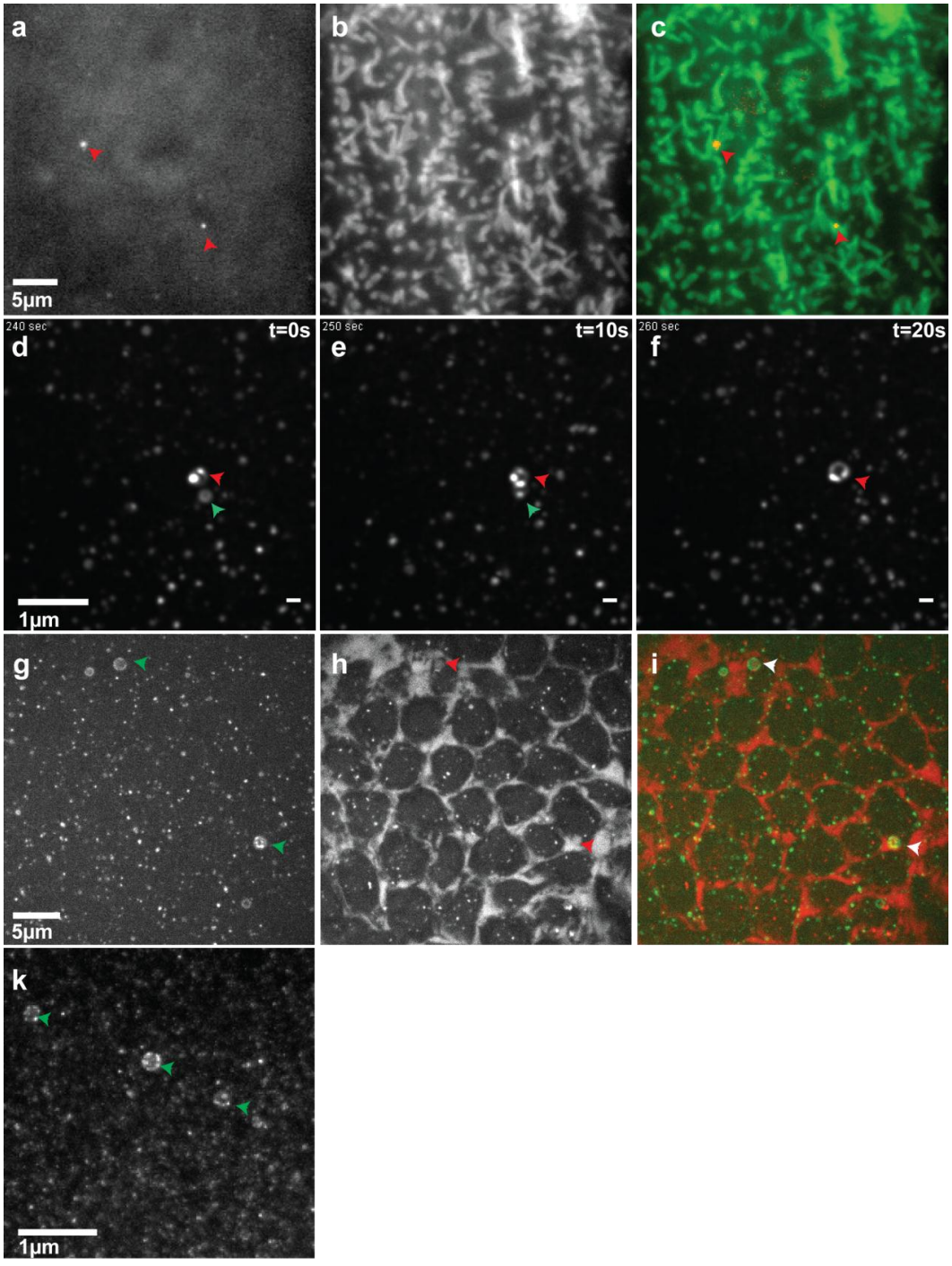

Figure 4.18 CG41099 localizes to apical vacuolar structures.

(a-c) GFP::CG41099 is present at the apical surface during cellularization. (a) TIRF view of the GFP::CG41099 puncta that are present at the protrusion plane during cellularization. (b) Apical membrane marked with the GAP43::mCherry (c) Merge of both channels. (d-e) GFP::CG41099-positive vacuoles are present under the apical membrane. Ectopically expressed GFP::CG41099 was analyzed by confocal microscopy. Fusion between two individual vacuoles can be observed (arrowheads). Notice that the protein is distributed into domains on the vacuoles. 2 µm z-stack is presented. (g-i) GFP::CG41099 expressed together with secCherry colocalize in subapical vacuoles. 2 µm z-stack is presented. (g) Subapical vacuoles originated from the pinching tubular intermediates are marked with GFP::CG41099 (green arrowheads). (h) These vacuoles are filled with secCherry cargo (red arrowheads). (i) Merge of both channels. (k) Immunostaining against endogenous CG41099 in the cellularizing embryo. Fluorescence immunostaining with an antibody raised against CG41099 stains vacuolar structures in wild type cellularizing embryos (arrowheads). Notice that staining is not uniformly distributed on the vacuoles, rather it is heterogeneously distributed around them. 6 µm z-stack is presented.
Parental crosses:
(a-c) y,w*; sqh > GAP43::mCherry/ αTub67C > Gal4; UAS- GFP::CG41099-PC/ αTub67C > Gal4. (d-f) y,w*; +/ αTub67C > Gal4; UAS-GFP::CG41099-PC/ αTub67C > Gal4. (g-i) y,w*; UAS-secCherry/ αTub67C > Gal4; UAS- GFP::CG41099-PC/ αTub67C > Gal4. (k) OregonR.

4.18 CG41099 controls the maturation of tubular intermediates at the apical plasma membrane

In the next step, my goal was to establish a relationship between Rabankyrin-5 and apical endocytosis. Because CG41099 gene is positioned in the heterochromatin region of the third chromosome, it is not possible to generate a mutant with the available genetic tools. In recent years a new tool for the gene knock down in the germ line was developed by Perrimon lab. It is based on the RNA interference with the use of the short hairpin constructs. This method was tested during the oogenesis and there is no information whether it is also suitable for cellularizing embryos (Ni, J-Q. et. al 2008)

To test this method I expressed shRNA targeting CG41099 in female germline with UAS/Gal4 system. I tested the efficiency of this RNAi method in reducing both the mRNA and the protein levels. The qPCR analysis revealed that the RNA level coding for Rabankyrin-5 was reduced 95-99% (Fig. 4.19 a). To check the variability between the samples analysis were performed both on a single and 10 embryos. Detected variability was below 5%.

In order to analyze the protein level of the CG41099 in the cellularizing embryos, I took advantage of the antibody that was raised against the protein. There was almost complete reduction in protein level in the shRNA expressing line comparing to wild type embryos (Fig. 4.19 b).

In the next step I analyzed the apical membrane and endocytic tubes in Rabankyrin-5 knock down embryos. I used secGFP to follow apical surface dynamics and endocytic vesicles. Surprisingly, the apical surface of cellularizing embryos was not affected. However, analysis of endocytic intermediates revealed that, while in control embryos vacuolar structures form rapidly (Fig. 4.19 d), in Rabankyrin-5-depleted embryos vacuoles form from long tubular membranes. These structures can extend for over 15 microns along the apico-basal axis of cell (Fig. 4.19 e). In addition, these extended membranes are budding in discrete portions. Instead, in the wild type embryos a single apical vacuole is budding from the apical plasma membrane. In both cases formed vacuoles travel towards the base of nuclei.

Interestingly, this phenotype is particularly prominent in ventral cells. To test whether apical endocytosis is more abundant in the ventral region of the embryo I compared the amount of budding vesicles between dorsal and ventral cells. In agreement with the observation coming from previous experiment, the mean amount of vesicles in ventral cells in wild type embryos was three times higher in comparison to the dorsal region (Fig. 4.19 f).

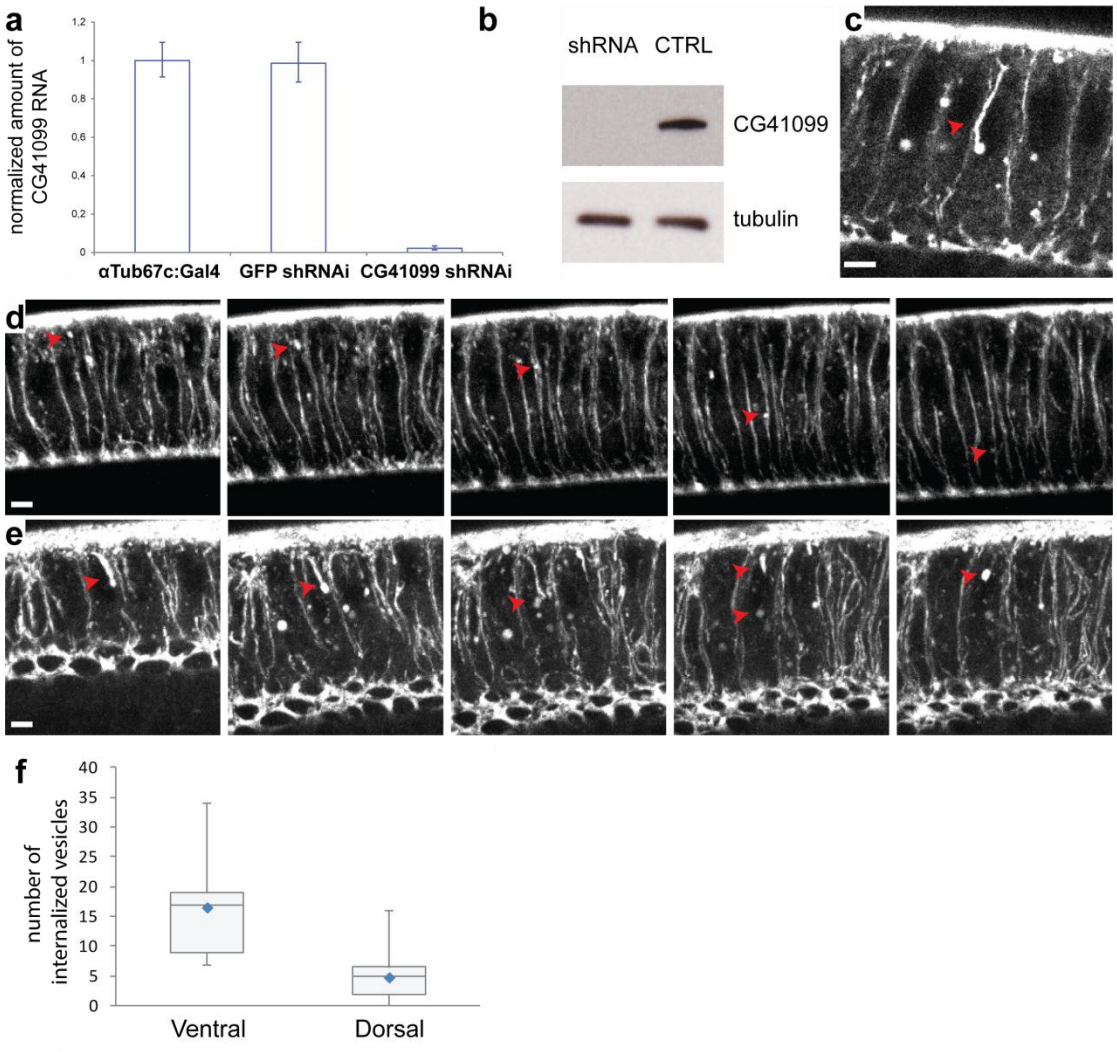

Figure 4.19 CG41099 controls maturation of the apical tubules.

(a) Expression of the Rabankyrin-5 shRNA reduces Rabankyrin-5 at both the mRNA and protein level. qRT-PCR shows a 98% reduction of Rabankyrin-5 mRNA in a shRNA-expressing line in comparison to the GAL4 driver line alone or to a line expressing GFP shRNA. (b) Western-blot analysis of the Rabankyrin-5 endogenous levels in Gal4 driver and in Rabankyrin-5 knock-down lines. Rabankyrin-5 protein level is undetectable in the cellularizing embryos expressing shRNA targeting the gene in comparison to GAL4 driver line embryos. Lower panel shows alpha-tubulin signal as a loading control. (c) Phenotypic characterization of ventral cells during cellularization in Rabankyrin-5 knock-down embryos. Single plane from the two-photon aquired image of the ventral cells of an embryo expressing Rabankyrin-5 shRNA and secGFP. Arrowheads indicate an elongated intracellular tube filled with secGFP. (d) Timecourse showing formation of the apical vacuoles in the embryos expressing secGFP. 5 micron z-projection stills from the ventral side of the embryo. Arrowheads indicate vacuoles filled with sec::GFP moving towards the base of the cells. Timepoints correspond to t=0s, t=100s, t=160s, t=190s, t=235s.

(e) Timecourse showing elongation of the intracellular tubes in the Rabankyrin-5 knock down embryos. 5 micron z-projection stills from the ventral side of the embryo expressing the Rabankyrin-5 shRNA and the secGFP. Arrowheads indicate maturation of the elongated intracellular tubes marked with the soluble GFP. Timepoints correspond to t=0s, t=225s, t=300s, t=525s, t=550s. Scale bar is 5 microns.
Parental cross:
(d) y,w*,UAS-secGFP/Y/+; +/ αTub67C > Gal4; +/ αTub67C > Gal4.
(c),(e) y,w*,v^1,UAS-secGFP/Y/+; /+; +/ αTub67C > Gal4; UAS-CG41099 shRNA/ αTub67C > Gal4.

4.19 Ultrastructural analysis of endocytic structures in cellularizing embryos

In order characterize the morphology of the endocytic structures involved in this novel pathway, Aleksandar Necakov performed correlative EM tomography on cellularizing embryos.

First, we analyzed the apical tubules coming from the apical region of the cells. These endocytic intermediates appeared as convoluted membrane structure. Similar to the 3D reconstruction (presented in Fig. 4.20) intracellular tubes consist of a neck and a vacuolar regions. The diameter of the vacuolar part is about 500 nm. Moreover, many invaginations protruding inside the vacuolar parts that could be observed. The presence of an area of ribosomal clearing around these structures is indicative of actin polymerization. A typical endocytic intermediate is presented in Fig. 4.20 a,b.

Next, we analyzed the membranes positive for CG41099. Because antibody against the CG41099 did not work for immunolabelling, we took advantage of the transgenic line expressing GFP::CG41099. By the combination of fluorescent microscopy and EM tomography we were able to reconstruct GFP::CG41099 positive membranes. GFP::CG41099 localizes to convoluted membranes detected close to the apical surface (Fig. 4.20.c-d). 3D reconstruction of these membranes revealed their toroidal-like structure. This suggests that the budded tubular membranes are able to self-fuse in a process similar to autophagosome formation (Xie and Klionsky 2007).

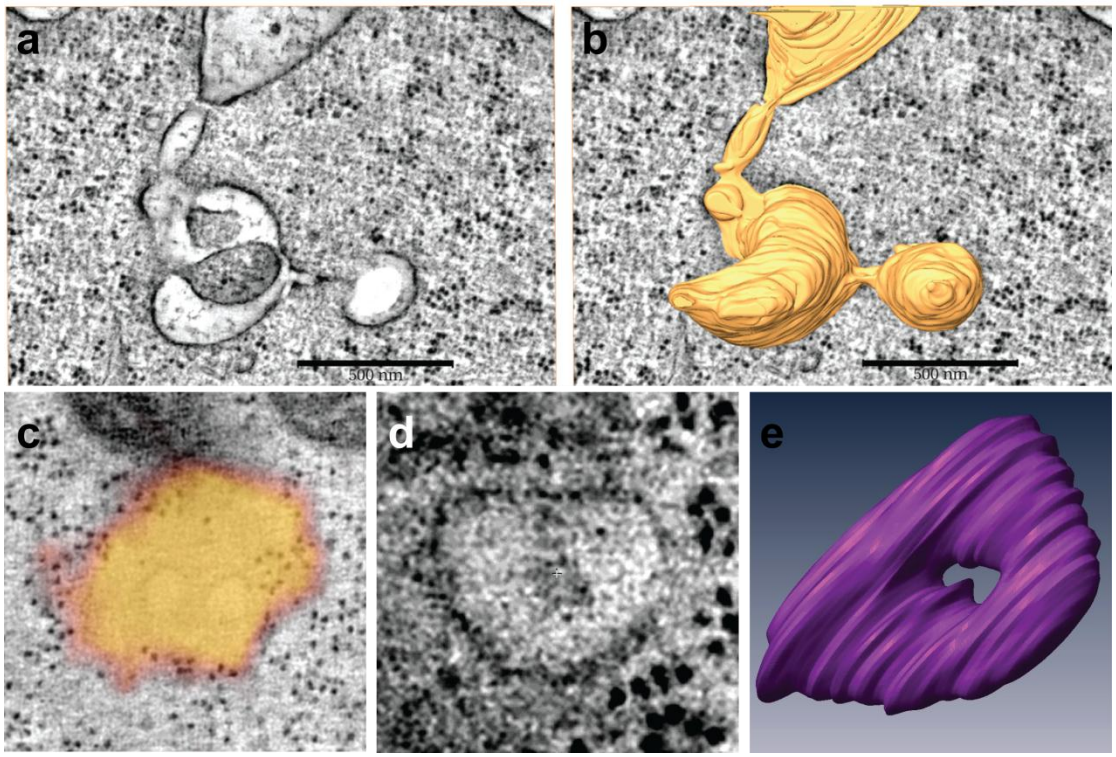

Figure 4.20 CG41099 controls maturation of the apical tubules.

(a-b) Endocytic tubular intermediates originating from the apical plasma membrane. EM tomography of an apical endocytic tubule showing multiple internal compartments in direct continuity with the apical plasma membrane. (a) A single section through an EM tomogram of a tubular endocytic structure in direct continuity with the apical plasma membrane. (b) Three-dimensional surface rendering of the tubular endocytic volume from the corresponding volume generated by EM tomography demonstrating the continuity of the tubular-endosomal structure with the apical plasma membrane at top. (c-e) Correlative light-electron micrograph showing the overlay of GFP::CG41099 fluorescence onto a corresponding EM tomogram of the same region. (d) High-magnification view of a section of the EM tomogram corresponding to the region underlying the GFP::Rabankyrin-5-positive spot labelled in panel (c). (e) Three-dimensional surface rendering of the convoluted, tubular-membranous, GFP::Rabankyrin-5-positive structure underlying the fluorescence spot marked in panel (c.) Scale bar= 500 nm

Chapter 5 Discussion

5.1 The apical plasma membrane of cellularizing *Drosophila* embryo undergoes specific morphological changes during development

The specialized function of many different epithelial cell types depends on the structural organization of their apical plasma membrane. Microvillous-like protrusions are involved in processes such as nutrient uptake, mechano- and photosensing, cell-to-cell adhesion and communication between cells (Frolenkov et al. 2004; Pellikka et al. 2002; Vasioukhin et al. 2000). Ruffling and formation of apical protrusions in the brush border of the gut and kidney epithelia control nutrient and solute uptake via macropinocytosis (Mercer and Helenius 2009). During embryonic development, for example in early starfish embryos, specialized apical protrusions are involved in stabilizing the position of the blastoderm inside the egg shell (Matsunaga et al. 2002). The shape and length of apical protrusions is tightly regulated and reflects their specialized function. For example, the length of mechano-sensory stereocilia present in the inner ear results in reception of specific wavelength of sound (Lin, Schneider, and Kachar 2005). While the length of apical microvilli originating from the follicle epithelium in maturing *Drosophila* egg chambers is necessary for the secretion of the vitelline components (Schlichting et al. 2006). These are only few examples of plasma membrane structures forming at the apical plasma membrane of polarized cells. In this thesis I focused on the mechanisms underlying the remodelling of the apical plasma membrane during early *Drosophila* development.

Previous electron microscopy studies had shown the presence of many microvilli-like protrusions at the apical surface of the early *Drosophila* embryo, which disappear at the onset of gastrulation (Turner and Mahowald 1976). These observations led to the model that villous projections are the initial pool of membrane, which is redistributed during cellularization. In my analysis I did not observe a massive accumulation of apical membrane prior to cellularization as it was previously suggested. Instead, in the initial phase of cellularization cells have many small villi that are elongating and are moving dynamically with the progress of the membrane furrow. Towards the end of cellularization these villi are reabsorbed and the apical membrane becomes flat. While the role of actin cytoskeleton in shaping the apical membrane is well

established, the organization of apical endocytosis during cell and tissue morphogenesis has been so far poorly investigated. Therefore, I addressed the contribution of membrane trafficking in controlling apical plasma membrane remodelling during cellularization.

5.2 Endocytosis drives plasma membrane flattening during epithelial morphogenesis

During the early stages of cellularization, endocytosis is particularly prominent at the invaginating furrow canals and is controlled by actin. (Sokac and Wieschaus 2008a) Cargo internalized at the furrow was detected in endocytic structures marked with Rab5. In addition, results presented by Pelissier et al. have shown that Rab5 has a crucial role in lateral membrane elongation during cellularization (Pelissier, Chauvin, and Lecuit 2003). However, these studies did not focus on the dynamics of the Rab5 machinery and did not address the role of endocytosis in apical remodelling during cellularization. By following the dynamics of endogenously tagged GFP::Rab5, I confirmed the results of Sokac, et al. The Rab5 signal is present at the furrow during first three stages of cellularization. However, during the fast phase of cellularization I discovered a second burst of endocytosis taking place at the apical surface that has never been described before. Rab5 signal at the apical membrane increases four-fold towards the end of cellularization. These apical Rab5 endosomes are highly dynamic and move towards the basal side of the cell in close proximity to invaginating furrow. My results demonstrated that this increase in apical Rab5 endosomes can be observed along both the dorsal-ventral and anterior-posterior axes, thus arguing for the presence of a general regulatory mechanism underlying the up-regulation of apical endocytosis.

To test whether apical endocytosis plays a role in controlling the morphology of apical membrane I decided first to analyze embryos expressing both, Rab5 and a plasma membrane marker. I found that appearance of apical Rab5 positive carriers coincide with the remodelling of the protrusions. To test directly whether endocytosis control apical morphology, I took advantage of flies carrying a temperature sensitive dynamin mutant allele (*shibire*^{TS}). I observed two phenotypes, first, blocking endocytosis resulted in the regression of the membrane furrow. This observation is consistent with previous reports showing that endocytosis is needed for furrow progression. Second, apical villi were

longer compared to wild type flies and the plasma membrane failed to flatten. The elongation of apical protrusions suggests that endocytosis plays an important role in controlling the shape of the apical membrane at the onset of gastrulation. Moreover, I showed that blocking dynamin activity during the fast phase of cellularization resulted in the complete depletion of Rab5 positive endocytic structures. This result indicates that dynamin activity is directly responsible for the up-regulation of Rab5 endosomes during membrane flattening.

What is the role of membrane flattening during cellularization? The timing of apical surface flattening led to the model that villous projections act as membrane reservoir. However, so far there is no direct evidence supporting this hypothesis, because there are no available tools to visualize the redistribution of internalized membranes during cellularization. Although the work of Pelissier et. al demonstrated that shibire is necessary for cellularization and that injection of dominant negative Rab5 during slow phase leads to a delay in furrow progression, there is no clear experiment addressing whether this effect is due to the function of Rab5 at the furrow or at the apical surface (Pelissier, Chauvin, and Lecuit 2003). The same limitation applies to the experiments done in shibire mutant background. By following both Rab5 and a soluble cargo, I could show that endosomes originating at the apical plasma membrane travel towards the base of the cells. This in principle could indicate that endocytic membranes are transported from the apical surface to the furrow.

One interesting observation is that endocytosis is more prominent in ventral cells. These cells will give rise to the mesoderm of the embryo. Ventral cells are morphologically distinct from the rest of the cellular blastoderm. They become longer during cellularization and the apical adherent junctions are located more apically comparing to their neighbours in the ectoderm (Leptin and Grunewald 1990). These cell shape changes immediately precede apical constriction and formation of ventral furrow. One possibility is that apical endocytosis could contribute to the redistribution of membranes in ventral cells during cell elongation. Another hypothesis is that membrane removal from the apical surface is necessary for proper apical constriction. Recent work by Lee et. al has shown that injection of dominant negative Rab5 or inhibition of dynamin activity results in apical constriction defects during *Xenopus* gastrulation (J.-Y.

Lee and Harland 2010). The same defects were observed in cells undergoing constricting during the morphogenesis of the neural tube. In addition, endocytosis was shown to control membrane removal during dorsal closure in *Drosophila* (Mateus et al. 2011). The data presented in this thesis show that the up-regulation of apical endocytosis precedes any visible change in the reduction of the apical surface area. Therefore, I hypothesis that endocytosis acts up-stream of apical constriction by removing membranes and thus facilitating the constriction of the actin-myosin network. Collectively all these data strongly argue that removal of apical membranes might be a general mechanism underlying apical constriction. To test this model it would be important to identify specific regulators of apical endocytosis.

5.3 The primary entry route for apical endocytic cargo is through endocytic tubules

To directly visualize apical endocytosis during surface flattening I developed a genetically encoded cargo uptake assay. Using this assay, I demonstrated the up-regulation of Rab5 endosomes corresponds to a *bona fide* increase in apical endocytosis. I observed a significant accumulation of internalized, fluorescently labelled cargo, underneath the apical surface shortly before the end of cellularization. Strikingly, this experiment revealed that the primary entry route for soluble cargos is through tubular intermediates that, upon budding from the plasma membrane form vacuolar-like structures. These structures originate at the very apical and subapical part of the plasma membrane. These tubular intermediates can extend up to 5 microns in length are surrounded by actin filaments. More importantly formation of these tubules is dynamin dependent. Interestingly, recent work of Levayer et. al has identified similar apical endocytic structures during germ-band extension in *Drosophila* (Levayer, Pelissier-Monier, and Lecuit 2011). These endocytic structures are involved in establishing planar polarity of apical adherence junctions during morphogenesis. They showed that tubular membranes serve as platforms for budding of clathrin-coated vesicles. My analysis of the apical tubular intermediates forming during cellularization revealed that these two structures are different. First, the structures described in this thesis bud off the plasma membrane as whole, and do not seem to serve as a platform for CCVs. Second, in the

analysis presented by Levayer et. al, blocking dynamin activity leads to accumulation of tubular intermediates at the plasma membrane. In contrast, apical endocytic structures present during cellularization are completely abolished in dynamin mutant. Interestingly, there is another type of tubular endocytic intermediates forming during cellularization. These structures were previously described by Sokac et. al. and their formation is restricted to the base of the furrow canal (Sokac and Wieschaus 2008a). In the shibire mutant these endocytic intermediates fail to detach from the plasma membrane, similar to the structures observed by Levayer et. al. Therefore the apical endocytic tubules present during cellularization form via a novel endocytic mechanism. Tubular endocytosis has been studied in mammalian cell culture and is associated, but not exclusive, for the internalization of GPI-anchored proteins. This pathway is referred to as the CLIC (clathrin-independent carriers) pathway and is controlled by the Rho GTPase (Sabharanjak et al. 2002; Lundmark et al. 2008). Ultra-structural analysis of the carriers presumably originating from endocytic tubes during cellularization revealed their complicated, doughnut-like shape. These endosomes resemble endocytic carriers previously associated to the CLIC pathway (Howes et. al 2010).

Although CLIC carriers have many morphological similarities to the endocytic tubules described in this thesis they do differ in size. While the structures present in *Drosophila* have a diameter of approx. 200-500 nm, the CLIC structures present in cell culture are approx. 40 nm (Lundmark et al. 2008). This might indicate that either these two endocytic structures do not represent the same pathway or that their morphology is not conserved between *Drosophila* and mammalian cells. One prominent regulator of the CLIC pathway is GRAF1. Therefore, the generation of GRAF1 knockout flies should help elucidating its *in vivo* function and a possible involvement of the CLIC pathway in regulating epithelial morphogenesis. Because tubular endocytosis has been observed also during germ-band extensions and dorsal closure, two key epithelial remodelling events required to complete embryogenesis in *Drosophila*, a detailed analysis of GRAF1 mutants should also help to clarify whether these different examples of tubular endocytosis are all regulated in a similar manner and all have a similar function (Levayer, Pelissier-Monier, and Lecuit 2011; Mateus et al. 2011).

In this thesis I identified two regulators of tubular endocytosis: dynamin and Rabankyrin-5.

5.4 The biogenesis of apical endocytic tubules is regulated by dynamin

Dynamin has been shown to be involved both in CME as well as clathrin-independent pathways (see Chapter 1.3.3.4). The classical view on dynamin function is related to its role in vesicle scission. By forming a helix around the neck of the vesicle and conformational changes mediated through GTP hydrolysis, dynamin generates force necessary to separate vesicles from the plasma membrane. An additional role of dynamin is to regulate actin dynamics. Indeed dynamin was shown to bind directly to actin bundles though its effector binding domain and indirectly through the association of its SH3 domain with other actin regulators (Ferguson and De Camilli 2012).

In this work, formation of apical tubular intermediates is completely abolished in embryos expressing temperature sensitive mutant of dynamin. This result is intriguing as previous reports describing tubular endocytosis imply that dynamin is not necessary for generation of endocytic tubes. For example, work presented by Sokac et. al shows that the role of dynamin in tubular endocytosis present at the furrow is necessary for vesicle scission (Sokac and Wieschaus 2008a). Conversely, work of Roemer et. al on CLIC/GEEC pathway suggests that formation and scission of tubular endocytic intermediates is dynamin independent (Römer et al. 2010). They proposed that dynamin is involved in the processing of the budded tubes. My work shows yet another function of dynamin, which is in generation of endocytic intermediates.

What could be the role of dynamin in this process? Because the role of dynamin in clathrin-independent endocytosis is associated with regulating actin dynamics, one hypothesis I put forward is that the role of dynamin in regulating apical endocytosis is also through regulation of actin. Elegant work in yeast has clearly demonstrated the requirement of actin during endocytosis, in particular for the invagination and scission of clathrin coated vesicles (Kaksonen, Toret, and Drubin 2005; Kübler and Riezman 1993). In polarized MDCK cells, actin has been recently shown to be required for apical

endocytosis under conditions that increase membrane tension (Boulant et al. 2011). Interestingly, during cellularizing, flattening of the apical surface is concomitant with the establishment of apical adherens junctions and a progressive lowering in the concentration of actin (Grevengoed et al. 2003; Thomas Lecuit 2004). The establishment of adherent junctions, which is expected to increase tension, in combination with the lower levels of actin could in principle favour membrane tubulation by delaying budding. Similar model would apply to the tubular structures identified by Levayer et. al during germ-band extension (Levayer, Pelissier-Monier, and Lecuit 2011). Because tubulation during cellularization can be observed not only at the plane of adherens junctions but also at the apical surface this model needs to take into account other factors. In my hypothesis formation of actin-rich apical protrusions would generate the spatially restricted tension of plasma membrane in order to promote tubular endocytosis.

5.5 Rab5 and its effector Rabankyrin-5 controls the processing of tubular endocytic membranes during apical flattening

The classical view on the role of Rab5 in endocytosis is that active Rab5 controls the fusion between CCVs and early endsomes. This is accomplished by Rab5 ability to recruit proteins to vesicles responsible for uncoating, fusion and motility (see Chapter 1.3.3.3). Simultaneous imaging of GFP::Rab5 and secreted mCherry revealed that Rab5 associates directly with cargo filled tubular invaginations. This indicates that Rab5 is able to form early endosomal structures directly at the plasma membrane.

To get better insight about the molecular mechanism underlying Rab5 function at the plasma membrane, I established a method for the affinity-based purification of Rab5-specific effectors operating during the early stages of embryonic development. I found that a *Drosophila* homolog of Rabankyrin-5 (CG41099) is the main effector of Rab5 in early embryos. In mammalian cell culture Rabankyrin-5 localizes to large vacuolar structures that correspond to macropinosomes (Schnatwinkel et al. 2004). However, the precise mechanism of Rabankyrin-5 in endocytosis is not known.

In my analysis Rabakyrin-5 localizes to tubular intermediates originating from the apical plasma membrane and persists on budded vesicles. Ultrastructural analysis of

Rabankyrin-5-positive structures revealed the existence of doughnut shaped endocytic membranes present close to the apical plasma membrane. This result suggests that their biogenesis relates to the budding and circular folding of tubular elements. Moreover, live imaging of Rabankyrin-5 knock down line demonstrated that, while in control embryos vacuolar structures formed rapidly, in Rabankyrin-5 depleted embryos this step was delayed, resulting in the formation of long tubular membranes that can extend for over 15 microns along the apico-basal axis of the cell. Therefore one of the roles of Rabankyrin-5 at the plasma membrane is to promote budding of endocytic tubes from the plasma membrane. Surprisingly, depletion of Rabankyrin-5 did not affect flattening of the plasma membrane. It is likely that long endocytic tubes can compensate for plasma membrane removal and drive apical flattening.

What could be the mechanism of Rabankyrin-5? Because there is no information about the interacting partners for Rabankyrin-5, its molecular function can be inferred only from its protein domain organization. Rabankyrin-5 contains 21 ankyrin repeats, which are protein domains associated with protein-protein interactions (Schnatwinkel et al. 2004). One possibility is that this Rab5 effector acts as a scaffolding protein linking budding factors to the plasma membrane. Another interesting hypothesis comes from the fact that ankyrin repeats have also mechano-sensing properties (G. Lee et al. 2006). It is proposed that ankyrin repeats are able to detect the tension of cytoskeleton and mechanically transfer this information onto other proteins. Therefore, Rabankirin-5 could take part in detecting and modulating tension of the plasma membrane leading to budding of intracellular tubes. Further experiments on Rabankyrin-5 are needed in order to elucidate its molecular function.

The role of Rab5 at the apical plasma membrane might be to regulate the biogenesis of these structures. In this case, Rab5 would recruit factors responsible to induce tubulation of the plasma membrane. For example actin dynamics has been shown to be regulated by Rab5. Work of Lanzetti et al suggests that the activation of Rab5 and binding to its effector RN-tre leads to cross-linking of actin fibers close to the plasma membrane. This promotes ruffling of the plasma membrane and formation of macropinosomes (Lanzetti, Palamidessi, and Areces 2004). In cellularizing embryo activation of Rab5 could have similar effect on actin dynamics thus promoting formation

of endocytic tubes. This hypothesis is challenged by the fact that Rab5 is lost from the membranes in dynamin mutant. This result suggests that dynamin acts upstream of Rab5 at the plasma membrane but does not exclude the possibility that Rab5 is also needed in this process. In order to address the role of Rab5 in generating endocytic tubes, there is a need for a tool to modulate Rab5 activity is spatial-temporal manner. This will be also important to separate the role of Rab5 at the furrow canal from the one at the apical plasma membrane. Unfortunately, my attempts to develop such approach did not yield positive results.

Another intriguing question is what could be the mechanism to activate apical endocytosis during cellularization? Polarization of the endocytic machinery is a feature common to many cell types. In gut and kidney epithelial cells endocytosis is stably up-regulated at the apical surface. This allows these cells to efficiently uptake solutes present in the environment. A different situation is present during cytokinesis. In this processes the endocytic machinery is rapidly reorganized in order to increase membrane delivery to the cleavage furrow. This reorganization is partially regulated by proteins controlling cell cycle and the cytoskeleton (for details, see Chapter 1.4.3). In order to better understand the mechanisms controlling the rapid rearrangement of the endocytic machinery during cellularization, it will be necessary to dissect the mechanism controlling the shift of the endocytosis. There are several possible models that would account for the observed shift in endocytosis. The up-regulation of apical endocytosis occurs during the maternal to zygotic transition. One possibility is that the expression of positive regulators of endocytosis peaks during the fast phase of cellularization. For example, the expression of an apically localized Rab5 GD/GTP exchange factor at cycle 14 could explain the gradual increase in apical endocytosis. Additional cues that promote endocytosis might be temporally regulated during cellularization. Prior to the apical endocytosis, actin dependent endocytosis can be detected at the furrow canals. The apical upregulation of endocytosis could be accomplished by shifting the localization of endocytic regulators from the furrow to the apical plasma membrane. For example Ras-related G proteins, including Rho1, Rac and Cdc42 could be involved in this process. Another possibility is that the up-regulation of PtdIns(4,5)P2 during fast phase of cellularization drives the up-regulation of apical endocytosis. PtdIns(4,5)P2 plays a crucial role in the recruitment of

endocytic components to the plasma membrane during CCV formation. It was also shown to promote formation of clathrin-independent structures like phagocytic cups (reviewed in van den Bout & Divecha 2009). Therefore the apical up-regulation of PtdIns(4,5)P2 would explain the observed increase in both clathrin-mediated endocytosis and clathrin-independent structures. Moreover, work on endocytosis in the female germline in *Drosophila* done by Compagnon et. al showed that PtdIns(4,5)P2 is promoting Rab5 association to membranes (Compagnon et al. 2009). Thus during cellularization, increasing amount of PtdIns(4,5)P2 would recruit Rab5 to endocytic intermediates originating from the apical plasma membrane. The up-regulation of the apical endocytic machinery during cellularization provides a framework for future studies aimed at characterizing the developmental mechanisms underlying the spatial-temporal activation of endocytosis during morphogenesis.

5.6 Conclusions

In summary the work presented in this thesis led to the identification of a novel endocytic mechanism underlying morphological remodelling during development. I demonstrate that apical surface flattening is a dynamin-dependent process associated with an increase in tubular endocytosis and formation of Rab5 endosomes. I found that cargo-filled tubular invagination bud-off from the plasma membrane as a whole leading to the formation of vacuolar like structures. Importantly, my data show that Rab5 localizes directly to these tubular plasma membrane invaginations as well as to intracellular apical vacuoles. Blocking dynamin resulted in the complete inhibition of both membrane tubulation and formation of Rab5 endosomes. Thus, I propose that the activation of tubular endocytosis initiates the formation of vacuolar–like Rab5 positive endosomes directly at the plasma membrane in a dynamin dependent manner. The elongation of tubular endocytic membranes observed in the knock-down of Rabnkyrin-5 embryos indicates that one function of the Rab5 machinery in this process is to control budding. Collectively, the effect of dynamin inhibition on surface morphology and on tubular endocytosis suggest that one function of this endocytic pathway is to control the rapid

removal of large quantities of membranes to drive surface flattening during epithelial morphogenesis (see model in Fig. 5.1).

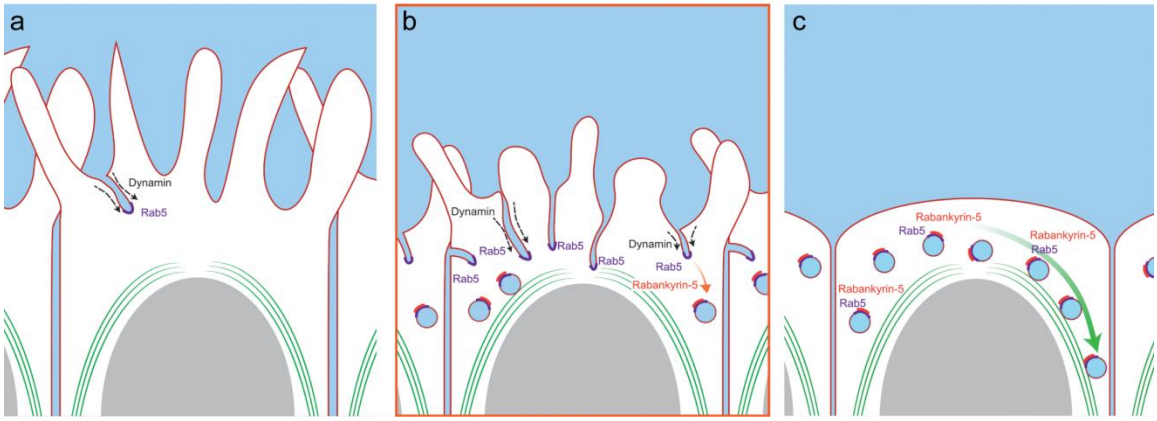

Figure 5.1 A model for remodeling of the apical surface by tubular endocytosis.

Early during cellularization (a) the apical surface is rich in villous protrusions. At this stage the abundance of tubular structures and apical Rab5 endosomes is low. During mid-cellularization (b) the upregulation of Rab5-positive tubular endocytic intermediates with a high surface to volume ratio allows for the rapid internalization of large amounts of membranes. These membranes are incorporated into Rab5-positive vacuoles that travel basally (green arrow, panel c), thus driving apical surface flattening (c). This tubular-endocytic pathway is dynamin dependent and controlled by the Rab5-effector Rabankyrin-5.

Appendices

Appendix A Vector map of pEOC

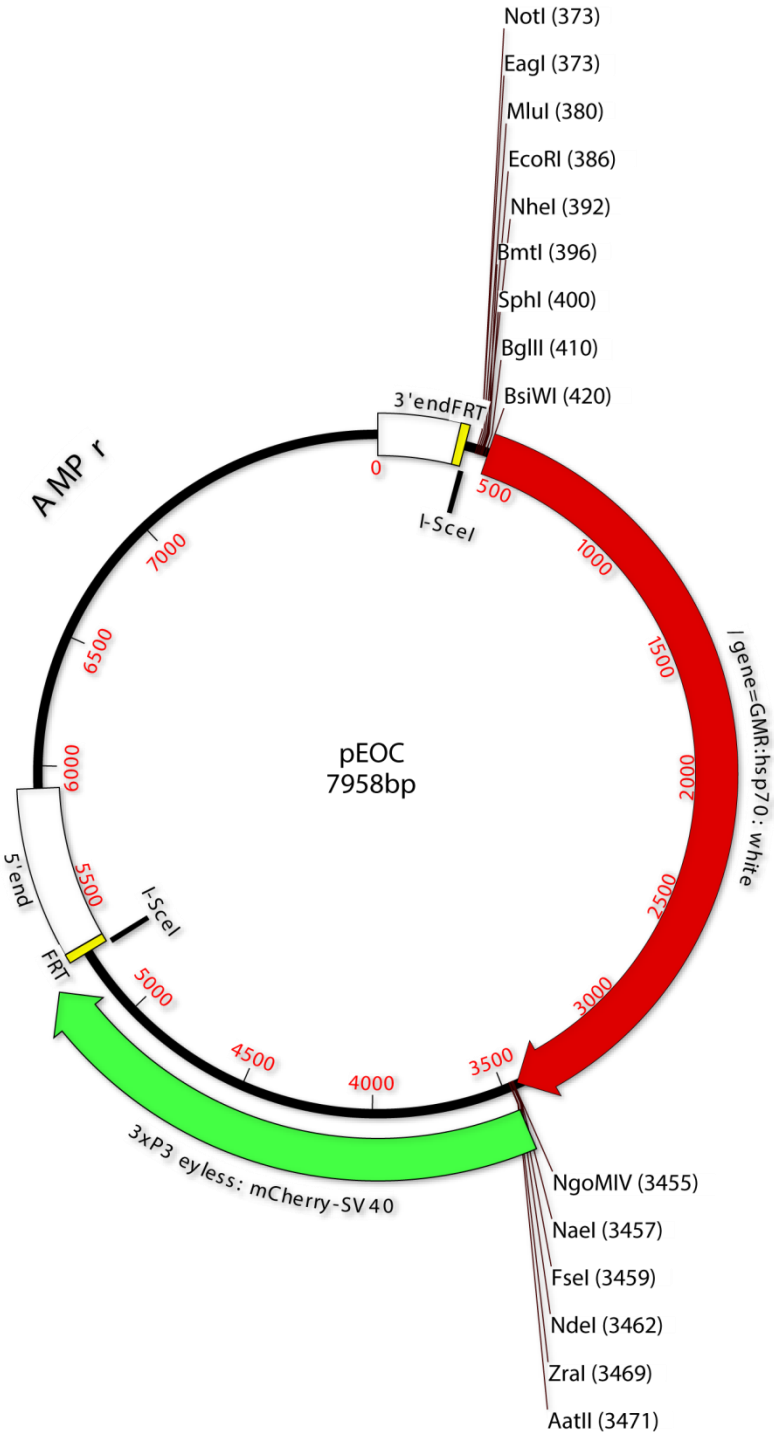

Appendix B Manuscript: Tubular endocytosis drives remodeling of the apical surface during epithelial morphogenesis in *Drosophila*

Tubular endocytosis drives remodeling of the apical surface during epithelial morphogenesis in *Drosophila*

Piotr Fabrowski[1]*, Aleksandar Necakov[1]*, Simone Mumbauer[1], Eva Loeser[1], Alessandra Reversi[1], Sebastian Streichan[1], John A.G. Briggs[1], and Stefano De Renzis[1]#

1 EMBL Heidelberg, Meyerhofstrasse 1, 69117 Heidelberg, Germany

* These authors contributed equally to this work

To whom correspondence should be addressed

Changes in cell shape are of fundamental importance during embryonic development [1-4]. Remodeling of cell morphology requires the expansion or contraction of plasma membrane domains, which in some instances also undergo more complex structural and functional reorganization that bring about specialized functions [5, 6]. While the role of the cytoskeleton in driving plasma membrane remodeling is well established [7], whether membrane trafficking also contributes remains an open question. Here we have identified a novel mechanism underlying the re-structuring of the apical surface during epithelial morphogenesis in *Drosophila*. We show that the retraction of villous protrusions and subsequent apical plasma membrane flattening is an endocytosis driven morphogenetic process. Quantitation of endogenously tagged GFP Rab5 dynamics revealed a massive increase in apical endocytosis that correlates with changes in apical morphology. By combining high-resolution imaging with a genetically encoded cargo uptake assay we show that this increase is accompanied by the formation of tubular plasma membrane invaginations that serve as platforms for the *de novo* generation of vacuolar Rab5-positive endosomes. We identify the Rab5 effector Rabankyrin-5 as a regulator of this pathway and demonstrate that blocking dynamin activity results in the complete inhibition of tubular endocytosis, in the disappearance of Rab5 endosomes and in the inhibition of surface flattening. These data collectively support a role for membrane trafficking in morphological remodeling. Surface flattening is thus an endocytosis-dependent morphogenetic process driven by the rapid internalization of large quantities of plasma membrane through tubular invagination and up-regulation of Rab5 endosome production.

The early *Drosophila* embryo is an ideal system for studying the mechanisms driving plasma membrane remodeling during epithelial morphogenesis. Over the course of one hour a syncitium of 6000 nuclei is sub-divided into an equal number of polarized epithelial cells through the invagination and growth of the apical plasma membrane by a process known as cellularization [8, 9]. Scanning electron microscopy studies revealed that during this process the apical plasma membrane undergoes a dramatic morphological re-organization characterized by the retraction of villous protrusions and flattening of the apical surface [10]. To characterize the membrane dynamics underlying surface flattening we applied Total Internal Reflection Fluorescence Microscopy (TIRF-M) to cellularizing *Drosophila* embryos (Fig. 1a) (see supplementary methods for a detailed description). As a first step, we imaged embryos expressing the plasma membrane marker peptide GAP43 (amino acids 1-20) tagged with the fluorescent protein mCherry [11]. Consistently with previous electron microscopy data [10], we observed a massive accumulation of membranes at the apical surface prior to cellularization. During the early phase of cellularization the apical surface of all blastoderm cells was densely covered with small, highly dynamic villous protrusions (Fig. 1b and Supplementary Movie S1). Over the course of cellularization these protrusions first began to elongate and broaden at mid-cellularization (Fig.1c), and were ultimately reabsorbed towards the end of cellularization as the apical plasma membrane flattened (Fig. 1d).

Considering this reduction in apical surface and changes in membrane organization we next asked whether membrane flattening is causally linked to endocytosis. One key regulator of endocytosis is the large GTPase dynamin [12]. Dynamin controls the scission of clathrin-coated vesicles from the plasma membrane [13] and has also been implicated in the biogenesis of a distinct set of endocytic

structures, including macropinosomes [14]. Using TIRF-M, we followed the dynamics of the GAP43-mCherry marked apical plasma membrane over the course of cellularization in embryos containing the *shibire*^{ts} mutation, a temperature sensitive allele of dynamin [15]. Whereas wild-type embryos imaged at the restrictive temperature (32 ^{0}C) undergo apical surface flattening without any morphological abnormality (Fig. 1e,f), this process was severely compromised in *shibire*^{ts} mutant embryos (Fig. 1g,h). Upon shifting embryos to the restrictive temperature the apical plasma membrane failed to flatten and the retraction of membrane protrusions did not occur (Fig. 1h,i and Supplementary Movie S2). This result shows that apical surface flattening is dynamin-dependent, suggesting that endocytosis might actively participate in this process.

To ask whether an increase in the rate of apical endocytosis might account for the decrease in the surface area of the plasma membrane during apical flattening, we developed a quantitative assay for monitoring the uptake of a soluble fluorescent tracer. To this end, we generated a genetically-encoded endocytic cargo consisting of EGFP fused to the secretion signal peptide of folded gastrulation (fog), a secreted signaling molecule expressed in early embryos [16]. This fusion protein, henceforth referred to as sec::GFP, is secreted, filing the extracellular space/perivitelline fluid with a soluble fluorescent tracer prior to cellularization. Using this assay we show that the number of endocytic structures increased approximately 5-fold over the course of cellularization, reaching a maximum during surface flattening (Fig. 2a,b,j and Supplementary Movie S3). Strikingly, this experiment also revealed that the primary entry route for soluble cargos is through tubular intermediates that, upon budding from the plasma membrane, form vacuolar-like structures (Fig. 2c-f). These structures formed primarily towards the end of cellularization, were particularly prominent in

ventral cells and originated from both the apical and the subapical region of the cell. Injection of pH-Rhodamine-labeled dextran (a pH-sensitive fluorogenic dye whose fluorescence intensity increases as the pH of its surroundings drops) further demonstrated that the newly formed vacuolar structures are acidified endosomal compartments (data not shown).

Given these changes in endocytic activity, we next asked whether the endosomal machinery also undergoes dynamic regulation during apical surface flattening. To this end, we used a homologous recombination-based strategy [17] to 'knock in' an enhanced GFP (EGFP) tag into the endogenous genomic locus of Rab5 (a small GTPase, conserved from yeast to humans, that controls endosome biogenesis [18]). TIRF-M imaging revealed that, during early cellularization, relatively few Rab5 positive endosomes exist at the apical plasma membrane (Fig. 2g,h and Supplementary Movie S4). In contrast, and consistent with a role of endocytosis in apical flattening, the number of these Rab5-positive endosomes increased three-fold during apical flattening (Fig. 2i,k and Supplementary Movie S4).

To test whether the apical increase in Rab5 did not simply result from an overall increase in expression levels, we imaged GFP-tagged-Rab5 expressing embryos over the entire apico-basal axis of the blastoderm during cellularization using two-photon microscopy. We observed no significant increase in Rab5 signal intensity over the course of cellularization (data not shown). In addition, we observed the formation of large Rab5 endosomes preferentially at the apical surface towards the end of cellularization (Supplementary Movie S5). Importantly, simultaneous imaging of GFP-Rab5 and secreted mCherry (sec::mCherry; a variant of sec::GFP in which the GFP was substituted with mCherry) revealed that Rab5 associates directly with cargo-filled tubular invaginations (Fig. 3a-d). We further showed using electron tomography

that tubular invaginations of the plasma membrane exist as convoluted structures surrounded by an area of ribosomal exclusion, which is suggestive of actin polymerization (Fig. 3e,f).

The data presented demonstrate that apical surface flattening is a dynamin-dependent morphogenetic process associated with an up-regulation of tubular endocytic intermediates and increasing levels of Rab5-positive endosomes. To identify proteins potentially involved in Rab-5 positive endosome biogenesis we carried out large-scale affinity chromatography in order to purify Rab5-specific effectors operating during these early stages of embryonic development. This experiment led to the identification of several proteins that were bound specifically to Rab5 in its active conformation (Fig. 4a). The most abundant effector identified by this approach was CG41099, the Drosophila homolog of human Rabankyrin-5 (Fig. 4a), a Rab5 effector linked to apical endocytosis in polarized MDCK cells [19]. In addition, Rabankyrin-5 has been shown to regulate macropinocytosis, a distinct form of endocytosis that involves the formation of large (0.2 - 10μm) vesicular structures [19]. We therefore tested whether tubular endocytosis at the apical surface is associated with Rabankyrin-5. Simultaneous imaging of EGFP-Rabankyrin-5 and sec::mCherry revealed that Rabankyrin-5 associates with apical vacuolar structures positive for sec::mCherry (Supplementary Fig. 1a-c). This result was confirmed using an antibody against Drosophila Rabankyrin-5 (Supplementary Fig. 1d). Moreover, correlative light-electron microscopy showed that Rabankyrin-5 GFP positive membranes are organized as convoluted tubular structures (Supplementary Fig. 2). Live imaging demonstrated that, while in control embryos vacuolar structures formed at the plasma membrane and moved towards the basal side of the cell with long range movement which are presumably microtubule dependent, in embryos expressing shRNAs against

Rabankyrin-5 (the knock-down of Rabankyrin-5 was almost complete at both mRNA and protein levels, Supplementary Fig. 3a,b) this step was impeded resulting in the formation of long tubular membranes extending for over 15 microns along the apico-basal axis of the cell (Fig. 4b and Supplementary Fig. S3c-l and Movies S6, S7). Using correlative light-electron microscopy we tracked one of these long tubular membrane filled with endocytic cargo (Fig. 4c). This long tubule extended parallel to microtubules and its basal tip appeared composed of multiple varicosities interconnected by a constricted membrane domain (Supplementary Fig. 4 and Supplementary Tomogram Movie, S8). We speculate that, at the functional level, this terminal region may serve as a platform for the budding and generation of vacuoles, in a process equivalent to the formation of vacuoles from the shorter tubular invaginations seen in wild-type embryos (Fig. 2c,f). In support of this hypothesis, we observed the sequential budding of vacuoles from the tip of elongated tubes by live imaging in Rabankyrin-5 depleted embryos (Supplementary Movie S7). The elongation of tubular endocytic membranes induced upon Rabankyrin-5 knock-down revealed that one role of the Rab5 machinery in this apical endocytic pathway is to control budding, and that other molecule/s must act upstream of Rabankyrin-5 in the initiation of tubular endocytosis.

Given the effect of dynamin inhibition on apical surface flattening we hypothesised that the high surface to volume ratio of tubular endocytic intermediates provides an efficient means by which to rapidly internalize large amounts of membrane in order to facilitate plasma membrane remodeling during morphogenesis. If this hypothesis is correct, then blocking dynamin activity, which inhibits membrane flattening, should also inhibit tubular endocytosis. To test this hypothesis we followed the internalization of sec::GFP in *shibire* mutant embryos. When embryos were heat-

shocked prior to surface flattening, formation of sec::GFP-containing tubular structures was completely abolished (Fig. 4d,e). Although a clear reliance upon dynamin for clathrin-mediated endocytosis has been demonstrated previously [20, 21] [13, 22], its role in clathrin-independent endocytic pathways and in apical endocytosis is less clear. The above result shows that dynamin is required for tubular endocytosis. We asked whether dynamin is also directly linked to the formation of Rab5 endosomes. We generated embryos expressing endogenously tagged GFP-Rab5 in a *shibire* mutant background. Strikingly, shifting the embryos to the restrictive temperature during surface flattening resulted in the almost complete disappearance of Rab5-positive endosomes within 2-5 min. (Fig. 4f,g). We conclude that dynamin is required for the initiation of tubular endocytosis and for the formation of Rab5 endosomes during surface flattening. The localization of Rab5 to tubular invaginations together with the rapid disappearance of Rab5 endosomes upon dynamin inhibition suggest that during surface flattening apical endosomes form directly at the plasma membrane rather than by fusion of incoming clathrin coated vesicles.

In summary, our data demonstrate that apical surface flattening is a dynamin-dependent process associated with the dynamic regulation and functional re-organization of both endocytosis and endosome biogenesis. Dynamin activity is required for both the initiation of tubular endocytosis as well as for *de novo* formation of apical Rab5 endosomes. The elongation of tubular endocytic membranes observed upon Rabankyrin-5 knock-down suggests that one role of the Rab5 machinery in this pathway is in mediating the formation of endosomes from tubular invaginations. Taken together these results are consistent with a model in which surface flattening is an endocytosis-dependent morphogenetic process driven by the rapid internalization of large quantities of plasma membrane via tubular endocytic intermediates. Given

the conservation of tubular endocytosis across different species [23] we propose that this endocytic pathway represents a general regulatory mechanism underlying plasma membrane remodeling during morphogenesis (see model in Fig. 4h,j).

Acknowledgments

We thank all members of the De Renzis and Briggs laboratories for helpful discussion. We thank A. Ephrussi, D. Gilmour, M. Kaksonen and J. Rink for critical reading of the manuscript. We thank the advanced light microscopy, the electron microscopy, the proteomics and protein expression core facilities (EMBL, Heidelberg) for their advice and assistance. We thank M. Kaksonen for sharing microscopy equipment. We thank the Bloomington Drosophila Stock Center and the Drosophila Genomics Resource Center for providing fly stocks and cDNAs. We thank the TRiP at Harvard Medical School (NIH/NIGMS R01-GM084947) for providing transgenic RNAi fly stocks used in this study and Adam Martin for providing the GAP43mcherry line. This work was supported by a Human Frontier Science Program Carrere Development Award (CDA) to Stefano De Renzis. Aleksandar Necakov was supported by an EIPOD postdoctoral fellowship.

Author contribution

The experiments were conceived and designed by P.F., A.N. and S.D.R.. P.F. developed the TIRF-M imaging protocol, generated the endogenously tagged GFP-Rab5 flies and performed the live imaging analysis together with A.N. and S.M. A.N. developed the correlative-light microscopy method in the early Drosophila embryo and performed the electron microscopy and tomography analysis with guidance from J.B. E.L. preformed the biochemical purification of the Rab5 effectors and A.R. performed the dextrane injection experiments and 2-photon movies. S.S analyzed the data shown in figure 7e-h and generated the graph shown in figure 7i. P.F., A.N. and S.D.R. analyzed together all the data and wrote the manuscript together with J.B.

Figure Legends

Figure 1. Endocytosis drives plasma membrane flattening during epithelial morphogenesis

(a) Schematic overview of TIRF imaging in the early *Drosophila* embryo. Embryos (cell membranes outlined in purple) are mounted such that the evanescent wave (green gradient) generated at the coverslip (blue rectangle) by total internal reflection of incident excitation light (dotted green lines) illuminates the apical plasma membrane (shown as purple protrusions). Nuclei are depicted as blue ovals.

(b-d) Apical view of cellularizing embryos expressing GAP43::mCherry using TIRF microscopy at progressive stages through cellularization (b = early (~ 5 min. into cellularization); c = middle (~ 20 min. into cellularization); d = late (~ 40 min. into cellularization). During the early phase of cellularization the apical plasma membrane is covered with small fillopodial-like protrusions (b) that thicken and elongate as cellularization proceeds. These protrusions progressively retract as the apical plasma membrane flattens (dotted red outline) towards the end of cellularization (d). Scale bar, 5 μm

(e-h) TIRF-M imaging of the apical plasma membrane in wt (e-f) and *shibire* mutant (g-h) embryos reared at 32 ºC over the course of cellularization. Progressive flattening of the apical plasma membrane was observed in wild type embryos (f), whereas surface flattening was impeded in *shibire* mutant embryos (h).
Scale bar, 10 μm.

(i) Quantification of the fractional surface area coverage by protrusions in wild type (pink line, +/- standard deviation) and *shibire* mutant (blue line, +/- standard deviation) embryos. Time zero corresponds to the timepoint at which embryos at mid-cellularization were shifted to the restrictive temperature (32 ºC)

Figure 2. Apical Rab5 endocytosis is upregulated during cellularization and coincides precisely with the timing of apical flattening

(a-b) Still frames from a time-lapse recording showing the upregulation of sec::GFP internalization. During early cellularization (a) sec::GFP localizes primarily to the extracellar space, whereas during late cellularization numerous internal sec:GFP-positive structures could easily be detected (b, white arrows)
Scale bar, 5 μm.

(c-f) Still frames from a 3.5 μm z-projection time-lapse recording under the apical surface showing formation of an intracellular vacuole filled with sec::GFP from a tube originating at the plasma membrane.
Timepoints correspond to (d) t=0s, (e) t=24s, (f) t=36s, (g) t=60s

(g-i) Still frames from a time lapse TIRF recording showing the upregulation of apical endosomal structures marked by endogenously tagged GFP::Rab5. A progressive increase in the number of apical Rab5 puncta between early (g), middle (h), and late (i) cellularization was observed. Scale bar, 5 μm.

(j) Quantification of sec::GFP-positive endocytic structures (tubules and vacuoles) over the course of cellularization (Blue line) including standard deviation (black bars). The early (yellow), mid- (green), and late (purple) stages of cellularization are highlighted. The number of internal sec::GFP-positive structures (tubules and vacuoles) was quantified in five independent z-sections separated by 0.2 μm, in nine separate 625 μm^2 surface regions, from three embryos (see methods for details).

(k) Quantification of endogenously tagged Rab5 endosomes at the apical surface over the course of cellularization. The early (yellow), mid- (green), and late (purple) stages of cellularization are highlighted. GFP::Rab5 signal intensity is represented as the normalized number of Rab5 particles vs. time (dark blue line) including standard deviation (light blue bars). n=3 embryos (see methods for details).

Figure 3. The primary entry route for apical endocytic cargo is through endocytic tubules that interact directly with Rab5

(a-d) sec::mCherry-positive endocytic structures (a) colocalize with endogenously tagged GFP::Rab5 (b). GFP::Rab5 (green), sec::mCherry (red) overlay (c). (d) Three dimensional rendering of a typical apical endocytic tubule labeled by sec::mCherry (red), co-labeled by endogenous GFP::Rab5 (green).
Scale bar, 500 nm.

(e-f) EM tomography of an apical endocytic tubule showing multiple internal compartments in direct continuity with the apical plasma membrane. A single section through an EM tomogram of a tubular endocytic structure in direct continuity with the apical plasma membrane (e). Three-dimensional surface rendering of the tubular endocytic volume from the corresponding volume generated by EM tomography demonstrating the continuity of the tubular-endosomal structure with the apical plasma membrane at top (f).
Scale bar, 500 nm

Figure 4. The biogenesis of apical endocytic tubules is regulated by dynamin and the Rab5 effector Rabankyrin-5.

(a) Coomasie staining of GST-Rab5 affinity chromatography products using 0-4 h embryo cytosolic fractions. Lane 1 (Mw) corresponds to a protein molecular weight ladder (corresponding protein sizes, in kDa, are shown at left). Lanes 2 and 3 (Rab5 GDP, Rab5 GTP) correspond to the proteins bound to GDP-loaded Rab5, and GTP-γ-S-loaded Rab5, respectively. The red asterisk marks the protein band identified by mass spectrometry as CG41099, the *Drosophila* homolog of mammalian Rabankyrin-5.

(b) Rabankyrin-5 knock-down results in the elongation of endocytic tubules along the apico-basal axis. Single plane two-photon optical cross-section of a Rabankyrin-5 siRNA embryo expressing sec::GFP showing a typical, elongated, sec::GFP-positive tubule (red arrow).
Scale bar, 5 μm.

(c) Ultrastructural characterization of an elongated endocytic tubule in a Rabankyrin-5 siRNA embryo. A single section from an EM tomogram of a Rabankyrin-5-siRNA embryo showing a typical elongated tubule that extends past the base of the nucleus (blue arrow indicates a nuclear pore at the base of the nucleus). Scale bar, 500 nm.

(d-e) Live imaging of internalized sec::GFP prior to cell flattening in *shibire* mutant embryos imaged at 18 ºC (d) and at 32 ºC (e), respectively . Multiple vacuolar and tubular structures were present in *shibire* mutant embryos imaged at 18 ºC (white arrowheads). In contrast, *shibire* mutant embryos reared at the non-permissive temperature (32 ºC) expressing sec::GFP showed no vacuolar or tubular structures.
Scale bar, 5 μm.

(f-g) Live imaging of GFP::Rab5 expressed at endogenous levels in *shibire* mutant embryos reared at the permissive temperature (18 ºC, panel f) and at the non-permissive temperature (32 ºC, panel g) during mid-cellularization. The punctate distribution of Rab5-positive endosomes was lost upon inhibition of dynamin activity and exhibited a diffuse cytoplasmic distribution.
Scale bar, 5 μm.

(h-j) A model for remodeling of the apical surface by tubular endocytosis.
Early during cellularization (h) the apical surface is rich in villous protrusions. At this stage the abundance of tubular structures and apical Rab5 endosomes is low. During mid-cellularization (i) the upregulation of Rab5-positive tubular endocytic intermediates with a high surface to volume ratio allows for the rapid internalization of large amounts of membranes. These membranes are incorporated into Rab5-positive vacuoles that travel basally (green arrow, panel j), thus driving apical surface flattening (j). This tubular-endocytic pathway is dynamin dependent and controlled by the Rab5-effector Rabankyrin-5.

Methods

TIRF microscopy

Embryos were dechorionated with 20% sodium hypochlorite solution and positioned on glass-bottom culture dishes (MatTek) in a drop of PBS solution. In order to produce a uniform interface between the vitelline membrane and the coverslip, a thin slab (~ 5mm) of 2% agar was placed on top of embryos prior to imaging. Time-lapse TIRF imaging was performed on an Olympus Biosystems Cell^R TIRF system using an Olympus APO N 60x oil objective (NA 1.49). The incident angle was set at the critical angle for total internal reflection with subsequent small, manual angular adjustments used to optimize signal from the apical membrane. All imaging was performed at room temperature unless stated otherwise. For experiments involving the temperature sensitive *shibire* mutant, either cold (18 ºC) or pre-warmed (32 ºC) PBS and agar were used for embryo mounting and live TIRF-M imaging was subsequently conducted in a temperature control chamber at either 18 ºC or 32 ºC.

Confocal and 2-photon microscopy

Embryos were positioned on siliconized glass-bottom culture dishes (MatTek) and immersed in PBS solution. Imaging was performed with a spinning disk confocal Ultraview VOX system (Perkin Elmer) using a 100x NA 1.3 oil immersion objective (Zeiss). 2 photon imaging was performed using Zeiss LSM 780 NLO system using a 63x NA 1.2 water immersion objective (Zeiss).

Correlative Light-Electron Microscopy

Correlative light-electron microscopy of *Drosophila* embryos was performed as previously described for yeast [24]. Briefly, Rabankyrin::GFP-expressing embryos were first preserved at near-native conditions by high-pressure freezing using a high pressure freezing machine (HPM 010; Bal-Tec). Embryos were subsequently processed by freeze substitution (FS) and embedding in Lowicryl HM20 (Electron Microscopy Sciences, Hatfield, PA) in an automated freeze substitution machine (AFS2; Leica). FS was performed at -90°C for 48–54 h with 0.1% (wt/vol) uranyl acetate in glass-distilled acetone. The temperature was then raised to -45°C at a rate of +5°C per hour, and samples were washed with acetone and infiltrated with increasing concentrations (10, 25, 50, and 75%; 4 h each) of Lowicryl in acetone while the temperature was further raised to -25°C. 100% Lowicryl was exchanged three times in 10-h steps and samples were UV polymerized at -25°C for 48 h, after which the temperature was raised to 20°C at a rate of +5°C per hour and UV polymerization continued for 48 h. 300-nm sections were cut with a microtome (Ultracut UCT; Leica) and a diamond knife (Diatome) and picked up on copper-palladium slot grids coated with separate layers of formvar and carbon. Blue (excitation 365 nm/ emission 415 nm) 100 nm TetraSpecks (Invitrogen) were pretreated (to reduce fluorescence intensity) with 0.1% Tween-20 for 10 min, washed twice by ultracentrifugation at 100,000 g, resuspended in PBS, and adsorbed to the EM grids by placing the grids section face-down onto a 15-µl drop of Tetraspecks for 10 min. Grids were then washed with three drops of water and blotted with filter paper. Embryo sections mounted on EM grids were placed on a droplet of water sandwiched between two glass coverslips and imaged face-down at room temperature using a widefield fluorescence microscope (model IX81; Olympus) fitted with a 100x, NA 1.45 objective, a camera (Orca-ER; Hamamatsu Photonics), and electronic

shutters and filter wheels (Sutter Instrument Co.). Fluorescence microscopy was accomplished with a lamp (X-Cite 120PC; EXFO Life Sciences) using 470/22-nm, and 377/50-nm filters for excitation of GFP/TetraSpecks, and Tetraspecks alone, respectively. Emission was imaged using a 520/35-nm filter for GFP/ TetraSpecks, and a 520/35-nm filter for TetraSpecks alone. The CCD camera, filter wheels, and shutters were controlled by MetaMorph software (Universal Imaging Corp.).

Electron tomography

Grids carrying embryo sections were post-stained with 2% uranyl acetate in 70% methanol and Reynolds lead citrate for contrast enhancement. 15-nm protein A–coupled gold beads were adsorbed on both sides of all grids as tomographic-fiducial markers. Grids were placed in a high-tilt holder (Model 2020; Fischione Instruments), and digital images were recorded on a camera (4k Eagle; FEI) as dual-axis tilt series over a -60° to 60° tilt range (1° increment) on a microscope (Tecnai TF30; FEI) operated at 300 kV. Tomograms were reconstructed using the IMOD software package (version 3.13.2; Kremer et al., 1996). Fiducial-based correlation was performed exactly as previously described [24].

Fly stocks

WT flies were Oregon-R; all stocks were maintained by standard methods at 25°C, unless otherwise specified.

y,w*;P[UASp:YFP::Rab5] (BL-9775)
y,w*; EGFP::Rab5/CyO (endogenous)
y,w*;;P[UASp:secmCherry]
y,w*,P[UASp:secGFP/Y]
y,w*;;P[UASp:secGFP]
y,sc*,v1; P[TRiP.HMS01228]attP2/TM3, Sb (CG41099 siRNA BL-34883)
y,sc*,v1; P[YFP-RNAi]attP2 (TRIP)
y,w*;P[UASp:EGFP::CG41099-PC]
w*; P[mat α Tub-Gal4VP16];[mat α Tub-Gal4VP16]
w*;; P[Sqh:Gap43mCherry]
Shibire (BL-7068)

GFP-Rab5 homologous recombination

To generate GFP-Rab5 expressed at endogenous levels we adapted the ends-out homologous recombination method [17]. An pEOC (pEndsOutmCherry) targeting vector was designed on the basis of the pRK1 vector by replacing the negative selection marker UAS-Rpr with 3xP3::mCherry [25] for more efficient screening purposes. In addition, the multiple cloning site was replaced by the NotI/MluI/EcoRI/SphI/BglII/BsiWI and the AatII/NdeI/NaeI sites. 5' 3.2 kbp and 3' 2 kbp homologous recombination arms were amplified from BACMID DNA containing the Rab5 locus (BACR22P10, BPRC). In addition, EGFP with a terminal Glycine-Alanine-Glycine-Alanine (GAGA) linker was inserted at the 5' end of the Rab5 coding sequence. Homologous arms were cloned into the pEOC vector and a homologous recombination targeting line on the third chromosome was generated. This targeting line was subsequently crossed to the 6939-hid line and the crossing scheme was followed as described [17]. Recombinant flies with the white marker segregating to the second chromosome were selected. The selection of false-positive insertions was performed by a screen against mCherry expression in the 3xP3 promoter pattern [26]. The *white* marker was removed using the Cre/ loxP system.

Correct insertion was confirmed by sequencing.

Cloning and antibody generation
UAS-secGFP and UAS-secmCherry were generated by fusion of the coding sequence of the folded gastrulation signal peptide (amino acids 1-22) to the fluorescent proteins EGFP and mCherry, respectively, and cloned into the pPW vector (DGRC) using the Gateway cloning system (Life Technologies).
cDNA for CG41099-PC (D-Rabankyrin) was reverse-transcribed from total RNA extracted from 0-4h old embryos. D-Rabankyrin was cloned into the pPGW vector (DGRC) using the Gateway cloning system (Life Technologies).
Antibodies against CG41099 were made in rabbit as follows: A fragment corresponding to amino acids 660-920 of CG41099-PC was cloned into the pET32 vector (Novagen) using BamHI and XhoI restriction sites. Protein was purified from BL21 E.coli cells (Stratagene) and sent for antibody production (Eurogentec). Antibodies were subsequently purified using affinity chromatography.

Western blot and Immunohistochemistry
For detection of endogenous Rabankyrin-5 protein 10 cellularizing embryos were lysed in SDS lysis buffer. Western blotting was achieved using the Western Lightning ECL kit (Perkin Elmer) according to the manufacturer's protocol. Rabbit anti-CG41099 (1:5000) and mouse anti-alpha-Tubulin (1:10 000, Sigma Aldrich, clone B-5-1-2) antibodies were used. Embryos were dechorionated for 3 min in 20% sodium hypochlorite solution and fixed in 4% paraformaldehyde (Electron Microscopy Sciences) and heptane (Sigma) for 20 min. Fixed embryos were incubated with an anti-CG41099 antibody (1:250). Alexa 488 (company) anti rabbit secondary antibodies were used (1:500). Imaging was performed with a spinning disk confocal Ultraview VOX system.

Quantitative PCR
RNA was extracted from 10 cellularizing embryos using the RNeasy Mini Kit (Qiagen) with additional DNA digestion performed 'on-column' using RNase-Free DNase (Qiagen). cDNA was synthesised with the Superscript III First strand synthesis System (Life Technologies).
qRT-PCR for CG41099 was performed with the SYBR Green PCR master mix (Applied Biosystems) using standard protocol with the following primers:

CG41099_1 CAGGGTGCAGACATTACAGC
CG41099_2 CGGACCATAACGGTGATTCT

and was normalised to the RPL32 gene with following primers:

RP49_1 GCTAAGCTGTCGCACAAA
RP49_2 TCCGGTGGGCAGCATGTG

Using an Applied Biosystems 7500 Real-Time PCR System.

Quantification and statistics
Quantification of intracellular signal in UAS::secGFP/+; Tub67::GAL4/+; Tub67::GAL4/+ embryos was performed manually. Intracellular tubes and vesicles positive for sec::GFP were counted from the Z-stack corresponding to the volume

between 4 to 5 microns under the apical membrane over the course of cellularization. Quantification was performed on 3 areas of 25 μm x 25 μm each (625 μm^2) in three different embryos.

GFP::Rab5 Signal quantification

GFP::RAB5 signal at the apical plasma membrane was imaged over the course of cellularization using TIRF microscopy and subsequently quantified using CellProfiler Image analysis software (www.cellprofiler.org). Briefly, 3 independent data sets were obtained each for both ectopically expressed YFP::RAB5 and for endogenous GFP::RAB5. Identification and segmentation of RAB5-positive puncta was accomplished using Cell Profiler, registration was verified manually, and the number and integrated intensity of puncta was quantified.

Both the number and integrated intensity of puncta were normalized by expressing their value over cellularization as a ratio to the mean value of the first 20 frames in each sequence.

Cell Profiler Reference

Lamprecht MR, Sabatini DM, Carpenter AE (2007) CellProfiler: free, versatile software for automated biological image analysis. Biotechniques 42(1):71-75. PMID: 17269487
(www.cellprofiler.org)

Quantification of the rate of apical surface flattening

First the images where corrected for bleaching by fixing the mean intensity at each time point to that of the initial image. Then the images where filtered using a mexican hat filter with values sigmax = 7, sigmay = 1, which was rotated according to angles in an interval from 0 to pi. The response images form a stack, where each plane corresponds to an angle from the interval, enhancing protrusions along the given angle. The maximum intensity projection of that stack was then segmented using Ilastik (ilastik: Interactive Learning and Segmentation Toolkit, Christoph Sommer, Christoph Straehle, Ullrich Koethe and Fred A. Hamprecht. 8th IEEE International Symposium on Biomedical Imaging, ISBI 2011) to yield a segmentation of the image. The skeleton of the image was then taken to compute the area in the image covered by protrusions.

Purification of Rab5 effectors from cellularizing *Drosophila* embryos

Rab5 effectors were purified as previously described [27] with the following modifications. Briefly, 0-4h. embryos were harvested, dechorionated for 2 minutes in bleach, washed in PBS 0.1% Triton X-100 and frozen at -80 ^{0}C. Thirty grams of packed embryos were diluted in 60ml of lysis buffer and homogenized in a Dounce tissue grinder at 4 ^{0}C and processed as described in [27]. Thereafter, the cytosolic fraction was divided in two aliquots and each aliquot was incubated with 1ml of packed GST-Rab5 beads loaded with either GDP (inactive) or GTP-γS (active). All the subsequent steps were performed as described in [2727].

Dextran injections

10 000 MW 647 Dextran, and pHrodo Red (Life Technologies) were injected into the perivitelline space of cellularizing embryos as described previously (Levayer et al. 2011). Embryos were covered with a thin layer of halocarbon oil 700/27 (1:2) (Sigma). The coverslip was placed on a microscope slide platform and embryos were

visualized using a standard 18 upright microscope equipped with a 10X objective (Zeiss). Microinjection was carried out with an Eppendorf 5242 microinjector.
Microinjection pipettes were pulled from borosilicate glass capillaries (1.2mm outer diamater x 0.94mm inner diamater, Harvard Apparatus), using a P-97 Flamming /brown puller (Sutter Instrument Co). 20 mg/m in PBS solution of dextran was used.

References

1. Harris, T.J. & Tepass, U. Adherens junctions: from molecules to morphogenesis. *Nat Rev Mol Cell Biol* **11**, 502-514 (2010).
2. Levayer, R., Pelissier-Monier, A. & Lecuit, T. Spatial regulation of Dia and Myosin-II by RhoGEF2 controls initiation of E-cadherin endocytosis during epithelial morphogenesis. *Nat Cell Biol* **13**, 529-540 (2011).
3. Fernandez-Gonzalez, R., Simoes Sde, M., Roper, J.C., Eaton, S. & Zallen, J.A. Myosin II dynamics are regulated by tension in intercalating cells. *Dev Cell* **17**, 736-743 (2009).
4. Martin, A.C., Kaschube, M. & Wieschaus, E.F. Pulsed contractions of an actin-myosin network drive apical constriction. *Nature* **457**, 495-499 (2009).
5. Lecuit, T. & Pilot, F. Developmental control of cell morphogenesis: a focus on membrane growth. *Nat Cell Biol* **5**, 103-108 (2003).
6. Mostov, K., Su, T. & ter Beest, M. Polarized epithelial membrane traffic: conservation and plasticity. *Nat Cell Biol* **5**, 287-293 (2003).
7. Harris, T.J., Sawyer, J.K. & Peifer, M. How the cytoskeleton helps build the embryonic body plan: models of morphogenesis from Drosophila. *Curr Top Dev Biol* **89**, 55-85 (2009).
8. Sisson, J.C., Field, C., Ventura, R., Royou, A. & Sullivan, W. Lava lamp, a novel peripheral golgi protein, is required for Drosophila melanogaster cellularization. *J Cell Biol* **151**, 905-918 (2000).
9. Lecuit, T. & Wieschaus, E. Polarized insertion of new membrane from a cytoplasmic reservoir during cleavage of the Drosophila embryo. *J Cell Biol* **150**, 849-860 (2000).
10. Turner, F.R. & Mahowald, A.P. Scanning electron microscopy of Drosophila embryogenesis. 1. The structure of the egg envelopes and the formation of the cellular blastoderm. *Dev Biol* **50**, 95-108 (1976).
11. Mavrakis, M., Rikhy, R. & Lippincott-Schwartz, J. Plasma membrane polarity and compartmentalization are established before cellularization in the fly embryo. *Dev Cell* **16**, 93-104 (2009).
12. Schmid, S.L. & Frolov, V.A. Dynamin: functional design of a membrane fission catalyst. *Annu Rev Cell Dev Biol* **27**, 79-105 (2011).
13. Ferguson, S.M. & De Camilli, P. Dynamin, a membrane-remodelling GTPase. *Nat Rev Mol Cell Biol* **13**, 75-88 (2012).
14. Liu, Y.W., Surka, M.C., Schroeter, T., Lukiyanchuk, V. & Schmid, S.L. Isoform and splice-variant specific functions of dynamin-2 revealed by analysis of conditional knock-out cells. *Mol Biol Cell* **19**, 5347-5359 (2008).
15. van der Bliek, A.M. & Meyerowitz, E.M. Dynamin-like protein encoded by the Drosophila shibire gene associated with vesicular traffic. *Nature* **351**, 411-414. (1991).

16. Dawes-Hoang, R.E. *et al*. folded gastrulation, cell shape change and the control of myosin localization. *Development* **132**, 4165-4178 (2005).
17. Huang, J., Zhou, W., Watson, A.M., Jan, Y.N. & Hong, Y. Efficient ends-out gene targeting in Drosophila. *Genetics* **180**, 703-707 (2008).
18. Zeigerer, A. *et al*. Rab5 is necessary for the biogenesis of the endolysosomal system in vivo. *Nature* **485**, 465-470 (2012).
19. Schnatwinkel, C. *et al*. The Rab5 effector Rabankyrin-5 regulates and coordinates different endocytic mechanisms. *PLoS Biol* **2**, E261 (2004).
20. van der Bliek, A.M. *et al*. Mutations in human dynamin block an intermediate stage in coated vesicle formation. *J Cell Biol* **122**, 553-563. (1993).
21. Sweitzer, S.M. & Hinshaw, J.E. Dynamin undergoes a GTP-dependent conformational change causing vesiculation. *Cell* **93**, 1021-1029. (1998).
22. Hinshaw, J.E. & Schmid, S.L. Dynamin self-assembles into rings suggesting a mechanism for coated vesicle budding. *Nature* **374**, 190-192. (1995).
23. Doherty, G.J. & McMahon, H.T. Mechanisms of endocytosis. *Annu Rev Biochem* **78**, 857-902 (2009).
24. Kukulski, W. *et al*. Correlated fluorescence and 3D electron microscopy with high sensitivity and spatial precision. *J Cell Biol* **192**, 111-119 (2011).
25. Sheng, G., Thouvenot, E., Schmucker, D., Wilson, D.S. & Desplan, C. Direct regulation of rhodopsin 1 by Pax-6/eyeless in Drosophila: evidence for a conserved function in photoreceptors. *Genes Dev* **11**, 1122-1131 (1997).
26. Horn, C., Jaunich, B. & Wimmer, E.A. Highly sensitive, fluorescent transformation marker for Drosophila transgenesis. *Dev Genes Evol* **210**, 623-629 (2000).
27. Christoforidis, S. & Zerial, M. Purification and identification of novel Rab effectors using affinity chromatography. *Methods* **20**, 403-410 (2000).

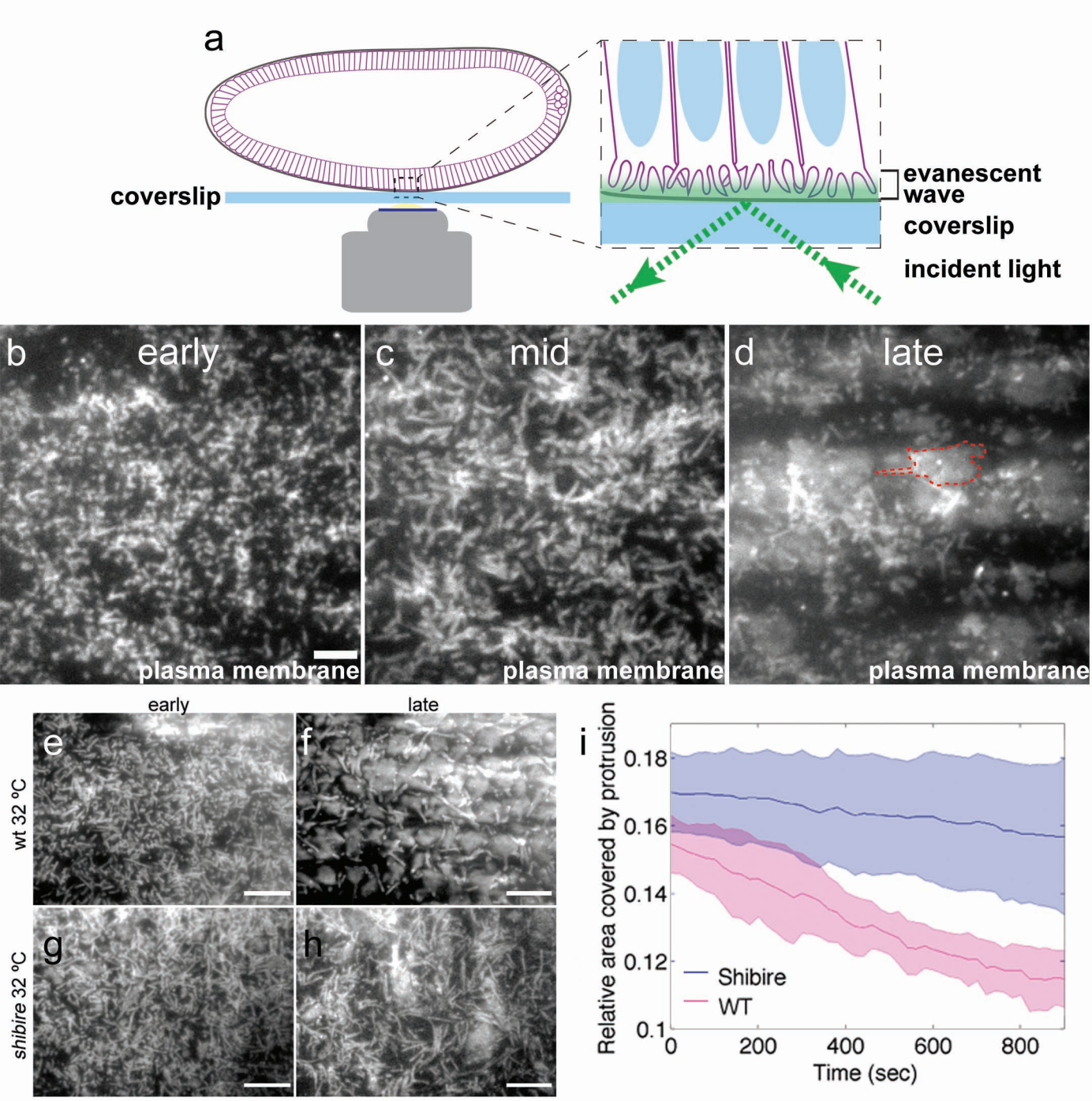

De Renzis, Figure 1

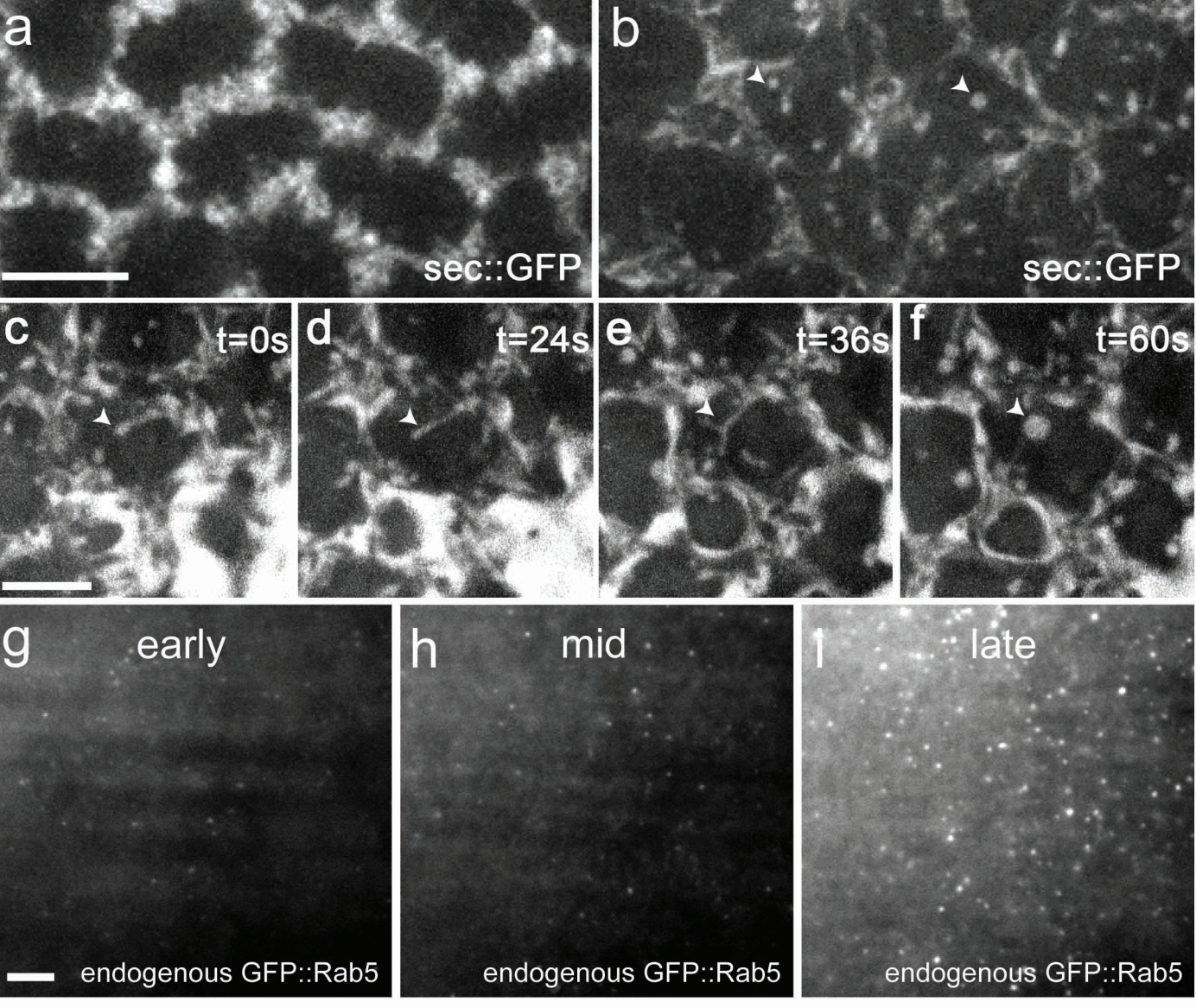

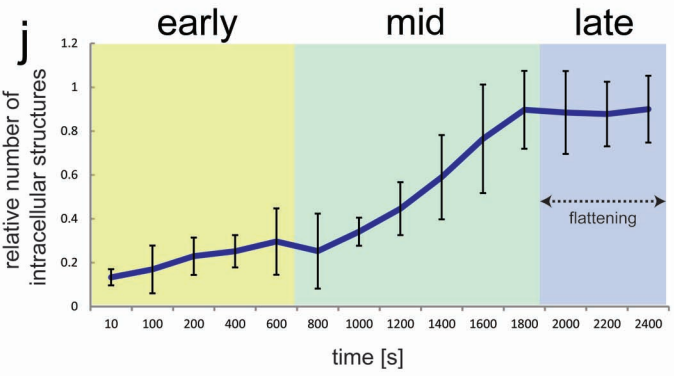

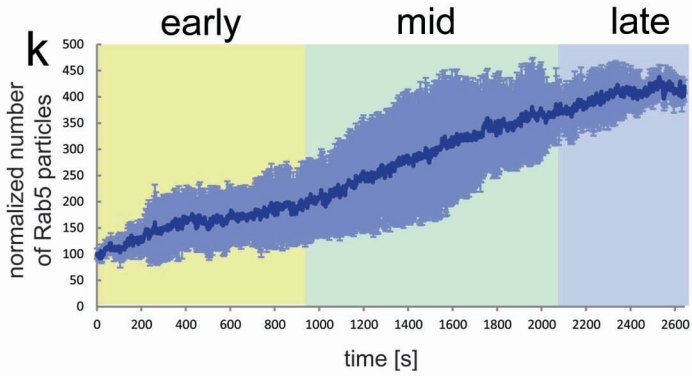

De Renzis, Figure 2

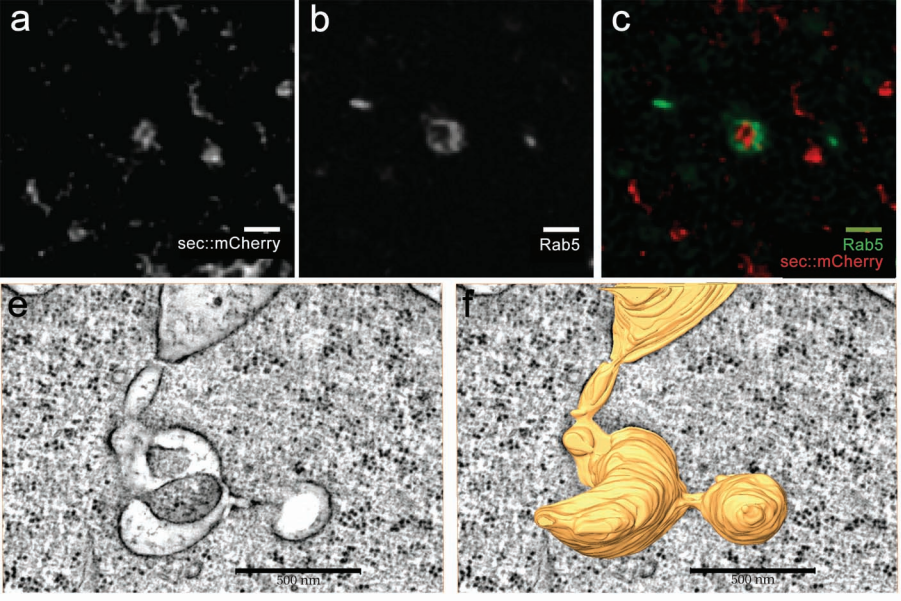

De Renzis, Figure 3

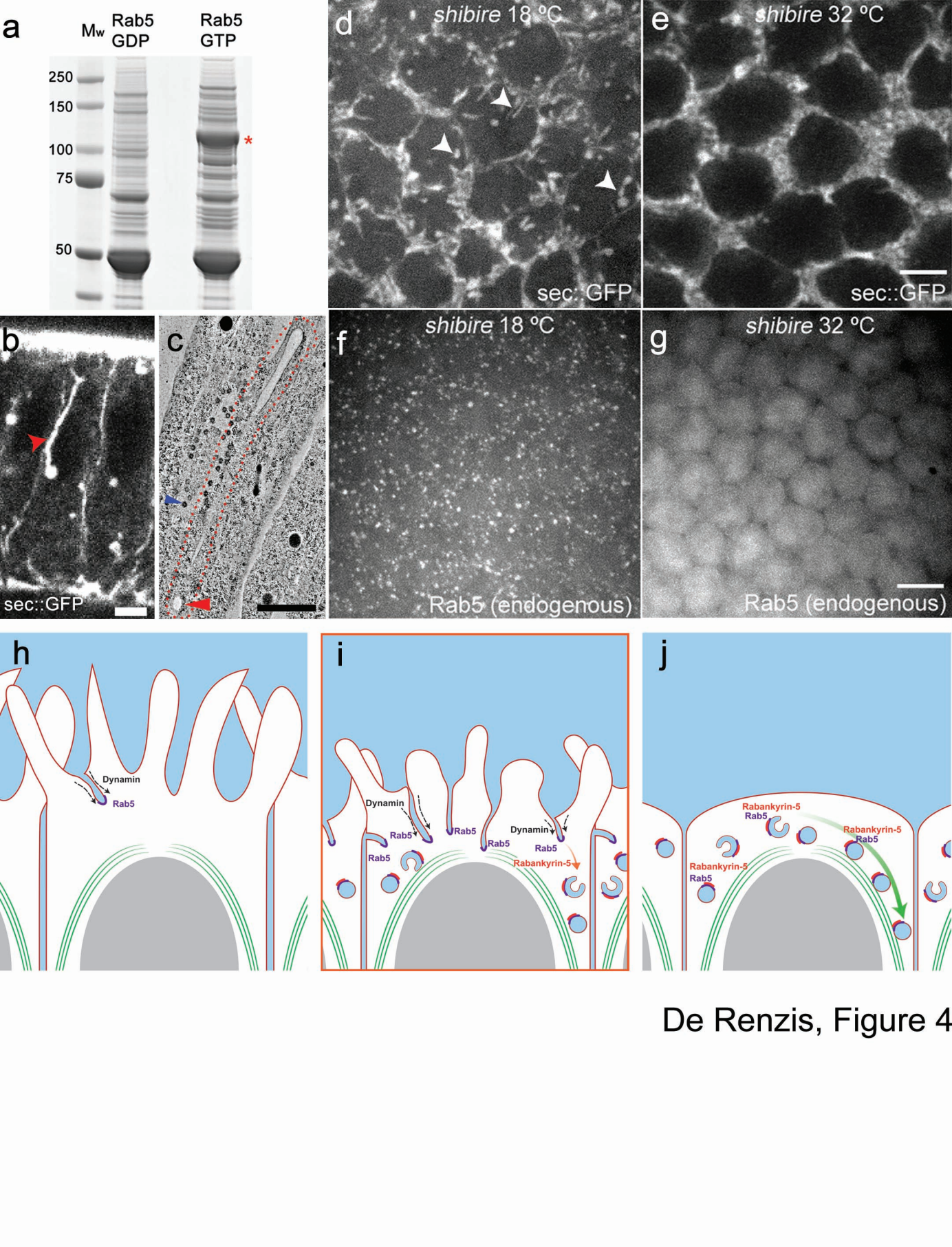

De Renzis, Figure 4

Bibliography

Bibliography

Adam, J C, J R Pringle, and M Peifer. 2000. “Evidence for Functional Differentiation Among Drosophila Septins in Cytokinesis and Cellularization.” *Molecular Biology of the Cell* 11 (9) (September): 3123–35.

Aghamohammadzadeh, Soheil, and Kathryn R Ayscough. 2009. “Differential Requirements for Actin During Yeast and Mammalian Endocytosis.” *Nature Cell Biology* 11 (8) (August): 1039–42. doi:10.1038/ncb1918.

Alexandrov, K, H Horiuchi, O Steele-Mortimer, M C Seabra, and M Zerial. 1994. “Rab Escort Protein-1 Is a Multifunctional Protein That Accompanies Newly Prenylated Rab Proteins to Their Target Membranes.” *The EMBO Journal* 13 (22) (November 15): 5262–73.

Arighi, Cecilia N, Lisa M Hartnell, Ruben C Aguilar, Carol R Haft, and Juan S Bonifacino. 2004. “Role of the Mammalian Retromer in Sorting of the Cation-independent Mannose 6-phosphate Receptor.” *The Journal of Cell Biology* 165 (1) (April): 123–33. doi:10.1083/jcb.200312055.

Baeg, G H, X Lin, N Khare, S Baumgartner, and N Perrimon. 2001. “Heparan Sulfate Proteoglycans Are Critical for the Organization of the Extracellular Distribution of Wingless.” *Development (Cambridge, England)* 128 (1) (January): 87–94.

Baldassarre, Massimiliano, Arsenio Pompeo, Galina Beznoussenko, Claudia Castaldi, Salvatore Cortellino, Mark A Mcniven, Alberto Luini, and Roberto Buccione. 2003. “Dynamin Participates in Focal Extracellular Matrix Degradation by Invasive Cells □” 14 (March): 1074–1084. doi:10.1091/mbc.E02.

Baonza, a, and a Garcia-Bellido. 2000. “Notch Signaling Directly Controls Cell Proliferation in the Drosophila Wing Disc.” *Proceedings of the National Academy of Sciences of the United States of America* 97 (6) (March 14): 2609–14. doi:10.1073/pnas.040576497.

Bar-Sagi, D, a Fernandez, and J R Feramisco. 1987. “Regulation of Membrane Turnover by Ras Proteins.” *Bioscience Reports* 7 (5) (May): 427–34.

Bardin, Allison J, and François Schweisguth. 2006. “Bearded Family Members Inhibit Neuralized-mediated Endocytosis and Signaling Activity of Delta in Drosophila.” *Developmental Cell* 10 (2) (February): 245–55. doi:10.1016/j.devcel.2005.12.017.

Barr, Francis a, and Benjamin Short. 2003. “Golgins in the Structure and Dynamics of the Golgi Apparatus.” *Current Opinion in Cell Biology* 15 (4) (August): 405–413. doi:10.1016/S0955-0674(03)00054-1.

Bennett, M K, N Calakos, and R H Scheller. 1992. “Syntaxin: a Synaptic Protein Implicated in Docking of Synaptic Vesicles at Presynaptic Active Zones.” *Science (New York, N.Y.)* 257 (5067) (July 10): 255–9.

Bento-Abreu, André, Ana Velasco, Erica Polo-Hernández, Concepción Lillo, Renata Kozyraki, Arantxa Tabernero, and José M Medina. 2009. “Albumin Endocytosis via Megalin in Astrocytes Is Caveola- and Dab-1 Dependent and Is Required for the Synthesis of the Neurotrophic Factor Oleic Acid.” *Journal of Neurochemistry* 111 (1) (October): 49–60. doi:10.1111/j.1471-4159.2009.06304.x.

Blanchette, Craig D, Youn-Hi Woo, Cynthia Thomas, Nan Shen, Todd a Sulchek, and Amy L Hiddessen. 2009. “Decoupling Internalization, Acidification and Phagosomal-endosomal/lysosomal Fusion During Phagocytosis of InlA Coated Beads in Epithelial Cells.” *PloS One* 4 (6) (January): e6056. doi:10.1371/journal.pone.0006056.

Bleil, JD, and MS Bretscher. 1982. “Transferrin Receptor and Its Recycling in HeLa Cells.” *The EMBO Journal* I (3): 351–355.

Bos, Johannes L, Holger Rehmann, and Alfred Wittinghofer. 2007. “GEFs and GAPs: Critical Elements in the Control of Small G Proteins.” *Cell* 129 (5) (June 1): 865–77. doi:10.1016/j.cell.2007.05.018.

Boucrot, Emmanuel, and Tomas Kirchhausen. 2007. “Endosomal Recycling Controls Plasma Membrane Area During Mitosis.” *Proceedings of the National Academy of Sciences of the United States of America* 104 (19) (May 8): 7939–44. doi:10.1073/pnas.0702511104.

Boucrot, Emmanuel, Saveez Saffarian, Rongying Zhang, and Tomas Kirchhausen. 2010. “Roles of AP-2 in Clathrin-mediated Endocytosis.” *PloS One* 5 (5) (January): e10597. doi:10.1371/journal.pone.0010597.

Boulant, Steeve, Comert Kural, Jean-Christophe Zeeh, Florent Ubelmann, and Tomas Kirchhausen. 2011. “Actin Dynamics Counteract Membrane Tension During Clathrin-mediated Endocytosis.” *Nature Cell Biology* 13 (9) (September): 1124–31. doi:10.1038/ncb2307.

van den Bout, Iman, and Nullin Divecha. 2009. “PIP5K-driven PtdIns(4,5)P2 Synthesis: Regulation and Cellular Functions.” *Journal of Cell Science* 122 (Pt 21) (November 1): 3837–50. doi:10.1242/jcs.056127. http://www.ncbi.nlm.nih.gov/pubmed/19889969.

Brandt, Annely, Fani Papagiannouli, Nicole Wagner, Michaela Wilsch-Bräuninger, Martina Braun, Eileen E Furlong, Silke Loserth, et al. 2006. “Developmental Control of Nuclear Size and Shape by Kugelkern and Kurzkern.” *Current Biology□: CB* 16 (6) (March 21): 543–52. doi:10.1016/j.cub.2006.01.051.

Bray, Sarah J. 2006. “Notch Signalling: a Simple Pathway Becomes Complex.” *Nature Reviews. Molecular Cell Biology* 7 (9) (September): 678–89. doi:10.1038/nrm2009.

Bucci. 1994. “Rab5a Is a Common Component of the Apical and Basolateral Endocytic Machinery in Polarized Epithelial Cells.”

Callaghan, Judy, Anne Simonsen, and JM Gaullier. 1999. “The Endosome Fusion Regulator Early-endosomal Autoantigen 1 (EEA1) Is a Dimer.” *Biochemical ...* 543: 539–543.

Callejo, Ainhoa, Joaquim Culi, and Isabel Guerrero. 2008. “Patched, the Receptor of Hedgehog, Is a Lipoprotein Receptor.” *Proceedings of the National Academy of Sciences of the United States of America* 105 (3) (January 22): 912–7. doi:10.1073/pnas.0705603105.

Cao, H, F Garcia, and M a McNiven. 1998. “Differential Distribution of Dynamin Isoforms in Mammalian Cells.” *Molecular Biology of the Cell* 9 (9) (September): 2595–609.

Caron, E, and a Hall. 1998. “Identification of Two Distinct Mechanisms of Phagocytosis Controlled by Different Rho GTPases.” *Science (New York, N.Y.)* 282 (5394) (November 27): 1717–21.

Carr, Chavela M, and Josep Rizo. 2010. “At the Junction of SNARE and SM Protein Function.” *Current Opinion in Cell Biology* 22 (4) (August): 488–95. doi:10.1016/j.ceb.2010.04.006.

Casanova, J E, G Apodaca, and K E Mostov. 1991. “An Autonomous Signal for Basolateral Sorting in the Cytoplasmic Domain of the Polymeric Immunoglobulin Receptor.” *Cell* 66 (1) (July 12): 65–75.

Caswell, Patrick, and Jim Norman. 2008. “Endocytic Transport of Integrins During Cell Migration and Invasion.” *Trends in Cell Biology* 18 (6) (June): 257–63. doi:10.1016/j.tcb.2008.03.004.

Chappie, Joshua S, Jason a Mears, Shunming Fang, Marilyn Leonard, Sandra L Schmid, Ronald a Milligan, Jenny E Hinshaw, and Fred Dyda. 2011. “A Pseudoatomic Model of the Dynamin Polymer Identifies a Hydrolysis-dependent Powerstroke.” *Cell* 147 (1) (September 30): 209–22. doi:10.1016/j.cell.2011.09.003.

Chavrier, P, JP Gorvel, and E Stelzer. 1991. “Hypervariable C-termmal Domain of Rab Proteins Acts as a Targeting Signal.”

Chen, H, S Fre, VI Slepnev, and MR Capua. 1998. “Epsin Is an EH-domain-binding Protein Implicated in Clathrin-mediated Endocytosis.” *Nature* 394 (August): 793–797.

Chen, H, V I Slepnev, P P Di Fiore, and P De Camilli. 1999. “The Interaction of Epsin and Eps15 with the Clathrin Adaptor AP-2 Is Inhibited by Mitotic Phosphorylation and Enhanced by Stimulation-dependent Dephosphorylation in Nerve Terminals.” *The Journal of Biological Chemistry* 274 (6) (February 5): 3257–60.

Chen, Y, and L C Norkin. 1999. “Extracellular Simian Virus 40 Transmits a Signal That Promotes Virus Enclosure Within Caveolae.” *Experimental Cell Research* 246 (1) (January 10): 83–90. doi:10.1006/excr.1998.4301.

Chesneau, Laurent, Daphné Dambournet, Mickaël Machicoane, Ilektra Kouranti, Mitsunori Fukuda, Bruno Goud, and Arnaud Echard. 2012. “An ARF6/Rab35 GTPase Cascade for Endocytic Recycling and Successful Cytokinesis.” *Current Biology : CB* 22 (2) (January 24): 147–53. doi:10.1016/j.cub.2011.11.058.

Christoforidis, S, H M McBride, R D Burgoyne, and M Zerial. 1999. “The Rab5 Effector EEA1 Is a Core Component of Endosome Docking.” *Nature* 397 (6720) (February 18): 621–5. doi:10.1038/17618.

Christoforidis, S, M Miaczynska, K Ashman, M Wilm, L Zhao, S C Yip, M D Waterfield, J M Backer, and M Zerial. 1999. “Phosphatidylinositol-3-OH Kinases Are Rab5 Effectors.” *Nature Cell Biology* 1 (4) (August): 249–52. doi:10.1038/12075.

Chu, D S, B Pishvaee, and G S Payne. 1996. “The Light Chain Subunit Is Required for Clathrin Function in Saccharomyces Cerevisiae.” *The Journal of Biological Chemistry* 271 (51) (December 20): 33123–30.

Clary, D O, I C Griff, and J E Rothman. 1990. “SNAPs, a Family of NSF Attachment Proteins Involved in Intracellular Membrane Fusion in Animals and Yeast.” *Cell* 61 (4) (May 18): 709–21.

Collins, Brett M, Airlie J McCoy, Helen M Kent, Philip R Evans, and David J Owen. 2002. “Molecular Architecture and Functional Model of the Endocytic AP2 Complex.” *Cell* 109 (4) (May 17): 523–35.

Compagnon, Julien, Louis Gervais, Mabel San Roman, Sophy Chamot-Boeuf, and Antoine Guichet. 2009. “Interplay Between Rab5 and PtdIns(4,5)P2 Controls Early Endocytosis in the Drosophila Germline.” *Journal of Cell Science* 122 (Pt 1) (January 1): 25–35. doi:10.1242/jcs.033027.

Conibear, Elizabeth, JN Cleck, and TH Stevens. 2003. “Vps51p Mediates the Association of the GARP (Vps52/53/54) Complex with the Late Golgi t-SNARE Tlg1p.” *Molecular Biology of the Cell* 14 (April): 1610–1623. doi:10.1091/mbc.E02.

Coppolino, M G, M Krause, P Hagendorff, D a Monner, W Trimble, S Grinstein, J Wehland, and a S Sechi. 2001. “Evidence for a Molecular Complex Consisting of Fyb/SLAP, SLP-76, Nck, VASP and WASP That Links the Actin Cytoskeleton to Fcgamma Receptor Signalling During Phagocytosis.” *Journal of Cell Science* 114 (Pt 23) (December): 4307–18.

Cox, D, D J Lee, B M Dale, J Calafat, and S Greenberg. 2000. “A Rab11-containing Rapidly Recycling Compartment in Macrophages That Promotes Phagocytosis.” *Proceedings of the National Academy of Sciences of the United States of America* 97 (2) (January 18): 680–5.

Crawford, J M, N Harden, T Leung, L Lim, and D P Kiehart. 1998. “Cellularization in Drosophila Melanogaster Is Disrupted by the Inhibition of Rho Activity and the Activation of Cdc42 Function.” *Developmental Biology* 204 (1) (December 1): 151–64. doi:10.1006/dbio.1998.9061.

Dambournet, Daphné, Mickael Machicoane, Laurent Chesneau, Martin Sachse, Murielle Rocancourt, Ahmed El Marjou, Etienne Formstecher, Rémi Salomon, Bruno Goud, and Arnaud Echard. 2011. “Rab35 GTPase and OCRL Phosphatase Remodel Lipids and F-actin for Successful Cytokinesis.” *Nature Cell Biology* 13 (8) (August): 981–8. doi:10.1038/ncb2279.

Dautry-Varsat, a, a Ciechanover, and H F Lodish. 1983. "pH and the Recycling of Transferrin During Receptor-mediated Endocytosis." *Proceedings of the National Academy of Sciences of the United States of America* 80 (8) (April): 2258–62.

Dawes-Hoang, Rachel E, Kush M Parmar, Audrey E Christiansen, Chris B Phelps, Andrea H Brand, and Eric F Wieschaus. 2005. "Folded Gastrulation, Cell Shape Change and the Control of Myosin Localization." *Development (Cambridge, England)* 132 (18) (September): 4165–78. doi:10.1242/dev.01938.

Deblandre, A, Eric C Lai, Chris Kintner, Gerald M Rubin, and San Diego. 2001. "Drosophila Neuralized Is a Ubiquitin Ligase That Promotes the Internalization and Degradation of Delta Salk Institute for Biological Studies" 1: 783–794.

Doherty, Gary J, Monika K Åhlund, Mark T Howes, Björn Morén, Robert G Parton, Harvey T McMahon, and Richard Lundmark. 2011. "The Endocytic Protein GRAF1 Is Directed to Cell-matrix Adhesion Sites and Regulates Cell Spreading." *Molecular Biology of the Cell* 22 (22) (November): 4380–9. doi:10.1091/mbc.E10-12-0936.

Doherty, Jason T, Kaitlin C Lenhart, Morgan V Cameron, Christopher P Mack, Frank L Conlon, and Joan M Taylor. 2011. "Skeletal Muscle Differentiation and Fusion Are Regulated by the BAR-containing Rho-GTPase-activating Protein (Rho-GAP), GRAF1." *The Journal of Biological Chemistry* 286 (29) (July 22): 25903–21. doi:10.1074/jbc.M111.243030.

Duclos, S, R Diez, J Garin, B Papadopoulou, a Descoteaux, H Stenmark, and M Desjardins. 2000. "Rab5 Regulates the Kiss and Run Fusion Between Phagosomes and Endosomes and the Acquisition of Phagosome Leishmanicidal Properties in RAW 264.7 Macrophages." *Journal of Cell Science* 113 Pt 19 (October): 3531–41.

Dyer, Naomi, Elena Rebollo, Paloma Domínguez, Nadia Elkhatib, Philippe Chavrier, Laurent Daviet, Cayetano González, and Marcos González-Gaitán. 2007. "Spermatocyte Cytokinesis Requires Rapid Membrane Addition Mediated by ARF6 on Central Spindle Recycling Endosomes." *Development (Cambridge, England)* 134 (24) (December): 4437–47. doi:10.1242/dev.010983.

Edwards, D C, L C Sanders, G M Bokoch, and G N Gill. 1999. "Activation of LIM-kinase by Pak1 Couples Rac/Cdc42 GTPase Signalling to Actin Cytoskeletal Dynamics." *Nature Cell Biology* 1 (5) (September): 253–9. doi:10.1038/12963.

Ehrlich, Marcelo, Werner Boll, Antoine Van Oijen, Ramesh Hariharan, Kartik Chandran, Max L Nibert, and Tomas Kirchhausen. 2004. "Endocytosis by Random Initiation and Stabilization of Clathrin-coated Pits." *Cell* 118 (5) (September 3): 591–605. doi:10.1016/j.cell.2004.08.017.

Emery, Gregory, Andrea Hutterer, Daniela Berdnik, Bernd Mayer, Frederik Wirtz-Peitz, Marcos Gonzalez Gaitan, and Juergen a Knoblich. 2005. "Asymmetric Rab 11 Endosomes Regulate Delta Recycling and Specify Cell Fate in the Drosophila Nervous System." *Cell* 122 (5) (September 9): 763–73. doi:10.1016/j.cell.2005.08.017.

Entchev, E V, a Schwabedissen, and M González-Gaitán. 2000. "Gradient Formation of the TGF-beta Homolog Dpp." *Cell* 103 (6) (December 8): 981–91.

Esko, Jeffrey D, and Scott B Selleck. 2002. "Order Out of Chaos: Assembly of Ligand Binding Sites in Heparan Sulfate." *Annual Review of Biochemistry* 71 (January): 435–71. doi:10.1146/annurev.biochem.71.110601.135458.

Fanto, M, and M Mlodzik. 1999. "Asymmetric Notch Activation Specifies Photoreceptors R3 and R4 and Planar Polarity in the Drosophila Eye." *Nature*: 523–526.

Farnsworth, C C, M C Seabra, L H Ericsson, M H Gelb, and J a Glomset. 1994. "Rab Geranylgeranyl Transferase Catalyzes the Geranylgeranylation of Adjacent Cysteines in the Small GTPases Rab1A, Rab3A, and Rab5A." *Proceedings of the National Academy of Sciences of the United States of America* 91 (25) (December 6): 11963–7.

Fasshauer, D, R B Sutton, a T Brunger, and R Jahn. 1998. "Conserved Structural Features of the Synaptic Fusion Complex: SNARE Proteins Reclassified as Q- and R-SNAREs." *Proceedings of the National Academy of Sciences of the United States of America* 95 (26) (December 22): 15781–6.

Felder, S, K Miller, G Moehren, a Ullrich, J Schlessinger, and C R Hopkins. 1990. "Kinase Activity Controls the Sorting of the Epidermal Growth Factor Receptor Within the Multivesicular Body." *Cell* 61 (4) (May 18): 623–34.

Ferguson, Shawn M, and Pietro De Camilli. 2012. "Dynamin, a Membrane-remodelling GTPase." *Nature Reviews. Molecular Cell Biology* 13 (2) (February): 75–88. doi:10.1038/nrm3266.

Ferguson, Shawn M, Shawn Ferguson, Andrea Raimondi, Summer Paradise, Hongying Shen, Kumi Mesaki, Agnes Ferguson, et al. 2009. "Coordinated Actions of Actin and BAR Proteins Upstream of Dynamin at Endocytic Clathrin-coated Pits." *Developmental Cell* 17 (6) (December): 811–22. doi:10.1016/j.devcel.2009.11.005.

Foe, V E, and B M Alberts. 1983. "Studies of Nuclear and Cytoplasmic Behaviour During the Five Mitotic Cycles That Precede Gastrulation in Drosophila Embryogenesis." *Journal of Cell Science* 61 (May): 31–70.

Ford, M G, B M Pearse, M K Higgins, Y Vallis, D J Owen, a Gibson, C R Hopkins, P R Evans, and H T McMahon. 2001. "Simultaneous Binding of PtdIns(4,5)P2 and Clathrin by AP180 in the Nucleation of Clathrin Lattices on Membranes." *Science (New York, N.Y.)* 291 (5506) (February 9): 1051–5. doi:10.1126/science.291.5506.1051.

Ford, Marijn G J, Ian G Mills, Brian J Peter, Yvonne Vallis, Gerrit J K Praefcke, Philip R Evans, and Harvey T McMahon. 2002. "Curvature of Clathrin-coated Pits Driven by Epsin." *Nature* 419 (6905) (September 26): 361–6. doi:10.1038/nature01020.

Franc, Nathalie. C Franc, Kristin White, R Alan B Ezekowitz, Phagocytosis and development: back to the future, Current Opinion in Immunology, Volume 11, Issue 1, 1 February 1999, Pages 47-52, doi: 10.1016/ S0952-7915

Frolenkov, Gregory I, Inna a Belyantseva, Thomas B Friedman, and Andrew J Griffith. 2004. "Genetic Insights into the Morphogenesis of Inner Ear Hair Cells." *Nature Reviews. Genetics* 5 (7) (July): 489–98. doi:10.1038/nrg1377.

Fujimoto, L M, R Roth, J E Heuser, and S L Schmid. 2000. "Actin Assembly Plays a Variable, but Not Obligatory Role in Receptor-mediated Endocytosis in Mammalian Cells." *Traffic (Copenhagen, Denmark)* 1 (2) (February): 161–71.

Futter, C E, a Pearse, L J Hewlett, and C R Hopkins. 1996. "Multivesicular Endosomes Containing Internalized EGF-EGF Receptor Complexes Mature and Then Fuse Directly with Lysosomes." *The Journal of Cell Biology* 132 (6) (March): 1011–23.

Fürthauer, Maximilian, and Marcos González-Gaitán. 2009. "Endocytosis and Mitosis: a Two-way Relationship." *Cell Cycle (Georgetown, Tex.)* 8 (20) (October 15): 3311–8.

Garrett, W S, L M Chen, R Kroschewski, M Ebersold, S Turley, S Trombetta, J E Galán, and I Mellman. 2000. "Developmental Control of Endocytosis in Dendritic Cells by Cdc42." *Cell* 102 (3) (August 4): 325–34.

Gaullier, J M, E Ronning, D J Gillooly, and H Stenmark. 2000. "Interaction of the EEA1 FYVE Finger with Phosphatidylinositol 3-phosphate and Early Endosomes. Role of Conserved Residues." *The Journal of Biological Chemistry* 275 (32) (August 11): 24595–600. doi:10.1074/jbc.M906554199.

Gersdorff, H Von, and G Matthews. 1994. "Dynamics of Synaptic Vesicle Fusion and Membrane Retrieval in Synaptic Terminals." *Nature*.

Giansanti, Maria Grazia, Giorgio Belloni, Maurizio Gatti, Nazionale Ricerche, Biologia Molecolare, and La Sapienza. 2007. "Rab11 Is Required for Membrane Trafficking and Actomyosin Ring Constriction in Meiotic Cytokinesis of Drosophila Males □" 18 (December): 5034–5047. doi:10.1091/mbc.E07.

Giraldez, Antonio J, Yuichiro Mishima, Jason Rihel, Russell J Grocock, Stijn Van Dongen, Kunio Inoue, Anton J Enright, and Alexander F Schier. 2006. "Zebrafish MiR-430 Promotes Deadenylation and Clearance of Maternal mRNAs." *Science (New York, N.Y.)* 312 (5770) (April 7): 75–9. doi:10.1126/science.1122689.

Gold, E S, D M Underhill, N S Morrissette, J Guo, M a McNiven, and a Aderem. 1999. "Dynamin 2 Is Required for Phagocytosis in Macrophages." *The Journal of Experimental Medicine* 190 (12) (December 20): 1849–56.

Goss, John W, and Derek K Toomre. 2008. "Both Daughter Cells Traffic and Exocytose Membrane at the Cleavage Furrow During Mammalian Cytokinesis." *The Journal of Cell Biology* 181 (7) (June 30): 1047–54. doi:10.1083/jcb.200712137.

Grabs, D, V I Slepnev, Z Songyang, C David, M Lynch, L C Cantley, and P De Camilli. 1997. "The SH3 Domain of Amphiphysin Binds the Proline-rich Domain of Dynamin at a Single Site That Defines a New SH3 Binding Consensus Sequence." *The Journal of Biological Chemistry* 272 (20) (May 16): 13419–25.

Grevengoed, Elizabeth E, Donald T Fox, Julie Gates, and Mark Peifer. 2003. “Balancing Different Types of Actin Polymerization at Distinct Sites: Roles for Abelson Kinase and Enabled.” *The Journal of Cell Biology* 163 (6) (December 22): 1267–79. doi:10.1083/jcb.200307026.

Grosshans, Jörg, Christian Wenzl, Hans-Martin Herz, Slawomir Bartoszewski, Frank Schnorrer, Nina Vogt, Heinz Schwarz, and H-Arno Müller. 2005. “RhoGEF2 and the Formin Dia Control the Formation of the Furrow Canal by Directed Actin Assembly During Drosophila Cellularisation.” *Development (Cambridge, England)* 132 (5) (March): 1009–20. doi:10.1242/dev.01669.

Groves, E, a E Dart, V Covarelli, and E Caron. 2008. “Molecular Mechanisms of Phagocytic Uptake in Mammalian Cells.” *Cellular and Molecular Life Sciences : CMLS* 65 (13) (July): 1957–76. doi:10.1007/s00018-008-7578-4.

Gruenberg, J, G Griffiths, and K E Howell. 1989. “Characterization of the Early Endosome and Putative Endocytic Carrier Vesicles in Vivo and with an Assay of Vesicle Fusion in Vitro.” *The Journal of Cell Biology* 108 (4) (April): 1301–16.

Gruenberg, Jean. 2001. “The Endocytic Pathway: a Mosaic of Domains.” *Nature Reviews Molecular Cell Biology* 2 (October): 1–10.

Gupta, Gagan D, M G Swetha, Sudha Kumari, Ramya Lakshminarayan, Gautam Dey, and Satyajit Mayor. 2009. “Analysis of Endocytic Pathways in Drosophila Cells Reveals a Conserved Role for GBF1 in Internalization via GEECs.” *PloS One* 4 (8) (January): e6768. doi:10.1371/journal.pone.0006768.

He, Bing, and Wei Guo. 2009. “The Exocyst Complex in Polarized Exocytosis.” *Current Opinion in Cell Biology* 21 (4) (August): 537–42. doi:10.1016/j.ceb.2009.04.007.

Henley, J R, E W Krueger, B J Oswald, and M a McNiven. 1998. “Dynamin-mediated Internalization of Caveolae.” *The Journal of Cell Biology* 141 (1) (April 6): 85–99.

Henne, WM, and E Boucrot. 2010. “FCHo Proteins Are Nucleators of Clathrin-mediated Endocytosis.” *Science ...* 328 (June).

Hershkos, Avram, Hannah Heller, Sarah Elias, and Aaron Ciechanover. 1983. “Components of Ubiquitin-Protein Ligase System” 258 (13): 8206–8214.

Hicke, L, and H Riezman. 1996. “Ubiquitination of a Yeast Plasma Membrane Receptor Signals Its Ligand-stimulated Endocytosis.” *Cell* 84 (2) (January 26): 277–87.

Hinshaw, JE, and SL Schmid. 1995. “Dynamin Self-assembles into Rings Suggesting a Mechanism for Coated Vesicle Budding.” *Nature*.

Hoepfner, Sebastian, Fedor Severin, Alicia Cabezas, Bianca Habermann, Anja Runge, David Gillooly, Harald Stenmark, and Marino Zerial. 2005. “Modulation of Receptor Recycling and Degradation by the Endosomal Kinesin KIF16B.” *Cell* 121 (3) (May 6): 437–50. doi:10.1016/j.cell.2005.02.017.

Horgan, Conor P, Melanie Walsh, Tomas H Zurawski, and Mary W McCaffrey. 2004. "Rab11-FIP3 Localises to a Rab11-positive Pericentrosomal Compartment During Interphase and to the Cleavage Furrow During Cytokinesis." *Biochemical and Biophysical Research Communications* 319 (1) (June 18): 83–94. doi:10.1016/j.bbrc.2004.04.157.

Howes, Mark T, Matthew Kirkham, James Riches, Katia Cortese, Piers J Walser, Fiona Simpson, Michelle M Hill, et al. 2010. "Clathrin-independent Carriers Form a High Capacity Endocytic Sorting System at the Leading Edge of Migrating Cells." *The Journal of Cell Biology* 190 (4) (August 23): 675–91. doi:10.1083/jcb.201002119.

Huang, Juan, Wenke Zhou, Annie M Watson, Yuh-Nung Jan, and Yang Hong. 2008. "Efficient Ends-out Gene Targeting in Drosophila." *Genetics* 180 (1) (September): 703–7. doi:10.1534/genetics.108.090563.

Hunter, C, and E Wieschaus. 2000. "Regulated Expression of Nullo Is Required for the Formation of Distinct Apical and Basal Adherens Junctions in the Drosophila Blastoderm." *The Journal of Cell Biology* 150 (2) (July 24): 391–401.

Huotari, Jatta, and Ari Helenius. 2011. "Endosome Maturation." *The EMBO Journal* 30 (17) (August 31): 3481–500. doi:10.1038/emboj.2011.286.

Ito, K, N Ishii, a Miyashita, K Tominaga, H Kuriyama, H Maruyama, M Shirai, M Naito, M Arakawa, and R Kuwano. 1999. "Molecular Cloning of a Novel 130-kDa Cytoplasmic Protein, Ankhzn, Containing Ankyrin Repeats Hooked to a Zinc Finger Motif." *Biochemical and Biophysical Research Communications* 257 (1) (April 2): 206–13. doi:10.1006/bbrc.1999.0430.

Jutras, Isabelle, and Michel Desjardins. 2005. "Phagocytosis: At the Crossroads of Innate and Adaptive Immunity." *Annual Review of Cell and Developmental Biology* 21 (January): 511–27. doi:10.1146/annurev.cellbio.20.010403.102755.

Kaksonen, Marko, Christopher P Toret, and David G Drubin. 2005. "A Modular Design for the Clathrin- and Actin-mediated Endocytosis Machinery." *Cell* 123 (2) (October 21): 305–20. doi:10.1016/j.cell.2005.09.024.

Karr, T L, and B M Alberts. 1986. "Organization of the Cytoskeleton in Early Drosophila Embryos." *The Journal of Cell Biology* 102 (4) (April): 1494–509.

Kelly, Bernard T, Airlie J McCoy, Kira Späte, Sharon E Miller, Philip R Evans, Stefan Höning, and David J Owen. 2008. "A Structural Explanation for the Binding of Endocytic Dileucine Motifs by the AP2 Complex." *Nature* 456 (7224) (December 18): 976–79. doi:10.1038/nature07422.

Kerr, M. C. 2006. "Visualisation of Macropinosome Maturation by the Recruitment of Sorting Nexins." *Journal of Cell Science* 119 (19) (October 1): 3967–3980. doi:10.1242/jcs.03167.

Kicheva, Anna, Periklis Pantazis, Tobias Bollenbach, Yannis Kalaidzidis, Thomas Bittig, Frank Jülicher, and Marcos González-Gaitán. 2007. "Kinetics of Morphogen Gradient Formation." *Science (New York, N.Y.)* 315 (5811) (January 26): 521–5. doi:10.1126/science.1135774.

Kilchherr, F, S Baumgartner, D Bopp, E Frei, and M Noll. 1986. “Isolation of the Paired Gene of Drosophila and Its Spatial Expression During Early Embryogenesis.” *Nature*.

Kinchen, Jason M, and Kodi S Ravichandran. 2008. “Phagosome Maturation: Going Through the Acid Test.” *Nature Reviews. Molecular Cell Biology* 9 (10) (October): 781–95. doi:10.1038/nrm2515.

Kirkham, Matthew, Akikazu Fujita, Rahul Chadda, Susan J Nixon, Teymuras V Kurzchalia, Deepak K Sharma, Richard E Pagano, John F Hancock, Satyajit Mayor, and Robert G Parton. 2005. “Ultrastructural Identification of Uncoated Caveolin-independent Early Endocytic Vehicles.” *The Journal of Cell Biology* 168 (3) (January 31): 465–76. doi:10.1083/jcb.200407078.

Kong, MMC, Ahmed Hasbi, and Michael Mattocks. 2007. “Regulation of D1 Dopamine Receptor Trafficking and Signaling by Caveolin-1.” *Molecular ...* 72 (5): 1157–1170. doi:10.1124/mol.107.034769.caveolar.

Kosaka, T, and K Ikeda. 1983. “Reversible Blockage of Membrane Retrieval and Endocytosis in the Garland Cell of the Temperature-sensitive Mutant of Drosophila Melanogaster, Shibirets1.” *The Journal of Cell Biology* 97 (2) (August): 499–507.

Kouranti, Ilektra, Martin Sachse, Nassim Arouche, Bruno Goud, and Arnaud Echard. 2006. “Rab35 Regulates an Endocytic Recycling Pathway Essential for the Terminal Steps of Cytokinesis.” *Current Biology□: CB* 16 (17) (September 5): 1719–25. doi:10.1016/j.cub.2006.07.020.

Kukulski, Wanda, Martin Schorb, Marko Kaksonen, and John a G Briggs. 2012. “Plasma Membrane Reshaping During Endocytosis Is Revealed by Time-resolved Electron Tomography.” *Cell* 150 (3) (August 3): 508–20. doi:10.1016/j.cell.2012.05.046.

Kutateladze, T G, K D Ogburn, W T Watson, T de Beer, S D Emr, C G Burd, and M Overduin. 1999. “Phosphatidylinositol 3-phosphate Recognition by the FYVE Domain.” *Molecular Cell* 3 (6) (June): 805–11.

Kölling, R, and CP Hollenberg. 1994. “The ABC-transporter Ste6 Accumulates in the Plasma Membrane in a Ubiquitinated Form in Endocytosis Mutants.” *The EMBO Journal* 13 (14): 3261–3271.

Kölsch, Verena, Thomas Seher, Gregorio J Fernandez-Ballester, Luis Serrano, and Maria Leptin. 2007. “Control of Drosophila Gastrulation by Apical Localization of Adherens Junctions and RhoGEF2.” *Science (New York, N.Y.)* 315 (5810) (January 19): 384–6. doi:10.1126/science.1134833.

Kübler, E, and H Riezman. 1993. “Actin and Fimbrin Are Required for the Internalization Step of Endocytosis in Yeast.” *The EMBO Journal* 12 (7) (July): 2855–62.

Lanzetti, Letizia, Valentina Margaria, Fredrik Melander, Laura Virgili, Myung-Hee Lee, Jiri Bartek, and Sanne Jensen. 2007. “Regulation of the Rab5 GTPase-activating Protein RN-tre

by the Dual Specificity Phosphatase Cdc14A in Human Cells." *The Journal of Biological Chemistry* 282 (20) (May 18): 15258–70. doi:10.1074/jbc.M700914200.

Lanzetti, Letizia, Andrea Palamidessi, and Liliana Areces. 2004. "Rab5 Is a Signalling GTPase Involved in Actin Remodelling by Receptor Tyrosine Kinases." *Nature* 221 (2001): 309–314.

Lasko, P. 1999. "RNA Sorting in Drosophila Oocytes and Embryos." *FASEB Journal : Official Publication of the Federation of American Societies for Experimental Biology* 13 (3) (March): 421–33.

Lecuit, T, and E Wieschaus. 2000. "Polarized Insertion of New Membrane from a Cytoplasmic Reservoir During Cleavage of the Drosophila Embryo." *The Journal of Cell Biology* 150 (4) (August 21): 849–60.

Lecuit, Thomas. 2004. "Junctions and Vesicular Trafficking During Drosophila Cellularization." *Journal of Cell Science* 117 (Pt 16) (July 15): 3427–33. doi:10.1242/jcs.01312.

Lecuit, Thomas, Pierre-François Lenne, and Edwin Munro. 2011. "Force Generation, Transmission, and Integration During Cell and Tissue Morphogenesis." *Annual Review of Cell and Developmental Biology* 27 (November 10): 157–84. doi:10.1146/annurev-cellbio-100109-104027.

Lecuit, Thomas, Reba Samanta, and Eric Wieschaus. 2002. "Slam Encodes a Developmental Regulator of Polarized Membrane Growth During Cleavage of the Drosophila Embryo." *Developmental Cell* 2 (4) (April): 425–36.

Lee, Gwangrog, Khadar Abdi, Yong Jiang, Peter Michaely, Vann Bennett, and Piotr E Marszalek. 2006. "Nanospring Behaviour of Ankyrin Repeats." *Nature* 440 (7081) (March 9): 246–9. doi:10.1038/nature04437.

Lee, Jen-Yi, and Richard M Harland. 2010. "Endocytosis Is Required for Efficient Apical Constriction During Xenopus Gastrulation." *Current Biology : CB* 20 (3) (February 9): 253–8. doi:10.1016/j.cub.2009.12.021.

Lee, Meng-Tse Gabe, Ashwini Mishra, and David G Lambright. 2009. "Structural Mechanisms for Regulation of Membrane Traffic by Rab GTPases." *Traffic (Copenhagen, Denmark)* 10 (10) (October): 1377–89. doi:10.1111/j.1600-0854.2009.00942.x.

Lee, P S, Y Wang, M G Dominguez, Y G Yeung, M a Murphy, D D Bowtell, and E R Stanley. 1999. "The Cbl Protooncoprotein Stimulates CSF-1 Receptor Multiubiquitination and Endocytosis, and Attenuates Macrophage Proliferation." *The EMBO Journal* 18 (13) (July 1): 3616–28. doi:10.1093/emboj/18.13.3616.

Leonid, A, and E Mostov. 1994. "Receptor-mediated Transcytosis of IgA in MDCK Cells Is via Apical Recycling Endosomes Materials and Methods" 125 (1): 67–86.

Leptin, M, and B Grunewald. 1990. "Cell Shape Changes During Gastrulation in Drosophila." *Development (Cambridge, England)* 110 (1) (September): 73–84.

Leung, S M, W G Ruiz, and G Apodaca. 2000. “Sorting of Membrane and Fluid at the Apical Pole of Polarized Madin-Darby Canine Kidney Cells.” *Molecular Biology of the Cell* 11 (6) (June): 2131–50.

Levayer, Romain, Anne Pelissier-Monier, and Thomas Lecuit. 2011. “Spatial Regulation of Dia and Myosin-II by RhoGEF2 Controls Initiation of E-cadherin Endocytosis During Epithelial Morphogenesis.” *Nature Cell Biology* 13 (5) (May): 529–40. doi:10.1038/ncb2224.

Levkowitz, G, H Waterman, E Zamir, Z Kam, S Oved, W Y Langdon, L Beguinot, B Geiger, and Y Yarden. 1998. “c-Cbl/Sli-1 Regulates Endocytic Sorting and Ubiquitination of the Epidermal Growth Factor Receptor.” *Genes & Development* 12 (23) (December 1): 3663–74.

Liang, Hsiao-Lan, Chung-Yi Nien, Hsiao-Yun Liu, Mark M Metzstein, Nikolai Kirov, and Christine Rushlow. 2008. “The Zinc-finger Protein Zelda Is a Key Activator of the Early Zygotic Genome in Drosophila.” *Nature* 456 (7220) (November 20): 400–3. doi:10.1038/nature07388.

Lim, Jet Phey, Jack T H Wang, Markus C Kerr, Rohan D Teasdale, and Paul a Gleeson. 2008. “A Role for SNX5 in the Regulation of Macropinocytosis.” *BMC Cell Biology* 9 (January): 58. doi:10.1186/1471-2121-9-58.

Lin, Harrison W, Mark E Schneider, and Bechara Kachar. 2005. “When Size Matters: The Dynamic Regulation of Stereocilia Lengths.” *Current Opinion in Cell Biology* 17 (1) (February): 55–61. doi:10.1016/j.ceb.2004.12.005.

Lingwood, Daniel, and Kai Simons. 2010. “Lipid Rafts as a Membrane-organizing Principle.” *Science (New York, N.Y.)* 327 (5961) (January 1): 46–50. doi:10.1126/science.1174621.

Liu, Allen P, Dinah Loerke, Sandra L Schmid, and Gaudenz Danuser. 2009. “Global and Local Regulation of Clathrin-coated Pit Dynamics Detected on Patterned Substrates.” *Biophysical Journal* 97 (4) (August 19): 1038–47. doi:10.1016/j.bpj.2009.06.003.

Liu, Ya-Wen, Andrew I Su, and Sandra L Schmid. 2012. “The Evolution of Dynamin to Regulate Clathrin-mediated Endocytosis: Speculations on the Evolutionarily Late Appearance of Dynamin Relative to Clathrin-mediated Endocytosis.” *BioEssays : News and Reviews in Molecular, Cellular and Developmental Biology* 34 (8) (August): 643–7. doi:10.1002/bies.201200033.

Luan, Peng, WE Balch, SD Emr, and CG Burd. 1999. “Molecular Dissection of Guanine Nucleotide Dissociation Inhibitor Function in Vivo.” *Journal of Biological Chemistry* 274 (21): 14806–14817.

Lundmark, Richard, and Sven R Carlsson. 2003. “Sorting Nexin 9 Participates in Clathrin-mediated Endocytosis Through Interactions with the Core Components.” *The Journal of Biological Chemistry* 278 (47) (November 21): 46772–81. doi:10.1074/jbc.M307334200.

Lundmark, Richard, Gary J Doherty, Mark T Howes, Katia Cortese, Yvonne Vallis, Robert G Parton, and Harvey T McMahon. 2008. “The GTPase-activating Protein GRAF1 Regulates

the CLIC/GEEC Endocytic Pathway." *Current Biology : CB* 18 (22) (November 25): 1802–8. doi:10.1016/j.cub.2008.10.044.

Luzio, J Paul, Paul R Pryor, and Nicholas a Bright. 2007. "Lysosomes: Fusion and Function." *Nature Reviews. Molecular Cell Biology* 8 (8) (August): 622–32. doi:10.1038/nrm2217.

Lyman, DF, and Bany Yedvobnick. 1995. "Drosophila Notch Receptor Activity Suppresses Hairless Function During Adult External Sensory Organ Development." *Genetics* 1505: 1491–1505.

Maniak, M, R Rauchenberger, R Albrecht, J Murphy, and G Gerisch. 1995. "Coronin Involved in Phagocytosis: Dynamics of Particle-induced Relocalization Visualized by a Green Fluorescent Protein Tag." *Cell* 83 (6) (December 15): 915–24.

Markgraf, DF, Franziska Ahnert, and Henning Arlt. 2009. "The CORVET Subunit Vps8 Cooperates with the Rab5 Homolog Vps21 to Induce Clustering of Late Endosomal Compartments." *... Biology of the Cell* 20: 5276–5289. doi:10.1091/mbc.E09.

Marks, B, M H Stowell, Y Vallis, I G Mills, a Gibson, C R Hopkins, and H T McMahon. 2001. "GTPase Activity of Dynamin and Resulting Conformation Change Are Essential for Endocytosis." *Nature* 410 (6825) (March 8): 231–5. doi:10.1038/35065645.

Martín-Bermudo, M D, a Carmena, and F Jiménez. 1995. "Neurogenic Genes Control Gene Expression at the Transcriptional Level in Early Neurogenesis and in Mesectoderm Specification." *Development (Cambridge, England)* 121 (1) (January): 219–24.

Mateus, Ana Margarida, Nicole Gorfinkiel, Sabine Schamberg, and Alfonso Martinez Arias. 2011. "Endocytic and Recycling Endosomes Modulate Cell Shape Changes and Tissue Behaviour During Morphogenesis in Drosophila." *PloS One* 6 (4) (January): e18729. doi:10.1371/journal.pone.0018729.

Mathavan, Sinnakaruppan, Serene G P Lee, Alicia Mak, Lance D Miller, Karuturi Radha Krishna Murthy, Kunde R Govindarajan, Yan Tong, et al. 2005. "Transcriptome Analysis of Zebrafish Embryogenesis Using Microarrays." *PLoS Genetics* 1 (2) (August): 260–76. doi:10.1371/journal.pgen.0010029.

Matsunaga, Maki, Isao Uemura, Miwa Tamura, and Shin-ichi Nemoto. 2002. "Role of Specialized Microvilli and the Fertilization Envelope in the Spatial Positioning of Blastomeres in Early Development of Embryos of the Starfish Astropecten Scoparius." *The Biological Bulletin* 202 (3) (June): 213–22.

Mavrakis M, Rikhy R, Lippincott-Schwartz J. Plasma membrane polarity and compartmentalization are established before cellularization in the fly embryo. Dev Cell. 2009 Jan;16(1):93-104.

Mazumdar, Aveek, and Manjari Mazumdar. 2002. "How One Becomes Many: Blastoderm Cellularization in Drosophila Melanogaster." *BioEssays : News and Reviews in Molecular, Cellular and Developmental Biology* 24 (11) (November): 1012–22. doi:10.1002/bies.10184.

McBride, H M, V Rybin, C Murphy, a Giner, R Teasdale, and M Zerial. 1999. “Oligomeric Complexes Link Rab5 Effectors with NSF and Drive Membrane Fusion via Interactions Between EEA1 and Syntaxin 13.” *Cell* 98 (3) (August 6): 377–86.

McLean MA, Rajfur Z, Chen Z, Humphrey D, Yang B, Sligar SG, Jacobson K. Mechanism of chromophore assisted laser inactivation employing fluorescent proteins. Anal Chem. 2009 Mar 1;81(5):1755-61.

McMahon, Harvey T, and Emmanuel Boucrot. 2011. “Molecular Mechanism and Physiological Functions of Clathrin-mediated Endocytosis.” *Nature Reviews. Molecular Cell Biology* 12 (8) (August): 517–33. doi:10.1038/nrm3151.

Mellman, I. 1996. “Endocytosis and Molecular Sorting.” *Annual Review of Cell and Developmental Biology* 12 (January): 575–625. doi:10.1146/annurev.cellbio.12.1.575.

Mellman, I, Helen Plutner, and Pentti Ukkonen. 1984. “Internalization and Rapid Recycling of Macrophage Fc Receptors Tagged with Monovalent Antireceptor Antibody: Possible Role of a Prelysosomal Compartment.” *The Journal of Cell Biology* 98 (April).

Meloty-Kapella, Laurence, Bhupinder Shergill, Jane Kuon, Elliot Botvinick, and Gerry Weinmaster. 2012. “Notch Ligand Endocytosis Generates Mechanical Pulling Force Dependent on Dynamin, Epsins, and Actin.” *Developmental Cell* 22 (6) (June 12): 1299–312. doi:10.1016/j.devcel.2012.04.005.

Mercer, Jason, and Ari Helenius. 2009. “Virus Entry by Macropinocytosis.” *Nature Cell Biology* 11 (5) (May): 510–20. doi:10.1038/ncb0509-510.

Michl, J, and JC Unkeless. 1983. “Modulation of Fc Receptors of Mononuclear Phagocytes by Immobilized Antigen-antibody Complexes. Quantitative Analysis of the Relationship Between Ligand Number.” *The Journal of …* 157 (June): 1746–1757.

Miletic, Ana V, Daniel B Graham, Kumiko Sakata-Sogawa, Michio Hiroshima, Michael J Hamann, Saso Cemerski, Tracie Kloeppel, et al. 2009. “Vav Links the T Cell Antigen Receptor to the Actin Cytoskeleton and T Cell Activation Independently of Intrinsic Guanine Nucleotide Exchange Activity.” *PloS One* 4 (8) (January): e6599. doi:10.1371/journal.pone.0006599.

Mirre, C, and L Monlauzeur. 1996. “Detergent-resistant Membrane Microdomains from Caco-2 Cells Do Not Contain Caveolin.” *American Journal of Cell Physiology*.

Morin, X, R Daneman, M Zavortink, and W Chia. 2001. “A Protein Trap Strategy to Detect GFP-tagged Proteins Expressed from Their Endogenous Loci in Drosophila.” *Proceedings of the National Academy of Sciences of the United States of America* 98 (26) (December 18): 15050–5. doi:10.1073/pnas.261408198.

Muhlberg, a B, D E Warnock, and S L Schmid. 1997. “Domain Structure and Intramolecular Regulation of Dynamin GTPase.” *The EMBO Journal* 16 (22) (November 17): 6676–83. doi:10.1093/emboj/16.22.6676.

Murphey, R. K. 2003. “Targeted Expression of Shibirets and Semaphorin 1a Reveals Critical Periods for Synapse Formation in the Giant Fiber of Drosophila.” *Development* 130 (16) (August 15): 3671–3682. doi:10.1242/dev.00598.

Murthy, Mala, Rita O Teodoro, Tamara P Miller, and Thomas L Schwarz. 2010. “Sec5, a Member of the Exocyst Complex, Mediates Drosophila Embryo Cellularization.” *Development (Cambridge, England)* 137 (16) (August): 2773–83. doi:10.1242/dev.048330.

Müller, H a, and E Wieschaus. 1996. “Armadillo, Bazooka, and Stardust Are Critical for Early Stages in Formation of the Zonula Adherens and Maintenance of the Polarized Blastoderm Epithelium in Drosophila.” *The Journal of Cell Biology* 134 (1) (July): 149–63.

Nakato, H, T a Futch, and S B Selleck. 1995. “The Division Abnormally Delayed (dally) Gene: a Putative Integral Membrane Proteoglycan Required for Cell Division Patterning During Postembryonic Development of the Nervous System in Drosophila.” *Development (Cambridge, England)* 121 (11) (November): 3687–702.

Ni, J-Q., Markstein, M., Binari, R., Pfeiffer, B., Liu, L-P., Villalta, C., Booker, M., Perkins, L. A., and Perrimon, N. (2008) Vector and Parameters for Targeted Transgenic RNAi in Drosophila melanogaster. Nature Methods 5, 49-51

Nielsen, E, S Christoforidis, S Uttenweiler-Joseph, M Miaczynska, F Dewitte, M Wilm, B Hoflack, and M Zerial. 2000. “Rabenosyn-5, a Novel Rab5 Effector, Is Complexed with hVPS45 and Recruited to Endosomes Through a FYVE Finger Domain.” *The Journal of Cell Biology* 151 (3) (October 30): 601–12.

Nien, Chung-Yi, Hsiao-Lan Liang, Stephen Butcher, Yujia Sun, Shengbo Fu, Tenzin Gocha, Nikolai Kirov, J Robert Manak, and Christine Rushlow. 2011. “Temporal Coordination of Gene Networks by Zelda in the Early Drosophila Embryo.” *PLoS Genetics* 7 (10) (October): e1002339. doi:10.1371/journal.pgen.1002339.

Nobes, C D, and a Hall. 1995. “Rho, Rac, and Cdc42 GTPases Regulate the Assembly of Multimolecular Focal Complexes Associated with Actin Stress Fibers, Lamellipodia, and Filopodia.” *Cell* 81 (1) (April 7): 53–62.

Ochoa, G C, V I Slepnev, L Neff, N Ringstad, K Takei, L Daniell, W Kim, et al. 2000. “A Functional Link Between Dynamin and the Actin Cytoskeleton at Podosomes.” *The Journal of Cell Biology* 150 (2) (July 24): 377–89.

Oh, P, D P McIntosh, and J E Schnitzer. 1998. “Dynamin at the Neck of Caveolae Mediates Their Budding to Form Transport Vesicles by GTP-driven Fission from the Plasma Membrane of Endothelium.” *The Journal of Cell Biology* 141 (1) (April 6): 101–14.

Oyler, G a, G a Higgins, R a Hart, E Battenberg, M Billingsley, F E Bloom, and M C Wilson. 1989. “The Identification of a Novel Synaptosomal-associated Protein, SNAP-25, Differentially Expressed by Neuronal Subpopulations.” *The Journal of Cell Biology* 109 (6 Pt 1) (December): 3039–52.

Padash Barmchi, Mojgan, Stephen Rogers, and Udo Häcker. 2005. "DRhoGEF2 Regulates Actin Organization and Contractility in the Drosophila Blastoderm Embryo." *The Journal of Cell Biology* 168 (4) (February 14): 575–85. doi:10.1083/jcb.200407124.

Pal, Arun, Fedor Severin, Barbara Lommer, Anna Shevchenko, and Marino Zerial. 2006. "Huntingtin-HAP40 Complex Is a Novel Rab5 Effector That Regulates Early Endosome Motility and Is Up-regulated in Huntington's Disease." *The Journal of Cell Biology* 172 (4) (February 13): 605–18. doi:10.1083/jcb.200509091.

Pan, Yonghua, Zhenyi Liu, Jie Shen, and Raphael Kopan. 2005. "Notch1 and 2 Cooperate in Limb Ectoderm to Receive an Early Jagged2 Signal Regulating Interdigital Apoptosis." *Developmental Biology* 286 (2) (October 15): 472–82. doi:10.1016/j.ydbio.2005.08.037.

Papoulas, Ophelia, Thomas S Hays, and John C Sisson. 2005. "The Golgin Lava Lamp Mediates Dynein-based Golgi Movements During Drosophila Cellularization." *Nature Cell Biology* 7 (6) (June): 612–8. doi:10.1038/ncb1264.

Parks, a L, K M Klueg, J R Stout, and M a Muskavitch. 2000. "Ligand Endocytosis Drives Receptor Dissociation and Activation in the Notch Pathway." *Development (Cambridge, England)* 127 (7) (April): 1373–85.

Payne, G S, D Baker, E van Tuinen, and R Schekman. 1988. "Protein Transport to the Vacuole and Receptor-mediated Endocytosis by Clathrin Heavy Chain-deficient Yeast." *The Journal of Cell Biology* 106 (5) (May): 1453–61.

Pelissier, Anne, Jean-Paul Chauvin, and Thomas Lecuit. 2003. "Trafficking Through Rab11 Endosomes Is Required for Cellularization During Drosophila Embryogenesis." *Current Biology* 13 (21) (October): 1848–1857. doi:10.1016/j.cub.2003.10.023.

Pelkmans, L, J Kartenbeck, and a Helenius. 2001. "Caveolar Endocytosis of Simian Virus 40 Reveals a New Two-step Vesicular-transport Pathway to the ER." *Nature Cell Biology* 3 (5) (May): 473–83. doi:10.1038/35074539.

Pellikka, Milena, Guy Tanentzapf, Madalena Pinto, Christian Smith, C Jane McGlade, Donald F Ready, and Ulrich Tepass. 2002. "Crumbs, the Drosophila Homologue of Human CRB1/RP12, Is Essential for Photoreceptor Morphogenesis." *Nature* 416 (6877) (March 14): 143–9. doi:10.1038/nature721.

Peplowska, Karolina, Daniel F Markgraf, Clemens W Ostrowicz, Gert Bange, and Christian Ungermann. 2007. "The CORVET Tethering Complex Interacts with the Yeast Rab5 Homolog Vps21 and Is Involved in Endo-lysosomal Biogenesis." *Developmental Cell* 12 (5) (May): 739–50. doi:10.1016/j.devcel.2007.03.006.

Pereira-Leal, J B, and M C Seabra. 2001. "Evolution of the Rab Family of Small GTP-binding Proteins." *Journal of Molecular Biology* 313 (4) (November 2): 889–901. doi:10.1006/jmbi.2001.5072.

Pfeffer, Suzanne R. 2005. "Structural Clues to Rab GTPase Functional Diversity." *The Journal of Biological Chemistry* 280 (16) (April 22): 15485–8. doi:10.1074/jbc.R500003200.

Polo S. Signaling-mediated control of ubiquitin ligases in endocytosis. BMC Biol. 2012 Mar 15;10:25

Postner, M a, and E F Wieschaus. 1994. “The Nullo Protein Is a Component of the Actin-myosin Network That Mediates Cellularization in Drosophila Melanogaster Embryos.” *Journal of Cell Science* 107 (Pt 7 (July): 1863–73.

Racoosin, E L, and J a Swanson. 1993. “Macropinosome Maturation and Fusion with Tubular Lysosomes in Macrophages.” *The Journal of Cell Biology* 121 (5) (June): 1011–20.

Raimondi, Andrea, Shawn M Ferguson, Xuelin Lou, Moritz Armbruster, Summer Paradise, Silvia Giovedi, Mirko Messa, et al. 2011. “Overlapping Role of Dynamin Isoforms in Synaptic Vesicle Endocytosis.” *Neuron* 70 (6) (June 23): 1100–14. doi:10.1016/j.neuron.2011.04.031.

Reider, Amanda, Sarah L Barker, Sanjay K Mishra, Young Jun Im, Lymarie Maldonado-Báez, James H Hurley, Linton M Traub, and Beverly Wendland. 2009. “Syp1 Is a Conserved Endocytic Adaptor That Contains Domains Involved in Cargo Selection and Membrane Tubulation.” *The EMBO Journal* 28 (20) (October 21): 3103–16. doi:10.1038/emboj.2009.248.

Reik, W, and J Walter. 2001. “Genomic Imprinting: Parental Influence on the Genome.” *Nature Reviews. Genetics* 2 (1) (January): 21–32. doi:10.1038/35047554.

De Renzis, Stefano, J Yu, R Zinzen, and Eric Wieschaus. 2006. “Dorsal-ventral Pattern of Delta Trafficking Is Established by a Snail-Tom-Neuralized Pathway.” *Developmental Cell* 10 (2) (February): 257–64. doi:10.1016/j.devcel.2006.01.011.

Ridley, a J, H F Paterson, C L Johnston, D Diekmann, and a Hall. 1992. “The Small GTP-binding Protein Rac Regulates Growth Factor-induced Membrane Ruffling.” *Cell* 70 (3) (August 7): 401–10.

Rink, Jochen, Eric Ghigo, Yannis Kalaidzidis, and Marino Zerial. 2005. “Rab Conversion as a Mechanism of Progression from Early to Late Endosomes.” *Cell* 122 (5) (September 9): 735–49. doi:10.1016/j.cell.2005.06.043.

Roberts, R L, M a Barbieri, K M Pryse, M Chua, J H Morisaki, and P D Stahl. 1999. “Endosome Fusion in Living Cells Overexpressing GFP-rab5.” *Journal of Cell Science* 112 (Pt 2 (November): 3667–75.

Rothberg, K G, J E Heuser, W C Donzell, Y S Ying, J R Glenney, and R G Anderson. 1992. “Caveolin, a Protein Component of Caveolae Membrane Coats.” *Cell* 68 (4) (February 21): 673–82.

Roulier, E M, S Panzer, and S K Beckendorf. 1998. “The Tec29 Tyrosine Kinase Is Required During Drosophila Embryogenesis and Interacts with Src64 in Ring Canal Development.” *Molecular Cell* 1 (6) (May): 819–29.

Roux, Aurélien, Katherine Uyhazi, Adam Frost, and Pietro De Camilli. 2006. "GTP-dependent Twisting of Dynamin Implicates Constriction and Tension in Membrane Fission." *Nature* 441 (7092) (May 25): 528–31. doi:10.1038/nature04718.

Royou, Anne, Christine Field, and JC Sisson. 2004. "Reassessing the Role and Dynamics of Nonmuscle Myosin II During Furrow Formation in Early Drosophila Embryos." *Molecular Biology of Cell* 15 (February): 838–850. doi:10.1091/mbc.E03.

Russell, J M. 2000. "Sodium-potassium-chloride Cotransport." *Physiological Reviews* 80 (1) (January): 211–76.

Römer, Winfried, Léa-Laetitia Pontani, Benoît Sorre, Carles Rentero, Ludwig Berland, Valérie Chambon, Christophe Lamaze, et al. 2010. "Actin Dynamics Drive Membrane Reorganization and Scission in Clathrin-independent Endocytosis." *Cell* 140 (4) (February 19): 540–53. doi:10.1016/j.cell.2010.01.010.

Sabharanjak, Shefali, Pranav Sharma, Robert G Parton, and Satyajit Mayor. 2002. "GPI-anchored Proteins Are Delivered to Recycling Endosomes via a Distinct Cdc42-regulated, Clathrin-independent Pinocytic Pathway." *Developmental Cell* 2 (4) (April): 411–23.

Saffarian, Saveez, Emanuele Cocucci, and Tomas Kirchhausen. 2009. "Distinct Dynamics of Endocytic Clathrin-coated Pits and Coated Plaques." *PLoS Biology* 7 (9) (September): e1000191. doi:10.1371/journal.pbio.1000191.

Saldanha, Sven, Beth Bragdon, Oleksandra Moseychuk, Jeremy Bonor, Prasad Dhurjati, and Anja Nohe. 2012. "Caveolae Regulate Smad Signaling as Verified by Novel Imaging and System Biology Approaches." *Journal of Cellular Physiology* (February) (October 5). doi:10.1002/jcp.24253.

Sapperstein, S K, D M Walter, a R Grosvenor, J E Heuser, and M G Waters. 1995. "P115 Is a General Vesicular Transport Factor Related to the Yeast Endoplasmic Reticulum to Golgi Transport Factor Uso1p." *Proceedings of the National Academy of Sciences of the United States of America* 92 (2) (January 17): 522–6.

Sato, Miyuki, Ken Sato, Paul Fonarev, Chih-Jen Huang, Willisa Liou, and Barth D Grant. 2005. "Caenorhabditis Elegans RME-6 Is a Novel Regulator of RAB-5 at the Clathrin-coated Pit." *Nature Cell Biology* 7 (6) (June): 559–69. doi:10.1038/ncb1261.

Schafer, Dorothy a. 2004. "Regulating Actin Dynamics at Membranes: a Focus on Dynamin." *Traffic* 5 (7) (July): 463–9. doi:10.1111/j.1600-0854.2004.00199.x.

Schejter, E D, and E Wieschaus. 1993. "Bottleneck Acts as a Regulator of the Microfilament Network Governing Cellularization of the Drosophila Embryo." *Cell* 75 (2) (October 22): 373–85.

Schier, Alexander F. 2007. "The Maternal-zygotic Transition: Death and Birth of RNAs." *Science (New York, N.Y.)* 316 (5823) (April 20): 406–7. doi:10.1126/science.1140693.

Schlichting, Karin, Michaela Wilsch-Bräuninger, Fabio Demontis, and Christian Dahmann. 2006. "Cadherin Cad99C Is Required for Normal Microvilli Morphology in Drosophila Follicle Cells." *Journal of Cell Science* 119 (Pt 6) (March 15): 1184–95. doi:10.1242/jcs.02831.

Schlossman, D M, S L Schmid, W a Braell, and J E Rothman. 1984. "An Enzyme That Removes Clathrin Coats: Purification of an Uncoating ATPase." *The Journal of Cell Biology* 99 (2) (August): 723–33.

Schnatwinkel, Carsten, Savvas Christoforidis, Margaret R Lindsay, Sandrine Uttenweiler-Joseph, Matthias Wilm, Robert G Parton, and Marino Zerial. 2004. "The Rab5 Effector Rabankyrin-5 Regulates and Coordinates Different Endocytic Mechanisms." *PLoS Biology* 2 (9) (September): E261. doi:10.1371/journal.pbio.0020261.

Schweisguth, F, J a Lepesant, and a Vincent. 1990. "The Serendipity Alpha Gene Encodes a Membrane-associated Protein Required for the Cellularization of the Drosophila Embryo." *Genes & Development* 4 (6) (June 1): 922–931. doi:10.1101/gad.4.6.922.

Schweitzer, Jill Kuglin, Alanna E Sedgwick, and Crislyn D'Souza-Schorey. 2011. "ARF6-mediated Endocytic Recycling Impacts Cell Movement, Cell Division and Lipid Homeostasis." *Seminars in Cell & Developmental Biology* 22 (1) (February): 39–47. doi:10.1016/j.semcdb.2010.09.002.

Seaman, Matthew N J. 2004. "Cargo-selective Endosomal Sorting for Retrieval to the Golgi Requires Retromer." *The Journal of Cell Biology* 165 (1) (April): 111–22. doi:10.1083/jcb.200312034.

Semerdjieva, Sophia, Barry Shortt, Emma Maxwell, Sukhdeep Singh, Paul Fonarev, Jonathan Hansen, Giampietro Schiavo, Barth D Grant, and Elizabeth Smythe. 2008. "Coordinated Regulation of AP2 Uncoating from Clathrin-coated Vesicles by Rab5 and hRME-6." *The Journal of Cell Biology* 183 (3) (November 3): 499–511. doi:10.1083/jcb.200806016.

Sever, S, a B Muhlberg, and S L Schmid. 1999. "Impairment of Dynamin's GAP Domain Stimulates Receptor-mediated Endocytosis." *Nature* 398 (6727) (April 8): 481–6. doi:10.1038/19024.

Shi, Feng, and Jane Sottile. 2011. "MT1-MMP Regulates the Turnover and Endocytosis of Extracellular Matrix Fibronectin." *Journal of Cell Science* 124 (Pt 23) (December 1): 4039–50. doi:10.1242/jcs.087858.

Shin, Hye-Won, Mitsuko Hayashi, Savvas Christoforidis, Sandra Lacas-Gervais, Sebastian Hoepfner, Markus R Wenk, Jan Modregger, et al. 2005. "An Enzymatic Cascade of Rab5 Effectors Regulates Phosphoinositide Turnover in the Endocytic Pathway." *The Journal of Cell Biology* 170 (4) (August 15): 607–18. doi:10.1083/jcb.200505128.

Shuster, C B, and D R Burgess. 2002. "Targeted New Membrane Addition in the Cleavage Furrow Is a Late, Separate Event in Cytokinesis." *Proceedings of the National Academy of Sciences of the United States of America* 99 (6) (March 19): 3633–8. doi:10.1073/pnas.052342699.

Simonsen, A, R Lippe, and S Christoforidis. 1998. “EEA1 Links PI (3) K Function to Rab5 Regulation of Endosome Fusion.” *Nature* 394 (JULY): 2–6.

Simpson, L, and E Wieschaus. 1990. “Zygotic Activity of the Nullo Locus Is Required to Stabilize the Actin-myosin Network During Cellularization in Drosophila.” *Development (Cambridge, England)* 110 (3) (November): 851–63.

Siniossoglou, S, and H R Pelham. 2001. “An Effector of Ypt6p Binds the SNARE Tlg1p and Mediates Selective Fusion of Vesicles with Late Golgi Membranes.” *The EMBO Journal* 20 (21) (November 1): 5991–8. doi:10.1093/emboj/20.21.5991.

Sisson, J C, C Field, R Ventura, a Royou, and W Sullivan. 2000. “Lava Lamp, a Novel Peripheral Golgi Protein, Is Required for Drosophila Melanogaster Cellularization.” *The Journal of Cell Biology* 151 (4) (November 13): 905–18.

van der Sluijs, P, M Hull, P Webster, P Mâle, B Goud, and I Mellman. 1992. “The Small GTP-binding Protein Rab4 Controls an Early Sorting Event on the Endocytic Pathway.” *Cell* 70 (5) (September 4): 729–40.

Sokac, Anna Marie, and Eric Wieschaus. 2008a. “Local Actin-dependent Endocytosis Is Zygotically Controlled to Initiate Drosophila Cellularization.” *Developmental Cell* 14 (5) (May): 775–86. doi:10.1016/j.devcel.2008.02.014.

Sokac, Anna Marie, and Eric Wieschaus 2008b. “Zygotically Controlled F-actin Establishes Cortical Compartments to Stabilize Furrows During Drosophila Cellularization.” *Journal of Cell Science* 121 (Pt 11) (June 1): 1815–24. doi:10.1242/jcs.025171.

Stein, Jennifer a, Heather Tarczy Broihier, Lisa a Moore, and Ruth Lehmann. 2002. “Slow as Molasses Is Required for Polarized Membrane Growth and Germ Cell Migration in Drosophila.” *Development (Cambridge, England)* 129 (16) (August): 3925–34.

Stenmark, H, G Vitale, O Ullrich, and M Zerial. 1995. “Rabaptin-5 Is a Direct Effector of the Small GTPase Rab5 in Endocytic Membrane Fusion.” *Cell* 83 (3) (November 3): 423–32.

Stimpson, HEM, and CP Toret. 2009. “Early-arriving Syp1p and Ede1p Function in Endocytic Site Placement and Formation in Budding Yeast.” *Molecular Biology of ...* 20: 4640–4651. doi:10.1091/mbc.E09.

Strigini, M, and S M Cohen. 2000. “Wingless Gradient Formation in the Drosophila Wing.” *Current Biology : CB* 10 (6) (March 23): 293–300.

Sundborger, Anna, Cynthia Soderblom, Olga Vorontsova, Emma Evergren, Jenny E Hinshaw, and Oleg Shupliakov. 2011. “An Endophilin-dynamin Complex Promotes Budding of Clathrin-coated Vesicles During Synaptic Vesicle Recycling.” *Journal of Cell Science* 124 (Pt 1) (January 1): 133–43. doi:10.1242/jcs.072686.

Suzuki DT, Grigliatti T, Williamson R. Temperature-sensitive mutations in Drosophila melanogaster. VII. A mutation (para-ts) causing reversible adult paralysis. Proc Natl Acad Sci U S A. 1971 May;68(5):890-3

Swanson, Joel a. 2008. “Shaping Cups into Phagosomes and Macropinosomes.” *Nature Reviews. Molecular Cell Biology* 9 (8) (August): 639–49. doi:10.1038/nrm2447.

Sweitzer, S M, and J E Hinshaw. 1998. “Dynamin Undergoes a GTP-dependent Conformational Change Causing Vesiculation.” *Cell* 93 (6) (June 12): 1021–9.

Sánchez-Mejorada, G, and C Rosales. 1998. “Signal Transduction by Immunoglobulin Fc Receptors.” *Journal of Leukocyte Biology* 63 (5) (May): 521–33.

Söllner, T, M K Bennett, S W Whiteheart, R H Scheller, and J E Rothman. 1993. “A Protein Assembly-disassembly Pathway in Vitro That May Correspond to Sequential Steps of Synaptic Vesicle Docking, Activation, and Fusion.” *Cell* 75 (3) (November 5): 409–18.

Sönnichsen, B, S De Renzis, E Nielsen, J Rietdorf, and M Zerial. 2000. “Distinct Membrane Domains on Endosomes in the Recycling Pathway Visualized by Multicolor Imaging of Rab4, Rab5, and Rab11.” *The Journal of Cell Biology* 149 (4) (May 15): 901–14.

Tabata, Tetsuya, and Yuki Takei. 2004. “Morphogens, Their Identification and Regulation.” *Development (Cambridge, England)* 131 (4) (February): 703–12. doi:10.1242/dev.01043.

Tadros, Wael, and Howard D Lipshitz. 2009. “The Maternal-to-zygotic Transition: a Play in Two Acts.” *Development (Cambridge, England)* 136 (18) (September): 3033–42. doi:10.1242/dev.033183.

Takei, PSMP Kohji, SL Schmid, and P De Camilli. 1995. “Tubular Membrane Invaginations Coated by Dynamin Rings Are Induced by GTP-Î³S in Nerve Terminals.” *Nature*.

Taylor, Marcus J, David Perrais, and Christien J Merrifield. 2011. “A High Precision Survey of the Molecular Dynamics of Mammalian Clathrin-mediated Endocytosis.” *PLoS Biology* 9 (3) (March): e1000604. doi:10.1371/journal.pbio.1000604.

Thomas, Jeffrey H, and Eric Wieschaus. 2004. “Src64 and Tec29 Are Required for Microfilament Contraction During Drosophila Cellularization.” *Development (Cambridge, England)* 131 (4) (February): 863–71. doi:10.1242/dev.00989.

Thompson, Heather M, Ahna R Skop, Ursula Euteneuer, Barbara J Meyer, and Mark a McNiven. 2002. “The Large GTPase Dynamin Associates with the Spindle Midzone and Is Required for Cytokinesis.” *Current Biology□: CB* 12 (24) (December 23): 2111–7.

Torroja, Carlos, Nicole Gorfinkiel, and Isabel Guerrero. 2004. “Patched Controls the Hedgehog Gradient by Endocytosis in a Dynamin-dependent Manner, but This Internalization Does Not Play a Major Role in Signal Transduction.” *Development (Cambridge, England)* 131 (10) (May): 2395–408. doi:10.1242/dev.01102.

Traub, Linton M. 2009. “Tickets to Ride: Selecting Cargo for Clathrin-regulated Internalization.” *Nature Reviews. Molecular Cell Biology* 10 (9) (September): 583–96. doi:10.1038/nrm2751.

Trimble, W S, D M Cowan, and R H Scheller. 1988. “VAMP-1: a Synaptic Vesicle-associated Integral Membrane Protein.” *Proceedings of the National Academy of Sciences of the United States of America* 85 (12) (June): 4538–42.

Turner, F.Rudolf, and a.P. Mahowald. 1976. “Scanning Electron Microscopy of Drosophila Embryogenesis.” *Developmental Biology* 50 (1) (May): 95–108. doi:10.1016/0012-1606(76)90070-1.

Ungar, Daniel, and Frederick M Hughson. 2003. “SNARE Protein Structure and Function.” *Annual Review of Cell and Developmental Biology* 19 (January): 493–517. doi:10.1146/annurev.cellbio.19.110701.155609.

Ungewickell, E, and H Ungewickell. 1995. “Role of Auxilin in Uncoating Clathrin-coated Vesicles.” *Nature*.

Vaccari, Thomas, Tor Erik Rusten, Laurent Menut, Ioannis P Nezis, Andreas Brech, Harald Stenmark, and David Bilder. 2009. “Comparative Analysis of ESCRT-I, ESCRT-II and ESCRT-III Function in Drosophila by Efficient Isolation of ESCRT Mutants.” *Journal of Cell Science* 122 (Pt 14) (July 15): 2413–23. doi:10.1242/jcs.046391.

Vadlamudi, Ratna K, Rozita Bagheri-Yarmand, Zhibo Yang, Seetharaman Balasenthil, Diep Nguyen, Aysegul a Sahin, Petra den Hollander, and Rakesh Kumar. 2004. “Dynein Light Chain 1, a P21-activated Kinase 1-interacting Substrate, Promotes Cancerous Phenotypes.” *Cancer Cell* 5 (6) (June): 575–85. doi:10.1016/j.ccr.2004.05.022.

Vasioukhin, V, C Bauer, M Yin, and E Fuchs. 2000. “Directed Actin Polymerization Is the Driving Force for Epithelial Cell-cell Adhesion.” *Cell* 100 (2) (January 21): 209–19.

Vitale, G, V Rybin, S Christoforidis, P Thornqvist, M McCaffrey, H Stenmark, and M Zerial. 1998. “Distinct Rab-binding Domains Mediate the Interaction of Rabaptin-5 with GTP-bound Rab4 and Rab5.” *The EMBO Journal* 17 (7) (April 1): 1941–51. doi:10.1093/emboj/17.7.1941.

Wang, Jack T H, Markus C Kerr, Seetha Karunaratne, Angela Jeanes, Alpha S Yap, and Rohan D Teasdale. 2010. “The SNX-PX-BAR Family in Macropinocytosis: The Regulation of Macropinosome Formation by SNX-PX-BAR Proteins.” *PloS One* 5 (10) (January): e13763. doi:10.1371/journal.pone.0013763.

Warn, R M, and M Robert-Nicoud. 1990. “F-actin Organization During the Cellularization of the Drosophila Embryo as Revealed with a Confocal Laser Scanning Microscope.” *Journal of Cell Science* 96 (Pt 1) (May): 35–42.

Warn, R M, and a Warn. 1986. “Microtubule Arrays Present During the Syncytial and Cellular Blastoderm Stages of the Early Drosophila Embryo.” *Experimental Cell Research* 163 (1) (March): 201–10.

Wennerberg, Krister, Kent L Rossman, and Channing J Der. 2005. “The Ras Superfamily at a Glance.” *Journal of Cell Science* 118 (Pt 5) (March 1): 843–6. doi:10.1242/jcs.01660.

Wenzl, Christian, Shuling Yan, Philip Laupsien, and Jörg Grosshans. 2010. "Localization of RhoGEF2 During Drosophila Cellularization Is Developmentally Controlled by Slam." *Mechanisms of Development* 127 (7-8): 371–84. doi:10.1016/j.mod.2010.01.001.

Wienke, D C, M L Knetsch, E M Neuhaus, M C Reedy, and D J Manstein. 1999. "Disruption of a Dynamin Homologue Affects Endocytosis, Organelle Morphology, and Cytokinesis in Dictyostelium Discoideum." *Molecular Biology of the Cell* 10 (1) (January): 225–43.

Worby, Carolyn a, and Jack E Dixon. 2002. "Sorting Out the Cellular Functions of Sorting Nexins." *Nature Reviews. Molecular Cell Biology* 3 (12) (December): 919–31. doi:10.1038/nrm974.

Xie Z, Klionsky DJ. Autophagosome formation: core machinery and adaptations. Nat Cell Biol. 2007 Oct;9(10):1102-9.

Yamada, E. 1955. "The Fine Structure of the Gall Bladder Epithelium of the Mouse." *The Journal of Biophysical and Biochemical Cytology* (5).

Yamashiro, D J, B Tycko, S R Fluss, and F R Maxfield. 1984. "Segregation of Transferrin to a Mildly Acidic (pH 6.5) para-Golgi Compartment in the Recycling Pathway." *Cell* 37 (3) (July): 789–800.

Yang, Zhibo, Ratna K Vadlamudi, and Rakesh Kumar. 2005. "Dynein Light Chain 1 Phosphorylation Controls Macropinocytosis." *The Journal of Biological Chemistry* 280 (1) (January 7): 654–9. doi:10.1074/jbc.M408486200.

Young, P E, T C Pesacreta, and D P Kiehart. 1991. "Dynamic Changes in the Distribution of Cytoplasmic Myosin During Drosophila Embryogenesis." *Development (Cambridge, England)* 111 (1) (January): 1–14.

Yu, Xinzi, Rytis Prekeris, and Gwyn W Gould. 2007. "Role of Endosomal Rab GTPases in Cytokinesis." *European Journal of Cell Biology* 86 (1) (January): 25–35. doi:10.1016/j.ejcb.2006.10.002.

Zeigerer, Anja, Jerome Gilleron, Roman L Bogorad, Giovanni Marsico, Hidenori Nonaka, Sarah Seifert, Hila Epstein-Barash, et al. 2012. "Rab5 Is Necessary for the Biogenesis of the Endolysosomal System in Vivo." *Nature* 485 (7399) (May 24): 465–70. doi:10.1038/nature11133.

Zerial, M, and H McBride. 2001. "Rab Proteins as Membrane Organizers." *Nature Reviews. Molecular Cell Biology* 2 (2) (February): 107–17. doi:10.1038/35052055. .

Zhang, Jing, Calliste Reiling, James B Reinecke, Iztok Prislan, Luis a Marky, Paul L Sorgen, Naava Naslavsky, and Steve Caplan. 2012. "Rabankyrin-5 Interacts with EHD1 and Vps26 to Regulate Endocytic Trafficking and Retromer Function." *Traffic (Copenhagen, Denmark)* 13 (5) (May): 745–57. doi:10.1111/j.1600-0854.2012.01334.x.

Zhang, Jun, Karen L Schulze, P Robin Hiesinger, Kaye Suyama, Stream Wang, Matthew Fish, Melih Acar, Roger a Hoskins, Hugo J Bellen, and Matthew P Scott. 2007. "Thirty-one

Flavors of Drosophila Rab Proteins." *Genetics* 176 (2) (June): 1307–22. doi:10.1534/genetics.106.066761.

Zigmond, SH, and JG Hirsch. 1972. "Effects of Cytochalasin B on Polymorphonuclear Leucocyte Locomotion, Phagocytosis and Glycolysis." *Experimental Cell Research* 73: 383–393.